A STUDY OF RAREFIED FLOWS

USING AN ELECTRON BEAM

D.C. Lillicrap

May 1969

A thesis submitted for the Degree of Doctor of Philosophy in the Faculty of Engineering of the University of London

ABSTRACT

Low Density flows over flat plates have been studied using the electron beam fluorescense technique. This technique has been improved to allow measurements to be made both close to the surface and the leading edge without appreciably disturbing the flow. Density profiles have been obtained throughout the merged layer and the near free molecular regime, including the disturbed region upstream of the leading edge. A flow field model is proposed, in which the near free molecular regime extends several dynamic mean free paths from the leading edge. The upstream limit of continuum flow is given approximately by $M^2/Re_{x,\infty} = \cdot 2$. The disturbance upstream of the leading edge might be a function of the wedge angle of the model but for the present 15° angle there was a 5% increase in density 3 mean free paths upstream.

Density profiles for different surface temperatures show that the surface temperature has a considerable effect on the density close to the surface. In addition the shock layer thickness and shock angle increase slightly as the surface temperature increases. The shock strength when plotted against $M/Re_{x,\infty}$ is largely independent of the surface temperature in spite of the above behaviour.

The theoretical basis, proposed by Muntz[1], for calculating rotational temperature from the electron beam measurements has

been examined and found to be incomplete. By taking account of the excitation by slow secondary electrons the correct rotational temperatures can be calculated over a wide range of densities.

ACKNOWLEDGEMENTS

The author gratefully acknowledges the advice and assistance of the following.

Dr. J.K. Harvey who supervised this project and whose expert advice during the design of the equipment enabled many potential problems to be avoided.

Dr. E.W.E. Rogers of the National Physical Laboratory who made the Low Density Tunnel available for this work.

Mr. C.J. Berry for his valuable assistance in running this facility. Without his experience and constant cooperation it would not have been possible to obtain so much useful data.

Mr. S.C. Metcalf for many suggestions and useful discussions and for providing the two nozzles used for the experiments. The surface pressure data presented here were also supplied by him.

The workshops and design office staff of Imperial College and the N.P.L. who manufactured many of the components required, often at short notice.

The Science Research Council for awarding the author a grant for the first eighteen months of this work.

CONTENTS

NOTATION

Symbols

An m	Transition probability from state n to state m.
B	Rotational Constant.
C	Chapman - Rubesin constant.
C_p	Specific heat at constant pressure.
D	Distance from electron beam source.
E	Energy.
eV	Electron volts.
h	Planks constant.
I	Intensity.
i_p	Primary beam current.
K	Rotational quantum number.
k	Boltzmann's constant.
M	Mach number.
n	Number density.
R	Gas constant.
Re	Reynolds number

T	Temperature in degrees Kelvin.
U	Velocity in free stream direction.
v	Vibrational quantum number.
x	Distance from leading edge of model measured parallel to surface.
y	Distance from surface of model.
Δ S	Shock wave thickness.
μ	Viscosity.
ρ	Density
γ	Ratio of specific heats.
α	Accomodation coefficient.
$\bar{V}$	Rarefaction parameter.
$\bar{\chi}$	Viscous interaction parameter.
σ (T)	Collision cross section.
$\nu_{n\,m}$	Frequency of emitted radiation for transition from state n to state m.

Subscripts

b	body molecule	p	peak value
f	free stream molecule	r	reflected
G.W.	Gas at the wall	R	rotational

i	incident	v	vibrational
J	jump conditions	w	wall
LE	leading edge	∞	free stream
MS	maximum slope	o	stagnation conditions

Suffixes

'	Upper state
''	Lower state

INTRODUCTION

Supersonic flows over bodies at high Reynolds numbers can now be accurately described in terms of classical boundary layers and shock waves. The processes of viscous dissipation and heat conduction are restricted to a relatively thin layer adjacent to the surface, the thickness of which is inversely proportional to the square root of the Reynolds number. On slender bodies the local streamline deflection induced by this layer is small and there is a negligible interaction between the boundary layer and inviscid flow field. As a result the inviscid flow field and the shock wave are determined by the body shape, and the displacement thickness of the boundary layer can be neglected. The shock wave is thin and the shock angles, and hence shock strength, are determined by the body geometry and free stream Mach number.

As M is raised the deceleration of the gas produces higher temperatures in the boundary layer and its thickness is therefore greater than that encountered at lower speeds for the same free stream Reynolds number. In fact the streamline deflection induced by the thick boundary layer is M^2 times the order of its value at low supersonic speeds. Consequently for the hypersonic regime $M>6$ the displacement effect of the boundary layer can no longer be neglected and there is a considerable induced pressure on the

body. Under some conditions it is convenient to consider this problem as the flow over an effective body shape, which is the true body shape plus the displacement thickness of the boundary layer.

At the altitudes of interest for hypersonic flight the density is only 10^{-3} or less times that at sea level. Therefore the Reynolds numbers are relatively low compared with the values for supersonic flight at lower altitudes. As the boundary layer thickness is proportional to $1 / \sqrt{Re_\infty}$, low Reynolds numbers lead to a stronger interaction between the boundary layer and inviscid flow. A more rigorous argument shows that the strength of the interaction depends on the Mach number times the local streamline deflection induced by the boundary layer. In fact, the interaction depends on $M^3 / \sqrt{Re_{x,\infty}}$ and therefore increases as the leading edge is approached. However, a point is reached where the concept of a distinct boundary layer and shock wave interacting with each other breaks down. For hypersonic flow the disturbance produced by a slender body is confined to a relatively thin layer near the surface, and as the leading edge is approached the thick boundary layer eventually fills the region between the shock wave and the surface to form a 'merged layer'. At the same time low Re_∞ and high M cause other effects such as velocity slip at the surface and shock thickening.

The general effect of merging and these low density phenomena is to reduce the surface pressure and heat transfer, as well as the shock strength, so that they tend to values that would be expected for the near free molecular flow that should exist at the leading edge. Within a few mean free paths of the leading edge the concept of a merged shock and viscous layer based on continuum ideas cannot be used and a kinetic theory description of the flow must be applied.

The purpose of the present study is to investigate in detail the merging of the shock wave and boundary layer and the flow over a sharp leading edge. Prior to the work now presented extensive surface pressure and heat transfer measurements had been made as discussed in Chapter 1. These were difficult to interpret, particularly since the values did not tend to the free molecular limits as the leading edge was approached. Conventional flow field measurements showed little promise of clarifying the situation since under the present conditions a thick boundary layer grows on any probe in the flow, similar to that over the surface of the body. In the case of a pitot probe this significantly alters the measured pressure and as yet there are no means of applying corrections for viscous effects in a shear layer. Hot wires have been used with only moderate success due to difficulties in interpreting the changes in resistance as

the wire is traversed through the flow. Finally it can be shown that any mechanical probe placed in the flow causes an appreciable disturbance particularly close to the surface or the leading edge.

To overcome these difficulties a narrow beam of well collimated electrons is used as a probe, since this does not appreciably disturb the flow. In nitrogen, and several other gases, the beam produces fluorescence the intensity of which is simply related to the density under the conditions of interest in rarefied gas dynamics. Therefore by using a suitable optical system and photomultiplier the intensity of fluorescence and hence the density can be measured. In the present study this technique has been developed so that reliable measurements can be made throughout the flow field, even close to the surface and the leading edge.

In a diatomic gas such as nitrogen, the electron beam technique can also in principle be used to obtain the rotational temperature of the gas by resolving the rotational fine structure of the fluorescence spectra. Muntz[1] has put forward a theory for calculating the rotational temperature which has been found to be incomplete. During the excitation of the gas by the electron beam, secondary electrons are produced which are shown to effect the rotational spectrum. A method is developed, which

includes the effect of secondary electrons, and is shown to give the correct rotational temperature over a wide range of conditions.

A flat plate was used for the experimental studies as it is a particularly suitable model for studying viscous interaction. For an inviscid fluid the flow over a flat plate at zero incidence consists of a Mach line originating at the leading edge. In the case of a real fluid a boundary layer grows on the surface causing a shock wave to be produced which interacts with the boundary layer as described above. The whole disturbance is then due to the viscosity of the gas and there are no superimposed pressure gradients due to the body shape.

The present experiments were performed in Mach 6 flows for a range of Reynolds numbers from 130 to 650 per cm.

1. SUMMARY OF PREVIOUS INVESTIGATIONS

1.1 Previous Aerodynamic Studies

As the interest in hypersonic flight has increased, viscous interaction has been recognized as an important phenomenon often dominating the flow over a large proportion of the body. It is therefore important to understand the development of high-speed rarefied flows over sharp leading edge flat plates, before attempting to deal with a more complicated body.

The earliest experiments by Becker[2] and Bertram[3][4] et al regarded the interaction as a displacement effect by the boundary layer which is only true if the interaction is weak. Lees and Probstein[5] treated the problem as a viscous interaction which could be divided into asymptotic regions called strong and weak interaction regimes. Weak interaction occurs when the streamline deflection induced by the viscous layer is small so that the self induced pressure gradient causes only small perturbations to the boundary layer. In contrast strong interaction occurs when the streamline deflection is large and the pressure gradient terms are of the same order of magnitude as the viscous stress terms in the boundary layer. Hayes and Probstein[6] have summarised this early theoretical work and discuss both regimes in terms of the viscous interaction parameter $\bar{\chi} = M^3 \sqrt{C_\infty / Re_{x,\infty}}$.

Therefore on a flat plate the strong interaction regime occurs close to the leading edge while the weak interaction regime is further downstream. Viscous interaction theories were in reasonable agreement with the experimental results provided the Reynolds number was not too low. However they must fail sufficiently close to the leading edge since they predict that the surface pressure tends to infinity as this edge is approached. Schaaf et al[7] and Nagamatsu et al[8][9] were the first to present surface pressure and heat transfer data, for low values of $Re_{x\infty}$, which were significantly lower than predicted by strong interaction. Although it is now known that the surface pressure data should have been corrected for an orifice effect, the discrepancy was a real one. Videl and Wittliff[10] later confirmed this and discussed the departure from strong interaction in terms of a so called rarefaction parameter $\bar{V} = M\sqrt{C / Re_{x,\infty}}$. They concluded that this parameter described the initial departure from strong interaction and showed that for their data, heat transfer and surface pressure deviated from strong interaction for $\bar{V} = .2$ and $.1$ respectively. It was also concluded that velocity slip at the surface was one of the dominant mechanisms causing the departure from strong interaction. Talbot[11] interpreted the rarefaction parameter as a Knudsen number and

proposed it as a useful correlating parameter in the slip flow region near the leading edge. Later it was shown that $\bar{V}$ only correlated the departure from strong interaction and is not valid further upstream. It was expected that the experimental data would tend to their free molecular limits at the leading edge. However, Chaun and Waiter[12] found that the measured surface pressure a few mean free paths from the leading edge was considerably above this limit.

In spite of the incomplete experimental results several theoretical models were proposed to explain the departure from strong interaction. Nagamatsu et al[8][9] proposed a slip flow model in which the formation of the shock was delayed in the slip flow region but this was based on the doubtful interpretation of schlieren photographs. Laurmann[13] suggested a model which lead to the boundary layer displacement thickness increasing as x^2 so that coalescing compression waves are produced which eventually form a linearised counterpart of a shock wave. Oguchi [14][15] proposed a model which treated the merged layer as a completely viscous wedge like flow with constant pressure. This assumption of constant pressure was not realistic in view of the induced pressure gradients in the strong interaction regime. Pan and Probstein[16] used a model based on the Navier - Stokes

equations and calculated the first order effects of shock wave curvature and thickness, transport behind the shock and velocity slip and temperature jump at the surface. However it was assumed that the shock wave thickness remained small compared with the shock layer thickness.

The first comprehensive study of the flow field in the merged layer was made by Mc. Croskey et al[17] who proposed a flow field model which could be used to test the validity of these theoretical studies. A schematic diagram of this model, Figure (1), shows typical mass flow profiles for the merged and strong interaction regimes. Merging of the shock wave and boundary layer occurred for rarefaction parameters between .15 and .2 and was accompanied by a marked reduction in shock strength below the Rankine-Hugonoit value. The shock wave was everywhere convex and slightly curved and in the merged regime was not thin compared with the shock layer thickness. As this study was made with various mechanical probes the details near the surface and leading edge are unreliable. However, the details of the shock wave structure should be reliable and Mc Croskey et al conclusively demonstrated that the theoretical flow models were incorrect as discussed in reference 17. Becker and Boylan[18] also made detailed flow field surveys of the merged layer and confirmed the reduction in shock strength as the leading edge was

approached. From their pitot tube readings they inferred that the slip velocity at the surface was as high as .6 of the free stream velocity. However such results must be treated with caution due to the considerable disturbance caused by the probe, particularly near the surface and also the uncertainty in the viscous corrections which must be applied to the readings.

A further difficulty which must be mentioned here is the interpretation of surface pressure measured through a small orifice in the surface of the model. Potter et al[19] (and subsequent papers) have discussed the effects that can arise at low densities when the model is not in thermal equilibrium with the ambient flow. The pressure on the surface of a probe or model is equal to the net transfer of momentum between the gas and the wall. However, the pressure indicated by a gauge connected to an orifice is determined by the condition of zero net flux of molecules into the orifice. Therefore such a gauge only records the surface pressure if equilibrium exists in the neighbourhood of the orifice. Potter et al used an empirical analysis of the nonequilibrium arising from heat flux, which showed that large corrections are required near the leading edge of flat plates in rarefied flows. It is not certain how accurate these are but a recent study by Bartz and Videl[20] concluded

that these empirical corrections underestimate the orifice effect and that the error could be in the order of 50%. This error appears to arise from the fact that there is a difference between the gas temperature in the cavity underneath the orifice and the temperature of the cavity, which is not accounted for in the correction procedure.

Harbour and Lewis[21] were the first to apply an electron beam to study the flow over a flat plate. The big advantage over previous techniques is that there is no appreciable disturbance to the flow and interpretation of the data is straight forward. They obtained density profiles through the shock layer which showed that the shock strength decreased as the leading edge was approached, in reasonable agreement with Mc Croskey et al[17]. These and other experiments defined the boundaries between the various flow regimes and therefore the matching points for theoretical studies. The most important feature of the merged layer was the reduction in strength and increase in thickness of the shock wave as the leading edge was approached, which must be accounted for in any theoretical model.

More recent work has been concentrated on the region close to the leading edge, so as to provide initial conditions for theoretical studies. Particular attention is being paid to the leading edge geometry and bluntness, and Joss et al[22]

have made surface pressure and hot wire measurements close to the leading edge for different edge thicknesses. There was no detectable change in the flow field or the surface pressure with increasing thickness, provided it was less than $\frac{1}{4}$ of a free stream mean free path. They therefore defined a sharp leading edge as one for which the Knudsen number is greater than 4. A similar study[23] was recently made with an electron beam to obtain the density field around sharp and slightly blunted leading edges. Even for a sharp leading edge an appreciable disturbance was found five mean free paths upstream. It was suggested that this upstream disturbance might be a function of the wedge angle which in these tests was 20°. Hickmann[24] using a 10° wedge angle, found a similar but smaller disturbance upstream of the leading edge. Further experiments will be needed to see how important the wedge angle is but it should be noted that if the lower wedge face is important, the definition of a sharp leading edge would depend upon the wedge angle as well as the leading edge radius.

These experiments, and other recent work such as that by Becker[25] and Nagamatsu et al[26], have produced a large amount of data which is difficult to correlate. This lead Potter[27] to introduce the concept of a Reynolds number at the wall

defined as $Re_w = Re_\infty(\mu_\infty/\mu_w)$. Some relation between viscosity and temperature is usually assumed to relate (μ_∞/μ_w) to (T_∞/T_w). This parameter has been partially successful in accounting for the effect of surface temperature and Becker[25] claims that $M_\infty/Re_{w,x}$ correlates surface pressure and slip velocity from the transition regime into the merged layer regime.

Following these detailed measurements for the merged layer, several theoretical studies were performed which dropped the assumption of a Rankine - Hugonoit or a slightly modified Rankine Hugonoit shock wave used in the earlier flow models. They fall into two broad groups, the first of which obtains separate solutions for the shock wave structure and viscous layer and then matches them at the shock wave - viscous layer interface. The second group obtain a set of equations valid throughout the flow field thus avoiding the need to match two solutions.

In the first group, Oguchi[28] has extended his earlier work[14][15] and that of Pan and Probstein[16], and Oguchi's work has in turn been developed further by Shorenstein and Probstein[29]. In the present form of this approach, solutions are obtained for the shock wave structure and the viscous layer which take account of the finite transport effects across

the shock wave - viscous layer interface. First order corrections are then applied for shock curvature velocity slip and temperature jump. The most serious criticism of this work is the assumption that the pressure gradient across the viscous layer can be neglected. This was based on an estimate by Oguchi[28] which showed that for a cold wall the pressure behind the shock is close to that on the surface. Within this limitation this approach gives results in reasonable agreement with experiments for Mach numbers between 10 and 26.

For the second group Laurmann[30] used the linearised Navier - Stokes equations, with a Von Mises coordinate system, which were valid for distances of O (^{1}/Re), or greater, from the leading edge. More recently Rudman and Rubin[31] obtained similar equations and carried out a more complete comparison with experimental results. The agreement was reasonable although the results presented here show that the initial conditions were not applied correctly. Garvine[32] in a similar study appears to recognise this problem although the paper is not yet available. A set of equations which are valid for continuum flow, are fed with initial conditions as generated by a kinetic theory approach over the first 10 or 20 mean free paths of the model.

One relatively recent development is the numerical solution

of the Boltzmann equation, or some approximation to it. Huang and Hartley[33A] used the Boltzmann equation with the B.G.K. model as the governing equation, and obtained solutions by a finite difference technique. Originally, computer storage requirements limited the study to M = 1.5 but Huang and Hwang[33B] have now extended this method to M = 5 and 10 flows. Unfortunately the agreement with experiment is poor and this appears to be due to a fault in the technique.

At the present time, data are available for all the flow regimes generated by high speed rarefied flows over flat plates. Heat transfer and surface pressure do not tend to their free molecular limits at the leading edge. Theoretical models for the merged layer describe the departure from strong interaction and give reasonable predictions of surface pressure, heat transfer and skin friction. Interest is now centred on the transition between continuum and near free molecular flow in the vicinity of the leading edge, and further studies are required to determine the upstream limit of the merged layer regime. A disturbance has been detected upstream of the leading edge but it is not known how this is affected by the wedge angle or the leading edge thickness of the model. In addition it is not clear what the relevant mean free path should be in the near free molecular

region, and in a paper to be published by Hamel and Cooper[34] two relevant mean free paths are proposed.

The data presented in this thesis, which has been obtained over the last two years, is intended to extend the present knowledge of the merged layer and near free molecular flow regimes. Emphasis has been placed on making reliable flow field measurements, which would give some quantative information about the jump conditions at the surface as well as the shock structure. The flow field measurements were made with an electron beam probe and a survey of this technique follows which highlights some of the problems and applications.

1.2 The Development of Electron Beam Probes

It was not until 1960 that electron beams were used in wind tunnel experiments, although there was extensive development work prior to this. Usually some form of electron gun is used to produce a narrow, well collimated beam of electrons of moderate energy(10-50 KeV). The beam is directed across the flow field when the gas in the locality of it is excited by collisions with the high energy electrons. Fluorescence is then produced by the decay of the excited molecular states and the intensity can be related to the density of the gas. In some cases when the

fluorescence spectrum has a rotational and vibrational fine structure, the rotational and vibrational temperatures can also be obtained. The relative intensities of the rotational and vibrational spectrum lines are measured and a mathematical model is used to relate these to the relevant temperature.

Much of the early work on the interaction of a beam of fast particles with gases was performed by Grun et al. As early as 1953 Grun and Schopper[35] measured the light yield of nitrogen and mixtures containing nitrogen, produced by excitation with α - particles. A spectroscopic study by Grun[36] using beams of α - particles and 50 KeV electrons showed that the second positive group of nitrogen was responsible for most of the light emission. It was deduced that this was excited principally by slow secondary electrons, in contrast to the present technique where most of the excitation is by fast primary electrons giving rise to the 1 st negative system of nitrogen. It should be noted that most of Grun's experiments were performed under conditions where large numbers of secondary electrons were produced and is therefore not directly relevant to the present technique. One important development from this work was the use of dynamic pressure stages to separate the high vacuum system where the beam is produced and accelerated, from the high pressure region containing the gas under investigation. Grun and Schumacher[37]

have described these stages and more recently Schumacher[38] has published criterion and graphs which can be used in their design. Schumacher[39] has dealt with many of the engineering problems associated with the use of electron beams in wind tunnels and this reference mentions many possible uses for them, listing the references concerned with the earlier feasability studies. The properties of a gas which can be determined depend very much on the structure of the gas in question. In general the density of the gas can be determined and in certain cases the rotational, vibrational, and translational temperatures can be measured. If the gas is flowing, there are various methods of obtaining at least an estimate of the velocity while in some gas mixtures the concentration of the constituent species can be measured. It is not proposed to describe these various techniques in detail but only to mention the ways in which electron beams have been applied to low density aerodynamics.

1.2.1 Density Measurements

The density of a gas is the easiest variable to measure and three distinct methods have been used. By far the simplest method is the attenuation method which Wada[40] used in a shock tube. A narrow beam of electrons was fired across the test

section into a detector which recorded the beam current. Due to collisions with molecules which scatter the beam as it crosses the test section the signal from the detector is a function of the density in the test section. Therefore after suitable calibration Wada was able to use this system to make quite reliable measurements of density. The big disadvantage is that the measurement is not a local one and the technique is only suitable for two dimensional or axi-symmetric flows. However it can be used at higher densities than other techniques; Wada's system could be used at a pressure of 10 m m Hg at room temperature. At lower pressures it has proved possible to relate the number of electrons scattered out of the beam, to the density of the gas. Schumacher and Aruja[41] found that the scattered intensity of the electrons was a linear function of the pressure from 10^{-5} mm Hg to about .1 mm Hg at room temperature. This arises from the fact that over this density range, the majority of electrons undergo only one collision in their passage through the gas. Schumacher et al[42] have proposed a vacuum gauge for the range from 10^{-5} mm Hg to 1 mm Hg which relies on the single scattering of electrons at low pressures and the attenuation of the beam at higher pressures. The biggest problem preventing the wide application of these techniques to wind tunnel measurements is that of obtaining good spacial resolution. However work is now in progress at

Oxford University which has considerably refined the measurement of scattered electron intensity, allowing good spacial resolution to be obtained.

The technique which has proved most useful makes use of the fluorescence produced by the beam. Schumacher and Gadamer[43] showed that it was feasable to use the intensity of fluorescence at a point as a measure of the local gas density. A 50 KeV beam of electrons produced a blue fluorescent line coincident with the beam, the intensity of which varied with the local gas density. Gadamer[44] has investigated the variation of the intensity of fluorescence with density for air while Muntz[1] has made similar measurements for nitrogen. In nitrogen the intensity varied linearly with density up to a value of 1.25×10^{16} molecules per c.c. At higher densities the intensity drops below that expected for a linear relation due to the 'quenching' of excited states by collisions with other molecules. In air, Gadamer showed that quenching leads to a non linear relation even at low densities. During these experiments a collimated beam of electrons was passed through the gas and collected by a Faraday cup. In contrast to Grun's experiments there was very little absorption of the beam so that the number of secondary electrons produced is relatively few. As a result the 1st negative system of nitrogen is relatively more intense than

the second positive system.

Muntz and Marsden[45] have made a general study of electron beams and specify a number of conditions which must be satisfied. They recommend that the beam should not attenuate or scatter outside the field of observation in its passage through the gas and the excitation of the molecules should be directly to the upper electronic state involved. The transition probability for the emission should be high, in the order of 10^7 sec^{-1}. These authors[45] examined the spectra of He, O_2, N_2 and NO and found suitable transitions for use in high speed flows in all cases except O_2. Inelastic and elastic collision cross sections for the scattering of moderate energy electrons, 5 to 50 KeV, by helium, argon and nitrogen were given which can be used to estimate the attenuation and scattering of the beam for any particular situation. Finally a general discussion was given of the emission intensity as a function of density including excitation by secondary electrons and quenching. One limitation which has largely been ignored is that the quenching is temperature dependent. Therefore if it is appreciable there is no unique relationship between density and intensity.

With due attention to design details, the fluorescence technique is a simple but valuable means of measuring density

in many rarefied flow problems. It has been used to determine the free stream conditions in hypersonic wind tunnels[46][47] as well as to investigate the flow over wedges, cones[48] blunt bodies[49][50] and flat plates[23][24]. It has also proved useful in studying underexpanded jets[51] and diffusion processes occuring in gas mixtures[52].

1.2.2 Rotational and Vibrational Temperature

As a means of measuring density the electron beam fluorescence technique is very valuable. In certain cases it can be extended to measure the temperature of the gas and hence its state at any locality in the flow without physical disturbances or reference to any other measurement. In principle this applies when the spectrum excited by the beam has a rotational and vibrational fine structure. The relative line or band intensities can then be used to calculate the relative population of the rotational or vibrational levels, assuming the excitation and emission processes are understood. If then the gas is in rotational or vibrational equilibrium the rotational or vibrational temperature, characteristic of that particular distribution, can be calculated.

At the present time rotational and vibrational temperatures have only been measured in air and nitrogen using the first

negative bands of nitrogen. To calculate the rotational temperature Muntz[1] assumed that molecules were excited directly from the ground state to the N_2^+ $B^2\Sigma$ states. These excited states then undergo spontaneous transitions to the N_2^+ $X^2\Sigma$ states giving rise to the 1st negative system of N_2^+. This process was assumed to be unaffected by gas kinetic collisions which was reasonable at the densities considered by Muntz. At higher densities quenching occurs as noted earlier and it is not known if this alters the relative line intensities. It was also thought that secondary electrons could be neglected but the arguments put forward were doubtful due to large uncertainties in the collision cross sections. Subsequent measurements by Robben and Talbot[53] and Morrone[51] seemed to indicate that the rotational temperature calculated using Muntz's theory was too high. In spite of this the method has been extensively used to study rarefied gas flows[48][49][50].

The apparent discrepancy between the measured and true rotational temperature led Askenes[54] to measure the temperature of a slowly flowing stream of nitrogen in thermal equilibrium with its surroundings. He demonstrated that the error increased with density and was larger at lower temperatures. A more recent study by Hunter[55] in static air has obtained similar

but larger errors. The larger errors could be due to the beam heating the air since it was not flowing as in reference 54. A new model was proposed by Hickman[56] in which the excitation as a combination of dipole and quadropole transitions, but this leads to errors similar to those of Muntz's theory. More recently Smith[57] has shown that secondary electrons could cause the discrepancies observed, while Maquire[58] has suggested that preferential quenching of the more highly populated levels is important. In the present work it has been shown that excitation by secondary electrons can seriously alter the relative line intensities but there is no evidence of preferential quenching.

For the determination of vibrational temperatures Muntz used the Frank Condon factors[59] to determine the relative intensities of the vibrational bands in the first negative system. The ratio of the (1,0) and (0,1) bands is reasonably sensitive to temperature over the range 500-4,000°K. This theoretical curve was used to read off the vibrational temperatures from the measured ratio of the band intensities.

A knowledge of the vibrational temperature would be useful in hypersonic flows to determine the degree of vibrational freezing. Harbour[47] in an attempt to determine absolutely the flow conditions in a Mach 18 to 26 nozzle has found that

the relative band intensities are dependent on the density at any given temperature. This was attributed to a higher quenching rate for the $V' = 1$ vibrational level than for the $V' = 0$ level. Further investigation of these secondary processes will be necessary before absolute measurements can be made in this way.

1.2.3 Translational Temperature and Velocity Distribution Functions

It is well known that the Doppler profile of an emission line is a direct representation of the velocity distribution of the emitters. If this function is a Boltzmann distribution then the translational temperature can be defined. Muntz[60] has shown that when helium is excited by a 20 KeV beam of electrons the Doppler profile of the line at 5015.67 Å can be used to measure the velocity distribution function of the atoms. A Fabry-Perot etalon was used since it has a high resolving power and is optically fast. He[61] went on to show that free jet expansions could be studied by this technique and the optical system used, allowed the fluorescence produced by the beam to be observed from a direction perpendicular or parallel to the flow direction. The half widths of the Doppler line profiles were used to calculate the static temperatures which were in reasonable agreement with the predictions of Hamel and Willis[62].

More recently Muntz[63] has given a performance envelope for this technique which at the present time is limited to helium. The 5015.67 Å line of helium is relatively intense and easily isolated from the rest of the spectrum by an interference filter. In contrast, for most molecular spectra the fine structure makes it necessary to use a high dispersion spectrometer in series with the etalon resulting in a low optical speed. If this problem can be overcome the Doppler technique would be very useful.

Electron beams have also been used for flow visualisation either by making use of some long life metastable state excited by the beam[59] or by traversing the beam through the flow field[64]. Finally it is possible to calculate the flow velocity from the Doppler shift associated with changing the direction of observation from perpendicular to parallel with the flow as in reference 59.

1.2.4 Present State of Electron Beam Techniques

In principle electron beams can be used to measure the flow velocity, density and static temperature from which all the variables for a point in the flow can be calculated without reference to any other measurements. In practice there are

many limitations and precautions which must be observed.

The measurement of density is straightforward if quenching is negligible. At higher densities, when quenching is appreciable, the intensity of fluorescence is not a unique function of the density since quenching is temperature dependent. This temperature dependence has not been investigated and calibration curves should not be used over a wide range of temperatures if it can be avoided.

Rotational and Vibrational temperatures measured using Muntz's[1] technique are too high. This error is thought to be due to neglecting excitation by secondary electrons and since this depends on both the density and temperature of the gas it is difficult to devise any empirical correction scheme. However, a scheme is proposed in this work for including the effect of secondaries, at least for rotational temperature measurements.

Those techniques relying on the Doppler effect are very promising but at the moment are limited to measurements in helium.

2. THE ELECTRON BEAM PROBE

2.1 General Discussion

The experimental study of viscous interaction on flat plates has reached the point where detailed flow field surveys are required both close to the surface and the leading edge of the model. In these circumstances mechanical probes, such as pitot tubes, are particularly unreliable. There are several sources of error but the most serious is the disturbance to the flow caused by the presence of the probe. In contrast a beam of electrons passing through the gas does not appreciably disturb the flow even though sufficient molecules are excited to produce a measureable intensity of fluorescence. This property is exploited in the electron beam probe to make measurements throughout the flow field without disturbing the flow.

The most common arrangement of the probe is to fire the beam of electrons through the gas at right angles to the flow direction. An optical system, which can be traversed parallel to the beam, is then used to observe the fluorescence from a small portion of the beam. By suitable measurements, as described in Chapter 1, the local density, rotational temperature and vibrational temperature can be determined for this small

region of the flow.

Usually one of the many conventional forms of electron guns is used to generate the beam which is then focussed and collimated down to the required size. Electron guns operate at considerably lower pressures than those encountered in low density wind tunnels and it is necessary to separate the gun chamber from the tunnel by dynamic pressure stages[37]. This is simply a narrow tube or orifice through which the beam passes into the tunnel. The speed of the diffusion pump and the conductance of the tube are matched so that the gun chamber is maintained at the required pressure. Schumacher[38] has given criteria for designing these dynamic pressure stages and it is a simple matter to calculate the required pumping speed.

2.2 Specification of Electron Gun

When designing the electron gun and its associated equipment there are several factors which must be considered. Beam current stability and filament lifetime are important but the most important consideration is the attenuation of the beam as it passes through the gas. Once the beam passes through the orifice of the dynamic pressure stage it will be attenuated in the sense that the current density will decrease along the path of

the beam. This is due to the electrons being scattered by collisions with molecules or atoms, although the total beam current measured over all angles will not be noticeably reduced. The differential scattering cross section is a complicated function of the scattering angle but is very much larger for small angles than large ones. Therefore the majority of electrons are scattered through small angles so that the beam is not spread too rapidly. Due to this behaviour the rate of attenuation of the beam will depend on the distance of the detector from the source, the size and acceptance angle of the detector, as well as the number density of the gas. Using values of the differential scattering cross section given by Schumacher et al[41][42] calculations have been performed for what might be a typical situation in a low density wind tunnel. A thin beam of 100 KeV electrons travelling through nitrogen at a number density of 5×10^{16} molecules/cc was considered. The number of electrons scattered outside a radius of .15 cm was calculated as a function of the product ρ. D where D is the distance from the source and ρ the density. The results, figure 2, indicate that near the source the small angle scattering is not sufficient to scatter the electrons outside a radius of .15 cm. For the present example small angle scattering becomes important about 4 cm form the source causing a large increase in the number of electrons

scattered 'out' of the beam. In this region the current density will vary considerably across the diameter of the detector which therefore measures some integral of the current density over this area. Only at large distances from the source, when the detector is in a region of uniform current density, will the attenuation in current density be measured.

Due to this complicated behaviour of the beam attenuation as measured by a detector of finite size it is essential to keep it as small as possible. There are two ways of doing this, the simplest is to reduce the distance the beam has to travel through the gas to a minimum. In studying boundary layers in hypersonic flows it should be possible to keep this distance down to about 5 cm. The second but more expensive way is to increase the energy of the electrons since the scattering cross section is smaller for higher energies. However, on examining the differential scattering cross section given by Schumacher it can be seen that there is little to be gained by increasing the energy of the electrons above 50 KeV. These two considerations will play a large part in the design of any electron beam probe.

The commonest form of electron guns are those used in Cathode Ray tubes and television tubes and can be obtained in cartridge form at very low prices. They therefore appear

attractive but suffer from two serious drawbacks, they cannot be operated at the high voltages required and use activated filaments. If these filaments are to have a reasonable lifetime the gun chamber has to be maintained at a pressure of less than $10^{-6}\mu$ Hg. To achieve this with reasonable pumping speeds two dynamic pumping stages are required which makes the alignment of the beam with the pumping orifices difficult.

The type of gun used in electron microscopes fulfills the role better except that the beam current normally available is low, but they produce a very narrow beam of high energy electrons, up to 100 KeV. As they use tungsten filaments the pressure in the gun chamber need only be less than $5 \times 10^{-4}\mu$ Hg which can be achieved with one dynamic pumping stage. The gun consists of a hairpin filament inside a grid or Wehnhelt cylinder which is mounted several millimetres above the anode, figure 3. The anode is earthed and a negative H.T. voltage is applied to the grid which is connected to the filament through a bias resistor. In this way automatic biasing is obtained since the H.T. current produces a potential drop across the bias resistor maintaining the filament at a potential several hundred volts above the grid potential. An electrostatic field is thus formed between the three electrodes which partially focusses the electrons. In

fact an image of the cathode is formed between the cathode and anode which acts as the source of electrons. In the present arrangement the filament is heated directly by a D.C. power supply floating at the H.T. voltage.

From the work of Muntz[1], Gadamer[44], Sebacker[65] and others it is apparent that a beam current of up to 1 mA would be desirable but this is larger than that obtained from electron microscope guns in normal use. However, Haine and Einstein[66] have shown that the beam current is increased by reducing the grid bias or the distance between the filament and the bottom of the grid. This causes an increase in source size and the angular spread of the electrons coming from the gun but since it is not required to focus the electrons on to a very small area this can be tolerated.

2.3 Description of Electron Beam Probe

The technique for density measurements was discussed in Chapter 1 and now a detailed description of the various components used in the experiments is given.

Figure 4 shows a schematic diagram of the complete electron gun arrangement including the electron optics used for alignment and producing a parallel beam. Below the gun are two pairs of

magnetic deflection coils used for directing the beam through the fine pumping aperature in the drift tube as shown. In addition a mechanical adjustment enables the grid and filament assembly to be tilted slightly with respect to the anode. This is to compensate for small misalignments of the filament in the grid which cause the beam to leave the gun at an angle to the axis. A further adjustment allows the whole gun to be rotated slightly with respect to the electron optics so that the beam can be directed towards the centre of the magnetic deflection yoke. Two magnetic lenses were used for focussing with their object and image distances arranged so that an image of the electron source several cm. in front of the drift tube would be the same size as the source. In fact, the first lens focusses the beam in front of the second more powerful lens which then focusses it into a narrow parallel beam.

These lenses used symmetrical soft iron shields with small air gaps. Liebmann and Grad[67] have published data which shows that for the present application serious aberrations would only arise from asymmetry in the lenses. This was minimised by accurately turning the shields from homogenenous soft iron and carefully locating them along the axis of the electron gun.

When initially setting up the electron gun for an experiment

some mechanical adjustment was usually necessary but thereafter the beam could easily be directed through the hole in the drift tube by systematic adjustment of the currents to the deflection yoke and lenses. These were supplied by constant current power supplies* stabalised to 1 part in 50,000 so that the beam required only minor adjustments for the lifetime of the filament. The conductance of the dynamic pressure stage was such that a 5 cm diffusion pump could maintain the pressure in the gun at less than 5×10^{-4} μ Hg against a pressure of over 1 mm Hg on the high pressure side. An ionization gauge monitored the pressure in the gun chamber and if this became too high a relay switched off the H.T. and filament current thus protecting the filament.

The electron beam probe was designed for a Mach 25 nitrogen tunnel similar to that described by Vas and Allegre[68]. Therefore to test the equipment a small vacuum chamber similar to the test section of this wind tunnel was set up as in figure 5. The beam entered the chamber through the drift tube and was collected at the far side by a carbon Faraday cup designed to minimise

---

* Designed and built by the electronics section of the Aeronautics department, Imperial College.

re-emission of electrons. The cup was large enough to collect all of the electrons leaving the drift tube except those few which undergo large angle scattering or more than one collision. To measure beam current the cup was connected to earth through a known resistor and the voltage across the resistor measured. Muntz et al[69] suggest that this is not a reliable method since the indicated current varies by about 100% for $\pm$ 10 volts change in cup potential. This effect was only eliminated when the pressure around the cup was reduced below 5 μHg. To confirm this a given beam current was measured using a range of standard resistors between the cup and earth. As the resistance increased the indicated current decreased in agreement with the earlier results. However, when the pressure was varied from one to several hundred microns of mercury there was no change in the indicated beam current. Fortunately it is only necessary for the indicated current to be proportional to the true beam current. To check this the intensity of fluorescence, produced by the beam in a slowly flowing gas stream at constant density, was measured for a range of beam currents. For a 1000 Ω load resistor the intensity varied linearly with beam current for currents up to 1 mA. This shows that although the potential of the Faraday cup increases with beam current the constant relating indicated current to actual beam current is constant.

Gas could be let into the chamber through a heat exchanger and the speed of the rotary pump was sufficient to maintain a flow of gas at a few metres per second through the chamber at pressures between 20 μHg and 1 mm Hg. The heat exchanger was designed to allow different coolants to be used down to liquid nitrogen temperature and was insulated by the vacuum around it once the chamber was evacuated. A Pirani gauge and a McLeod gauge were provided for measuring the pressure in the chamber so that if the temperature of the gas was known its density could be calculated.

The beam could be observed through a window in the side of the test chamber using the optical system shown in figure 6. One lens and mirror were mounted on a two axis traverse gear which allowed any point within a 5 cm square to be observed with a positional accuracy of $\pm$ .025 mm on each axis. With the beam at the focus of this first lens a parallel beam of light was incident on all the mirrors making it possible to traverse along either axis without changing the focus of the second lens. The lenses must be positioned so that the second one focusses the light on the slit in front of the photomultiplier or monochromator. To do this a knife edge was mounted vertically in the chamber in the position that would be occupied by the beam and illuminated from behind by a diffuse light source.

A sharp image of the knife edge could readily be obtained on the front of the slit which remained in focus for all positions of the vertical traverse. For density measurements, an E.M.I. 9502S photomultiplier was used with a .1 mm wide slit in front of it. An interference filter centred on 3900 Å with a half band width of 100 Å was placed in front of the slit so that measurements could be made under normal lighting conditions.

2.4 The Optimum Operating Conditions

It is important to obtain the maximum beam current and filament lifetime compatable with the beam diameter and stability required. The parameters involved were mentioned when specifying the electron gun and in this case the emission current from the filament was measured as a function of the filament heater current, the grid bias resistor, the H.T. voltage and the filament position relative to the grid. The best position for the filament was found to be between .25 and .5 mm above the bottom of the grid and for this position characteristics such as those in figure 7 were obtained. (At present the highest H.T. voltage available was 30 Kv although the equipment was designed for use up to 50 Kv). A useful feature of these characteristics is the sharp saturation in the emission current,

due to the negative feedback, which can be used to stabilise the total beam current by increasing the filament heater current until the saturation knee is reached. This occurs for a heater current of 2.7 to 2.8 amps when an emission current of approximately a milliamp could be obtained. By systematic adjustment of the grid bias resistor and electron optics more than 90% of the emitted current could be directed through the drift tube and collected by the Faraday cup. Under the present operating conditions the hairpin filaments had a lifetime of between 10 and 15 hours which is adequate for most wind tunnel applications.

Although a current of 1 mA is sufficient it is necessary that this be contained in a narrow reasonably parallel beam of electrons. The intensity of fluorescence is proportional to the current density and therefore the variation in current density across the beam can be obtained by an Abel tranformation from the measured intensity profile. For the present discussion it is sufficient to use the variation in intensity as an indication of the electron distribution and hence beam size. The slit in front of the photomultiplier was .1 mm wide and orientated so that its length was parallel to the beam. Figure 8 shows typical profiles, obtained by traversing across the beam 1.3 cm in front of the drift tube, for a wide range of pressures at room temperature. Interpretation of these profiles is

complicated by quenching above 400 μHg and the peak of each distribution was difficult to determine with any accuracy. However, it is apparent that the effect of scattering is to redistribute the electrons causing a broadening of the distribution and a reduction in the peak value. The parameter ρ.D governs the scattering of the beam and for this particular arrangement a detector 2 mm in diameter would record practically all of the primary beam for values of ρ.D up to 2 x 10^{-6} grams cm^{-2}.

The profiles for the higher pressures, greater than 600 μHg, do not tend to zero intensity even 1 mm outside the primary beam diameter. This is due to the 'halo' around the beam produced by low energy secondary electrons. There appears to be no halo produced at lower pressures but this was thought to be due to the intensity of the halo being too low to be measured. To overcome this the slit was rotated through 90^{o} so that a cross section of the beam was observed. For a pressure of 32 μHg and a primary beam diameter of .5 mm the slit length was varied from 1 to 3 mm. Figure 9 shows there is a rapid increase in the photomultiplier signal as the slit length is increased to 1.5 mm followed by a more gradual rise for longer slits. This indicates that even at this pressure there is a halo around the beam which is not of negligible intensity. Fortunately the intensity of the halo

appears to vary in the same way as the intensity of fluorescence produced by the primary beam. For nitrogen Wada[40], and Harbour and Lewis[21] have shown linear calibration curves for pressures up to 500 μHg at room temperature.

The beam was usually used with a slit 2 mm long by .1 mm wide orientated so as to observe a cross section of the beam. This should minimise errors due to the spreading of the beam but before each experiment tests were performed in a static gas to ensure that the slit was long enough to observe the fluorescence due to the whole of the primary beam.

2.5 The Validity of Room Temperature Calibrations

If absolute density measurements are to be made the electron beam probe must be calibrated using a stream of gas at a known temperature and pressure. Calibration carried out in a static gas are not reliable since the beam might heat up the gas in its vacinity. The gas must be flowing at a velocity of at least a few metre per second to carry away the excited ions and any metastable excited molecules produced by the high energy electrons. It is usually only convenient to carry out such a calibration at room temperature and it is therefore necessary to establish its validity over the range of temperatures encountered in high Mach number low density wind tunnels. For room temperature

nitrogen the de-excitation of the N_2^+ $B_2\Sigma$ states by collisions with other molecules becomes important above 500 μHg pressure : causing the intensity of the bands to fall below that which would be expected for a linear relation between intensity and density. Muntz[1] gives the following expression for the intensity of a spectral line under these conditions

$$I = \frac{n h c \nu_{nm}}{1 + \frac{2n\sigma(T)\sqrt{4\pi RT}}{A_{nm}}} \qquad \ldots(1.2)$$

This shows that quenching depends on the temperature, through the variable $\sigma(T) \cdot \sqrt{T}$, as well as the density, but a search of the literature has failed to reveal any information on the variation of $\sigma(T)$. Harbour and Lewis[21] suggested that the quenching cross section varied with temperature as does the conventional collision cross section when the quenching term can be shown to vary as $nT/\mu(T)$. An attempt is made here to justify this assumption and to determine what corrections must be applied in the present experiments.

If any calibration curve is to be useful the sensitivity of the photomultiplier must not vary during the course of an experiment. An optical system was therefore introduced which

allowed an image of the filament of a standard lamp to be formed on the slit in front of the photomultiplier the output of which was measured for a range of currents supplied to the lamp. This current was determined by passing it through a standard shunt and measuring the voltage across it. The true temperature of the filament was obtained from the calibration supplied by the manufacturers and the spectral radiance for each temperature (obtained from the tables of DeVos[70]) plotted against the photomultiplier output. Calibration curves obtained in this way on three consecutive days are shown in figure 10 which demonstrate that the photomultiplier sensitivity is practically constant over this period.

To investigate the temperature dependence of quenching a 2 mm long slit was placed in front of the photomultiplier to observe a cross section of the beam and thus avoid errors due to the scattering of the beam. For room temperature measurements the heat exchanger was filled with water. The temperature of the gas flowing through the test chamber was assumed to be the same as the water temperature which was measured with a mercury thermometer. A room temperature calibration was then obtained simply by varying the pressure and measuring the photomultiplier output and beam current. A second calibration curve was obtained

at 76° K, as liquid nitrogen was readily available and this is close to the free stream static temperature obtained in many low density tunnels. To prevent the cold gas from the heat exchanger from mixing with the warmer gas already in the test chamber a pipe was mounted as shown in figure 11. A shielded and calibrated thermocouple was mounted just downstream of the beam to record the temperature of the gas stream. On filling the heat exchanger with liquid nitrogen the thermocouple indicated a steady drop in temperature until a value very close to that of the liquid was obtained after half an hour. However, this did not necessarily mean the gas flowing through the chamber was at this temperature since the radiative heat transfer between the thermocouple and its surroundings is comparable to the convective heat transfer at these low densities. Further indication of the temperature of the gas comes from the intensity of fluorescence at low densities which should be proportional to the density but independent of the temperature. However, as the density is calculated from the measured pressure and temperature if the temperature is higher than that indicated by the thermocouple the intensity would be lower than expected. This effect was observed initially but when the gas was pre-cooled before it entered the heat exchanger there was good agreement between the curves for both tempeatures, figure 12, and quenching was less effective at lower temperatures.

In order to check the assumption of Harbour and Lewis the room temperature curve was used to calculate a curve for 76°K. There was good agreement between the measured and calculated curves but this experiment alone is not enough to justify the assumption. In the present heat exchanger the gas passes through a narrow bore coil and then expands into a considerably larger bore tube a few inches upstream of the measuring station. During this expansion some condensation of the gas could occur the effects of which would be similar to those shown in figure 12. This has not been considered further since the present experiments were performed in the density range for which the curves are linear and independent of temperature. Figure 12 is presented to establish that the experimental results need not be corrected in any way for quenching while also giving some justification for the assumption that the quenching term varies as $nT/\mu(T)$.

3. EXPERIMENTAL STUDIES

3.1 The Setting up Procedure and Free Stream Measurements

The object of this thesis is to extend the current knowledge of high speed rarefied flows over sharp leading edge flat plates. Detailed flow field measurements in the merged and transition regimes have been made with particular attention paid to the influence of surface temperature. As far as possible accurate quantitative measurements, free from probe interference, have been made which provide a criterion for testing recent theoretical studies.

3.1.1 Installation of Electron Beam Probe in the Low Density Tunnel

The experiments were performed in the Low Density Tunnel at the National Physical Laboratory, because of delays in completing the Mach 20 nitrogen tunnel at Imperial College. The N.P.L. tunnel which has been described in reference 71 is considerably different from the nitrogen tunnel for which the electron beam probe was originally designed. A contoured nozzle, described in Appendix I, is mounted in a large test chamber so that the flow emerges into it as a free jet. After some modifications the electron gun was mounted horizontally so that the beam of electrons was directed across the exit plane of the nozzle. In addition to the drift tube, a mounting

sting was bolted to the end of the gun assembly. This supported the model on the axis of the nozzle and provided adjustments to its axial position and incidence.

The shock layer studies were performed using the technique described in Appendix II and the arrangement of the electron gun, model and optical system shown in figure 13. The optical system was mounted on a three axis traverse gear so that measurements could be made at points along the beam. A resolution of .15 mm was achieved in the beam direction and 2 mm in the flow direction. In order that the aperature of the lens was not reduced by the model as the point of observation approached the model surface, the optical axis was inclined as shown. As the electron beam was at the focus of this lens, the plane mirror directed a parallel beam of light through the window in the side of the tunnel. An optical system similar to that described in Chapter 2 then focussed the light onto a slit in front of the photomultiplier. This arrangement while satisfactory is far from ideal but it was impractical to extensively modify the equipment already in existance.

3.1.2 Setting Up Procedure

The alignment of the electron beam, the model and the various components of the optical system involved a lengthy

but not difficult procedure. To do this the model was first set up on the centre line of the nozzle and the axis of the gun aligned with one of the holes through its surface. To facilitate the initial alignment of the optics a wire, made luminous by passing a current through it, was used. This was strung across a metal bracket which held it in the same position that would be occupied by the electron beam. Final adjustments were made by running the beam with the test tank pumped down to about 50μ Hg pressure. The focus was adjusted to give the sharpest possible cut off at the surface of the model and then the position of the beam was plotted using the remaining two axes of the traverse gear. By suitable adjustments the traverse gear could be made to move parallel to the beam over its entire length. The final test was to measure the intensity offluorescence along the length of the beam, when the results shown in figure 14 were obtained.

3.1.3 Absolute Determination of Free Stream Density

One potential use of the electron beam is to measure the absolute value of the free stream density. This with a knowledge of the stagnation conditions, could then be used to calculate the free stream Mach number.

The beam was therefore calibrated by using the heat exchanger,

shown in figure 5, which was mounted on the tunnel in place of the nozzle. The electron beam was directed across the exit of the heat exchanger and a calibration curve obtained as described in Chapter 2. Measurements were made on two consecutive days (figure 15) and the reproducable accuracy was about 1% while the absolute value of the density was estimated to be accurate to better than 1%.

The calibration curve can be accurately established but practical difficulties with the present equipment limited its usefulness. This curve will only be strictly valid so long as the electron gun is not disturbed or the optics are not moved other than to traverse along the beam. It was not easy to satisfy the condition since the nozzle had to be replaced with the heat exchanger, the calibration performed; and then the nozzle replaced. However the calibration curve obtained was used in determining the free stream density for a stagnation pressure of 74.6 mm Hg, and a stagnation temperature of 693° K. From the pitot pressure, measured with a .310 cm diameter internally champfered pitot tube, the Mach number was calculated as 6.41 and the free stream density was 1.87×10^{-7} grams/cm^3. The value obtained from the electron beam measurement was 1.81×10^{-7} grams/cm^3 so that the two values agree well within the accuracy of the several measurements involved. It was not

necessary to apply any corrections for quenching at this density.

This initial check seemed to indicate that the electron beam could be used to determine the absolute value of the density. However measurements made over an extended period of time, and a large number of different runs showed that there was as much as a 15% variation for the intensity of fluorescence in the free stream. Some of this variation was due to genuine changes in the density arising from differences in the Mach number for each run. As discussed in Appendix I, this was occasionally as much as 2% and was due to different rates of cooling of the nozzle by the liquid nitrogen. Such a variation of the Mach number could account for 10% of the scatter in the free stream density. As the actual scatter was larger than this, the results were examined to see if there was any systematic variation with the beam current or the test chamber pressure. No such variation could be found but possibly it was masked by the variation in Mach number since the pitot pressure was not measured for every run during these preliminary measurements. A further possibility, which could not be investigated, was impurities in the nitrogen, particularly oxygen which would seriously affect the intensity of fluorescence.

As the electron beam probe would require frequent calibration it was not used to make absolute measurements. Instead, for

fill the remaining aerodynamic tests, the Mach number was calculated from the ratio of the free stream pitot pressure to the stagnation pressure. The corrections to the pitot pressure for viscous effects were small, 1 to 3% for the range of free stream conditions used in the experiments. The stagnation temperature was measured with a Nickel-Chrome Advance thermocouple, calibrated against the standards of the N.P.L. It was therefore possible to calculate all the free stream conditions to the accuracy required and the density was always measured in terms of the free stream density, readings of which were made before and after each set of measurements.

3.2 Shock Layer Measurements

The electron beam probe was used to obtain the density profiles at several axial stations along the length of the model. In the first place the effect of surface temperature on the growth of the shock layer was investigated by circulating different coolants through the model. Secondly detailed flow field measurements were made around the leading edge to investigate the disturbance upstream of the leading edge.

3.2.1 The Effect of Surface Temperature on the Growth of the Shock Layer

This first experiment was performed in the smaller nozzle

using the flow conditions summarised in table A1.1. The models were constructed from high conductivity copper with a solid rib down the centre through which the holes for the beam passed, figure 16. On either side of this central rib were cavities through which a coolant could be circulated to within 1 cm of the leading edge. The wedge angle of the model was 15° and the holes for the beam were 0.5 mm diameter.

To obtain a density profile through the shock layer, the model was mounted parallel to the nozzle axis with one of the holes directly opposite the end of the drift tube. This required careful positioning of the model but once this was done it was only necessary to push the drift tube firmly into the counter-bored hole on the underside of the model. Apart from near the leading edge, such a seal is acceptable due to the small pressure differences and the large mean free paths. Close to the leading edge, where there is little or no counter-bore, the tube was araldited to the underside of the model. The remaining holes in the model were sealed off. Some difficulties were experienced with the narrow drift tubes as they were too small to be cooled by circulating water through them. A satisfactory design consisted of a length of stainless steel hypodermic tube with .125 mm of copper deposited on the outside. The deposit of copper was sufficient to prevent local hot spots being produced,

which otherwise melted the stainless steel.

Once the model and drift tube had been set up by eye, the tunnel was evacuated and the electron beam operated. The magnetic focusing and deflection controls were used to maximise the beam current coming through the hole in the model. If this was adequate (0.1 to 1 mA), then the electron beam and the diffusion pump evacuating the gun were switched off and the system outgassed for at least half an hour and prefereably more. The thermistor gauge[72], used to monitor the pressure in the drift tube, could then be calibrated against the McLeod gauge. This completed the setting up of the electron beam and the required flow conditions could now be established. Finally, with the beam operating, the pressure in the drift tube was set equal to that on the surface of the model. A density profile through the shock layer was obtained by simultaneously measuring the intensity of fluorescence and beam current at several points through the shock layer and normalising the results to a constant beam current. The position of the model surface could be determined to within .125 mm from the sharp drop in the photomultiplier signal, as the point of observation was traversed onto the surface.

After each traverse of the shock layer the pitot pressure was measured .25 cm ahead of the leading edge, and used to calculate the free stream conditions.

The above procedure was used to obtain density profiles at different axial stations on the model from .175 cm to 5.71 cm from the leading edge. This was done first with water and then liquid nitrogen circulating through the model. Some difficulties were experienced in circulating the liquid nitrogen and it was necessary to insert a vapour trap immediately prior to the inlet pipes on the model. Sufficient liquid could then be circulated through the model to hold all but the leading edge at the temperature of the liquid. Typical sets of density profiles are shown in figures 17 and 18 for both cases.

The surface temperature distribution was measured, using a series of thermocouples inserted into the electron beam holes. Quartz inserts were fitted into the holes so that the bead forming the thermocouple was positioned just below the surface. Thermally conducting paint was then used to fill the hole so that the surface was uninterrupted. The biggest criticism of this method is that several insulated leads were fixed to the underside of the model, thus reducing the heat transfer to this face. This is an important point since the model is a wedge with one side parallel to the free stream. The upper and lower faces are not thermally isolated, and over the solid leading edge the heat transfer to the underside will be important in determining the temperature. For the water cooled case, figure 19, this was

obviously not important sice the leading edge is only a few degrees hotter than the rest of the model. However, for the liquid nitrogen case the temperature .175 cm from the leading edge was approximately 100° K. Under normal operating conditions it might be slightly higher, but this does not affect any of the qualitative conclusions drawn from the results.

The density profiles, figures 17 and 18, show the expected decrease in shock strength as merging occurs. For the case shown this corresponds to a rarefaction parameter $\bar{V}$ of .16 and occurs approximately 2.5 cm from the leading edge. Therefore downstream of this point the shock strength should be equal to the Rankine-Huganoit value for the measured shock angle and free stream Mach number. The Rankine-Hugonoit value for the density ratio was 2.38 for the water cooled case and 2.16 for the liquid nitrogen case while the measured values were 1.8 and 1.69 respectively.

This discrepancy is not due to a coalescing of the shock layer and the nozzle boundary layer. However, there is an appreciable blockage effect causing an increase in the Mach number above that for the empty nozzle. This results from a strong interaction between the nozzle boundary layer and the shock layer on the underside and side plates of the model, causing a disturbance to propogate upstream through the subsonic

part of the nozzle boundary layer. At a stagnation pressure of 74.6 mm Hg the Mach number was increased by .1 when the model was in the flow. This would correspond to a thinner nozzle boundary layer leading to a greater expansion of the flow and possibly some flow angularity, i.e. away from the axis of the nozzle the free stream flow is no longer parallel to the model surface. This is only a tentative suggestion but a flow angularity of almost 3° would explain the observed results.

To determine the conditions and gradients in the flow approaching the shock, axial pitot traverses were made at different heights above the model surface. At the highest Reynolds number, 650 per cm, measurements 2 cm above the model are not affected by the nozzle boundary layer, figure 20. 2.5 cm above the surface there is some loss of stagnation pressure in front of the shock layer due to this layer coalescing with the nozzle boundary layer. However it should have been possible to study the shock layer over at least 5 cm of the model. Another feature clearly shown is the decrease in shock strength towards the trailing edge of the model in spite of the fact that within the $\pm$ .25 mm accuracy of the measured shock position, the shock wave was straight over this region. Some decrease in the shock strength is to be expected due to the expansion at the trailing edge, but this would also be associated with a decrease in the

shock angle as the shock wave tended to a Mach wave sufficiently far down stream. Due to this unexplained behaviour of the shock strength, only measurements within 2.5 cm of the leading edge have been used when analysing the results for the smaller nozzle.

This experiment was continued in the larger nozzle when pitot traverses established that even 7.5 cm from the leading edge, there was a 1 cm wide region of uniform flow between the shock layer and the nozzle boundary layer. In addition, from Appendix I, the flow angularity was shown to be only.24° at the most. It was therefore possible to study the effect of the trailing edge by fixing different length extension plates to it. Pitot traverses were performed for 2.5 and 5 cm extensions. No differences in shock strength were detected over the first 2.5 cm of the model but further downstream it was between 5 and 6% lower for the shorter extension. For the 5 cm extension a virtually straight shock of constant strength existed from 2.5 to 5 cm downstream of the leading edge. Further downstream the shock angle decreased and there was a corresponding decrease in shock strength in agreement with the Rankine-Hugonoit values, as shown in figure 21. Therefore it appears that the trailing edge effect extends approximately 7.5 cm upstream but to investigate this further requires more attention to the trailing edge geometry. However it can be concluded that when a 5 cm extension

plate is used the flow over at least the first 5 cm of the model is not influenced by this trailing edge effect.

Using this extended model further density profiles were obtained and the density ratio across the shock wave was found to agree with the Rankine-Hugonoit values.

3.2.2 The Flow Field Around the Sharp Leading Edge

Theorectical studies, which use finite difference schemes, require initial conditions at the upstream limit of the flow regime for which they are valid. Unrealistic initial conditions are often applied at the leading edge but recent flow field surveys[22][23][24], show that there is an appreciable disturbance extending a few free stream mean free paths upstream of the leading edge.

For the larger nozzle a useful inviscid core can be obtained for a Reynolds number as low as 130 per cm (Appendix I). This corresponds to a free stream mean free path of .63 mm and since the primary beam diameter is only .5 mm it was possible to examine the upstream disturbance. The electron beam was directed across the leading edge and the optics were masked so that there was no change in aperature when traversing along it. In addition the narrow drift tube was shortened so that the shock wave generated by it did not influence the flow around the

leading edge. The distance between this tube and the leading edge was measured and the end of the tube used as a reference position for the traverses along the beam. Density profiles were obtained approximately 1 and 3 mean free paths upstream and were noted to be slightly asymmetric as shown in figures 22 and 23.

This flow field study of the leading edge region was extended 1.25 cm downstream of the leading edge when the density profiles shown in figure 24 were obtained. The free stream density profile upstream of the model is also shown and due to the gradients there and the diffuse nature of the shock wave it is difficult to determine the transition from one to the other. As a result the free stream density used to normalise the profiles cannot be accurately determined and ρ/ρ_∞ is only accurate to within 5%.

The merging of the nozzle boundary layer and the shock layer just downstream of this leading edge region should not sericusly effect the results since the shock layer is supersonic throughout.

This completes the experimental studies and results are now available from which the development of the flow field can be traced, from the first disturbance upstream of the model, to the weak interaction regime towards the trailing edge.

4. Discussion and Correlation of Results

An experimental study has been made of the various flow regimes for high speed rarefied flows over a sharp leading edge flat plate. The Mach number varied from 5.7 to 6.5 while the range of Reynolds numbers was 130 - 650 per cm. For the lowest Reynolds numbers the flow was sufficiently rarefied for the near free molecule region in the vacinity of the leading edge to be investigated. The first disturbance to the free steam was found a few mean free paths upstream of the leading edge. There was then a transition regime extending several mean free paths downstream of the leading edge until continuum flow was established giving rise to the merged regime. In this regime there is no shock wave distinct from the boundary layer and the whole flow field is described as a shock layer. Further downstream the density profiles showed a distinct shock wave and boundary layer separated by an inviscid region.

It will be demonstrated that this is a weak interaction regime and not a strong interaction as for Mach numbers greater than about 8[27]. From the density profiles a flow field model is built up and the extent of each regime is defined as far as

possible. This model is then used as a criterion for comparing the latest theoretical studies of the problem.

4.1 Correlation of Experimental Results

4.1.1 Shock Layer Shape

Before the shock layer shape can be discussed it is necessary to define the position and thickness of the shock wave. Usually the point of maximum slope in the density or pitot profile is taken as the position of the shock wave, as illustrated in figure 25a. This definition has been used for most of this thesis and is reasonable except when very close to the leading edge. The density profiles plotted in figure 24 show that as the leading edge is approached, the point of maximum slope moves closer to the peak of the profile. At the same time the peak moves closer to the surface. Therefore this definition gives a ratio of the shock thickness to the shock layer thickness which tends to infinity at the leading edge.

Therefore a more suitable definition is used when dealing with the near free molecular flow regime within a few mean free paths of the leading edge.

The actual shock shape for the merged and weak interaction regimes is plotted in figure 26 for both surface temperatures.

For the cold wall the temperature is assumed to be uniform and equal to 78^{o} K for which $T_w / T_o = .11$. Increasing the surface temperature leads to an increase in the shock layer thickness and the shock angles.

Several correlating parameters have been suggested for the merged layer and Mc Croskey[73] plotted Y_{MS} / X against $\bar{V}_\infty$. While the cold wall data correlated well, the data of Chaun and Waiter[12] for an adiabatic wall was as much as 100% higher. When the present data and that of Chaun and Waiter were plotted against $\bar{V}_\infty$ there was a systamatic increase in Y_{MS} / X with T_w / T_o for a given $\bar{V}_\infty$. Therefore a parameter using conditions at the wall as the reference should be more suitable. It is convenient to introduce a Reynolds number at the wall, $Re_{w,x} = Re_{x,\infty} \mu_\infty / \mu_w$, as Potter[27] did when correlating low density drag data for spheres and cones. Becker[25] has used this concept to discuss the transition from continuum to kinetic flow. It was shown that the Knudsen number at the wall changes from a dependence on $\bar{V}^2_{x,\infty}$ to a dependence on $M_\infty C_\infty / Re_{x,\infty}$. Therefore in the upstream region of the merged layer where the flow is near free molecular a Knudsen number based on $M_\infty C_\infty / Re_{w,x}$ is more appropriate. Shorenstein and Probstein[29] in a recent theoretical study introduced the parameter $\frac{M^2 C_\infty}{Re_{x,\infty}} \left(\frac{T_w}{T_o}\right)^{\frac{1}{2}}$ which

is simply related to the Knudsen number at the wall through:-

$$\frac{M^2 C_\infty}{Re_{x,\infty}} \left(\frac{T_w}{T_o}\right)^{\frac{1}{2}} = \bar{V}_{x,\infty}^2 \left(\frac{T_w}{T_o}\right)^{\frac{1}{2}} = \frac{M}{Re_{w,x}} \left(\frac{T_\infty}{T_w}\right)^{\frac{1}{2}} \left(\frac{2}{\gamma-1}\right)^{\frac{1}{2}} \quad \ldots(1.4)$$

Having obtained this expression Becker then proceeded to use $\frac{M}{Re_{w,x}}$ and claims that this is justified by the results. However the correlation of the shock shape in terms of this parameter was not good and in the present case the temperature ratio $(T_\infty / T_w)^{\frac{1}{2}}$ has been retained. In figure 27 the present results and Chaun and Waiter's data have been plotted against $\frac{M}{Re_{w,x}} \cdot \left(\frac{T_\infty}{T_w}\right)^{\frac{1}{2}}$ using the maximum slope definition for the shock wave position.

The correlation is remarkably good up to values of .1 in this parameter showing that the dependence on the temperature ratio $(T_\infty / T_w)^{\frac{1}{2}}$ is reasonable when conditions at the wall are used as a reference. If the free stream conditions are used as the reference then $(T_w / T_o)^{\frac{1}{2}}$ is the appropriate ratio.

For values of $\frac{M}{Re_{w,x}} \left(\frac{T}{T_w}\right)^{\frac{1}{2}}$ greater than .1 the correlation breaks down. This correponds to a distance in the order of 10 static mean free paths downstream of the leading edge. Hamel and Cooper[34] have discussed the flow in this near free molecular flow regime in terms of two relevant mean free paths.

They are the mean free path for collision of an emitted or body molecule, λ_b, with a free stream molecule, and the mean free path of a free stream molecule with a body molecule, λ_f. For hard sphere molecules the ratio of λ_f to λ_b is the speed ratio, i.e. $\lambda_f / \lambda_b = S_\infty$. This point will be discussed in more detail when dealing with the near free molecular flow regime in the vacinity of the leading edge. At present it can only be suggested that the breakdown in the correlation against $\frac{M}{Re_{w,x}} (\frac{T_\infty}{T_w})^{\frac{1}{2}}$ is due to the fact that the static mean free path at the wall is not the characteristic length for this regime.

Figure 27 also indicates the mean of Mc Croskey's[73] results which lies considerably below the present data. To consider this further it is necessary to use the position of the peak in the density or pitot pressure profile, Y_p, in place of Y_{MS}. Theoretical studies invariably use Y_p for the shock wave position and some recent experimental data is also presented in this form. In figure 28 the present data is replotted in terms of Y_p / X and the first point to note is that the correlation is not as good as before. In addition to Mc Croskey's data that of Harbour and Lewis[21] for similar flow conditions is also shown. Harbour and Lewis's measurements should be the more reliable as they were made with an electron beam probe. This probe does not appreciably disturb the flow while the pitot

tubes and hot wires used by Mc Croskey have been shown to cause considerable disturbances. It is therefore interesting to note that Harbour and Lewis's results are closer to the present data. In addition the recent data of Becker[25] are in better agreement with the present results than those of Becker and Boylan[18].

The scatter in the experimental data is considerable, $\pm$ 25%, and does not appear to vary systematically with M_∞, $Re_{x,\infty}$ or T_w / T_o. It is therefore difficult to make reliable comparisons with theory but Shorenstein and Probstein have already noted the agreement between their predictions and the results of Becker and Boylan[18] and Mc Croskey et al[17]. However they failed to compare with the results of Harbour and Lewis and Becker's results are now available all of which show higher values of Y_p / X than predicted by the theory. The present results are in reasonable agreement with these two references and it therefore appears that the theoretical model is at fault although the error is not serious. This point will be persued further when a new flow field model is proposed and compared in detail with the different theoretical approaches. However it is worth commenting that the theory of Huang and Hwang[33B] does not describe the development of the shock layer properly while Rudman and Rubin's [31] approach leads to a virtually constant value of Y_p / X of between .7 and .8.

4.1.2 Shock Thickness

It is often stated that when the shock wave and boundary layer merge there is a rapid thickening of the shock wave. While this is true to some extent it is not as pronounced as many flow field models show. In fact at the upstream end of the merged layer the shock wave is becoming thinner as illustrated by plotting contours of constant density around the leading edge, figures 29 and 30. This clearly shows that the peak in the density profile moves towards the surface as the leading edge is approached and occurs on the surface at the leading edge. At the same time the shock wave becomes thinner but if the maximum slope definition of the shock wave is used then the ratio of the shock thickness to shock layer thickness becomes infinite at the leading edge.

Due to this difficulty of defining the shock wave the maximum slope definition has been used for $\bar{V} \leq 1$. Values of $\Delta S / Y_{MS}$ are plotted in figure 31 where a remarkably good correlation is obtained over a wide range of Mach numbers, Reynolds numbers and T_w / T_o. This implies that ΔS varies in the same way as Y_{MS} with the ratio T_w / T_o. The increase in $\Delta S/Y_{MS}$ for the present data occurs for a $\bar{V}_{\infty}$ of .15 indicating the beginning of the merged layer in agreement with other studies (17)(18). As pointed out above the continued rise in this

ratio for the larger values of $\bar{V}_{\infty}$ is due to Y_{MS} decreasing faster than ΔS and does not mean that shock waves continues to get thicker.

For values of $\bar{V}_{\infty}$ greater than 1 the density profiles indicate a gradual rise to a peak value followed by a sharp drop as the surface is approached. It is difficult to define characteristic points for these profiles and therefore the somewhat arbitrary definition of Becker and Boylan[18] is used. From figure 25 the shock thickness is $Y_p - Y_A$ while the shock position is $(Y_p + Y_A) / 2$.

Using this definition some of the present data has been compared with Becker and Boylan's values $\Delta S / Y_{MEAN}$ in figure 32, for values of $\bar{V}_{\infty}$ between .3 and 2. There is reasonable agreement at a $\bar{V}_{\infty}$ of .5 but for larger values there is rapid divergence of the two set of data. It is dangerous to infer too much from this since Becker and Boylan used pitot tubes and hot wire which could drastically disturb the thin shock layer, very close to the leading edge, as suggested in Appendix II. However some of the difference is probably due to a breakdown in the correlation with $\bar{V}_{\infty}$. As mentioned earlier Hamel and Cooper have shown that there are two effective mean free paths for this regime related by $\lambda_f / \lambda_b = S_{\infty}$. The speed ratio, S_{∞}, should therefore be important rather than the Reynolds

number or surface temperature. This is clearly the case for the data presented in figure 32. The results for the present experiment show that there is no dependence on Reynolds number or T_w / T_o for the range considered. For Becker and Boylan's data the Reynolds number and T_w / T_o are similar so that the only difference is the Mach number. Therefore the difference in $\Delta S / Y_{MEAN}$ appears to be due to the difference in Mach number, or speed ratio, although the results of Becker and Boylan should be treated with caution.

4.1.3. Shock Strength

The density profiles and figures 29 and 30 clearly show that the merged layer is made up of a relatively thick shock wave with a viscous layer between it and the surface. The most striking effect of this merging is the reduction of the shock strength as the leading edge is approached. This has been discussed by Oguchi[28] and Shorenstein and Probstein[29] and was shown to be due to finite transport effects behind the shock due to its contact with the viscous layer. The actual processes involved are discussed when comparing the flow field model with their theoretical model but the shock strength and its correct correlation should give some insight into these processes.

As the density is the parameter measured in the present

experiment the ratio of the maximum density to the free stream density is defined as the shock strength. Within a few mean free paths of the leading edge it was anticipated that the free stream mean free path would be important in determining the shock strength. Therefore the shock strength for several different experiments has been plotted against $\frac{M\ C^*}{Re_{x,\infty}}$, which is approximately λ_{∞} / X. The Chapman - Rubesin constant C^* is based on Eckert's[21] reference temperature T^* given by $T^* / T_o \simeq$ $1/6(1 + 3\ T_w / T_o)$. This is approximately the mean temperature in the shock layer and is more appropriate than T_w or T_∞ particularly if T_o and M_∞ are high.

Figure 33 reveals the remarkable result that this parameter correlates the shock strength for more than 100 free stream mean free paths from the leading edge. In fact for the present data the correlation extends to the downstream limit of the merged regime. Further support for this correlation comes from the Mach 9.4 data of Hickman[24]. It has been noted in the present experiment that the peak in the density profile moves closer to the surface as the leading edge is approached. However, even 3 mean free paths from the leading edge there is still a distinct peak in the profile. In constrast Hickman's profiles do no show such a peak ten or more mean free paths from the leading edge. This is consistent with the fact that the

resolution of the optical system for his experiment appears to be worse than .5 mm measured along the beam which would not be sufficient to resolve the peak in the profile close to the leading edge. Due to this only data for $M C^{*} / Re_{x,\infty}$ up to value of .05 has been plotted and this is in good agreement with the present data. Therefore this simple parameter $M C^{*} / Re_{x,\infty}$ correlates the shock strength for a range of Reynolds numbers from 320 to 6,000 per cm and Mach numbers from 5.74 to 25.5. This data also includes results for a cold wall $T_w / T_o = .11$ and the adiabatic case $T_w / T_o \simeq 1$. The physical significance of this and the theoretical results plotted will be discussed in connection with a new flow field model presented later.

4.2 Surface Pressure

For completeness the surface pressure distribution is discussed here although the measurements were not performed by the author. The results are taken from an earlier study[74] which used the same flow conditions as the present experiments. Corrections were applied for the orifice effect which arises when the model is not in thermal equilibrium with the ambient flow. The corrections applied, using the theory of Kinslow and Arney[75], increased the surface pressure by approximately 20% and 5% for $T_w / T_o = .11$ and .44 respectively. Bartz and Videl[20]

have recently studied these empirical methods for correcting pressure data and concluded that they underestimate the effect possibly by as much as 20% $\pm$ 20%. No precise estimates were made for the accuracy of Kinslow and Arney's method as applied to the present data but as errors similar to those suggested by Bartz and Videl are possible, the pressure could have been underestimated by as much as 8% for $T_w / T_o = .11$. However, an error of this magnitude will not alter any of the qualitative conclusions in this thesis.

The corrected surface pressures increased with T_w / T_o and in figure 34 the more reliable data for $T_w / T_o = .44$ is plotted against the viscous interaction parameter χ_∞. Comparison with weak and strong interaction theory shows that the surface pressure deviates from 1st order weak interaction theory for $\chi_\infty \simeq 8$ and there is no region of strong interaction. The usual criterion for strong interaction is $\chi \simeq$ O(10) while merging occurs for $V_{\infty,x} \gtrsim .1$ to .2. Therefore as Potter[27] has suggested, because $\chi_{\infty,x} = V_{\infty,x} M_\infty^2$, strong interaction will not occur over much of the plate unless $M_\infty \gtrsim 8$. As a result the region downstream of the merged layer is a weak interaction regime for the present Mach 6 flows, which explains the surface pressure variation in figure 34.

4.3 Temperature Jump and Slip Velocity

Reliable solutions to the Navier - Stokes equations, describing the flow over a body in the continuum limit, can only be obtained if the correct boundary conditions are applied at the surface. It is therefore necessary to examine in detail the Knudsen layer, of the order of a mean free path thick, which separates the outer continuum flow from the body surface. For this layer collisions with the surface are more significant than intermolecular collisions so that the velocity distribution function is not locally Maxwellian and the Navier - Stokes equations are not valid. Therefore the correct boundary conditions to be used with the Navier - Stokes equations are the conditions at the outer edge of the Knudsen layer.

Provided the density of the gas is sufficiently high for the mean free path to be neglected compared with the physical dimensions of the problem, the Knudsen layer can be ignored without causing serious errors. Under these conditions the Navier - Stokes equations can be used by applying the boundary conditions $u = 0$ and $T = T_w$ at the surface. However, for the present flow conditions, realistic boundary conditions for the Navier - Stokes equations can only be obtained by considering the Knudsen layer. The simplest approach is to ignore the thickness of this layer but to apply appropriate slip boundary

conditions at the surface. The conditions are obtained by considering the velocity or temperature profile for the continuum flow, for which the Navier - Stokes equations are valid, to be extrapolated uniformly up to the surface. Alternatively the solutions for the Knudsen layer and the Navier - Stokes equations can be matched at the interface between the continuum flow and the Knudsen layer. Only a few of the recent theoretical solutions can be mentioned here but first it is useful to consider the simple approach proposed by Maxwell.

To calculate the slip velocity over a surface it is convenient to group the molecules into two streams. One stream consists of molecules approaching the surface and the other of molecules that have just struck it and are receding from it. The slip velocity can then be regarded as the nett mass velocity of these two streams. If the slip velocity is U_w then the average tangential velocity of the molecules approaching the surface will be

$$U_I = U_w + \lambda \frac{\partial U}{\partial Y}$$

For the reflected molecules if the accommodation coefficient for tangential momentum is f then their average velocity will be

$$U_R = (1 - f) \cdot U_I \qquad \ldots(2.4)$$

Therefore since $U_w = \frac{1}{2}(U_I + U_R)$ it can be shown that

$$U_w = \frac{2 - f}{f} \lambda \frac{\partial U}{\partial Y}$$

Similar arguements show that the temperature jump is given by $T_J = \frac{2 - \alpha}{\alpha} \lambda \frac{\partial T}{\partial Y}$. The slip velocity and temperature jump occur together and the important parameter is the enthalpy jump. Patterson[76] has considered this problem and related the temperature jump to the slip velocity through the expression

$$T_J = (T_{GW} - T_w)$$
$$= \frac{75\pi}{128} \lambda \left(\frac{\partial T}{\partial Y}\right) + \frac{U^2_{GW}}{4 C_p} \frac{\gamma}{\gamma - 1} \qquad \ldots(3.4)$$

Recent studies have attempted to represent the gas - surface interaction more realistically. Shen[77] has pointed out that the procedures of Patterson and others lead to difficulties if more than tangential momentum exchange and thermal accommodation coefficients are incorporated in the slip boundary conditions. Shen calculates the velocity slip and temperature jump to be used with the Navier - Stokes equations from the asymptotic behaviour of the Knudsen layer towards its outer edge. A linearized Boltzmann equation is used and the resulting simultaneous integral equations are solved using a variational principle. It was demonstrated that this procedure allows the coefficient for normal momentum exchange to be incorporated in

addition to the usual tangential and thermal accommodation coefficients. There have been many similar studies by Cercignani et al and recently[78] a new set of boundary conditions have been proposed for the Navier - Stokes equations. Another feature of gas - surface interactions which has been investigated is the dependence of the slip coefficients on the molecular model assumed for the calculations. Most work has been done using the Krook model but Loyalka and Ferziger[79][80] by extending Cercignani's method to the Knudsen layer but for the full linear Boltzmann equation, has shown that both the slip velocity and temperature jump are virtually independent of the model.

In spite of the large effort to understand gas - surface interactions there is very little information on the effect of such interactions on the growth of the shock layer over a flat plate. Pitot tube readings have been used to obtain an estimate of the slip velocity although these are not reliable. The density and surface pressure data presented in this work can be used to obtain a quite reliable estimate of the temperature jump. Care was taken to obtain reliable density measurements to within .25 mm of the surface and the value at the wall could be obtained by extrapolating the profile. Then the temperature of the gas at the wall can be calculated from the equation of state using

the measured surface pressure corrected for orifice effects. Due to the uncertainty in these corrections the temperature calculated in this way could be as much as 8% low for $T_w / T_o = .11$. However, this does not effect any of the qualitative conclusions discussed below.

The calculated values of T_{GW} are compared with the measured surface temperature in figures 35 and 36 where the error bars represent the experimental error only.

One of the most striking features of figure 35 is the rapid rise in T_{GW} over the first 50 mean free paths of the model which is a distance of 1.75 cm. A positive temperature jump, which would be expected for continuum flow and a stagnation temperature of 700° K, is not established until this distance downstream of the leading edge. Figure 36 reveals another interesting point, within 10 mean free paths of the leading edge the estimated temperature behind the shock is fortuitously equal to T_{GW}. This estimation is made using the approximate calculations discussed in Appendix II but should be accurate enough to show that the temperature gradient across the shock layer is small. Therefore neglecting the temperature gradient in equation (3.4) an estimate can be made of the slip velocity. A value of $U_{GW} / U_\infty = .32$ was obtained which for a $\bar{V}_\infty$ of .56 is in good agreement with

Becker and Boylan's[18] results. This is not a general way of obtaining slip velocity and it is fortuitous that $(\frac{\partial T}{\partial Y})$ across the shock layer is small for this particular case. The results presented and similar data at higher Reynolds numbers clearly show that the temperature gradient can be positive or negative depending on the value of T_w / T_o and M_∞.

The variation of T_{GW} for $T_w / T_o = .42$ suggests that continuum flow is not established over the first 40 - 50 free stream mean free paths. At the same time the flow is not free molecular since a disturbance has been detected upstream of the leading edge, figures 29 and 30, and the density at the leading edge is $1.3 \pm .05 \rho_\infty$. Therefore some of the molecules reflected off the surface must propogate upstream of the leading edge where they act as scattering centres for the oncoming free stream molecules. A 5% rise in density was detected approximately $3\lambda_\infty$ upstream of the leading edge from which it is deduced that the mean free path of the reflected molecules is of the same order as λ_∞. This behaviour suggests the idea of two effective mean free paths for this regime[34] as mentioned earlier in connection with the shock shape and thickness. The reflected, or body molecules, become collision dominated in a distance of several λ_b while the free stream molecules become collision dominated over a distance of several λ_f. With the same

approximations as Hamel and Cooper[34] for hard sphere molecules

$$\lambda_b \simeq \lambda_\infty \frac{\rho_\infty}{\rho_{LE}}$$

where ρ_{LE} is the density at the leading edge.

Further

$$\lambda_f \simeq S_\infty \lambda_b = .84\, M_\infty \lambda_b$$

Therefore $\lambda_f \simeq .65\, M_\infty \lambda_\infty$ Since $\frac{\rho}{\rho_{LE}} \simeq \frac{1}{1.3}$

In terms of more familiar aerodynamic quantities this becomes:-

$$\lambda_f \simeq \frac{M^2}{Re_\infty}$$

If the transition from the free stream to continuum flow is assumed to occur over $5\lambda_f$, the condition for continuum flow is $\frac{M^2}{Re_{x,\infty}} < .2$. This is based on the approximate value of λ_f at the leading edge which will not be the mean value for the near free molecular transition regime. λ_f will decrease as the slip velocity decreases but this will be counteracted to some extent by the decreasing density near the surface downstream of the leading edge. As the density near the surface, and hence the mean density in the shock layer, are dependent on the surface temperature the condition for continuum flow will vary with T_w / T_o. It is not possible to examine this dependence on T_w / T_o from the present data and the above condition is

therefore only approximately true.

It is interesting to note, from figure 35, that the condition for continuum flow ($M^2 / Re_{x,\infty} < .2$) is satisfied just upstream of the point where a positive temperature jump is first established. For the case shown $\frac{M^2}{Re_{x,\infty}} = .2$ corresponds to a point approximately $24\lambda_\infty$ downstream of the leading edge while the temperature jump becomes positive $40\lambda_\infty$ downstream. In this respect it should be noted that the values of T_{GW} could be a few percent low due to underestimating the corrections for orifice effects to the measured surface pressure.

4.4 Flow Field Model

4.4.1 Near Free Molecular Flow Regime

Prior to this study the flow field model most commonly used as a guide to theoretical work was that of Mc Croskey et al[17]. This conclusively demonstrated the merging of the shock wave and boundary layer and the associated departure from a Rankine - Hugonoit shock wave. However the upstream limit of the merged layer was not defined but several theoretical studies assumed the flow was free molecular at the leading edge. This was contrary to experimental values of surface pressure and heat transfer which were considerably above their free molecular

values. The present flow field studies show that there is no free molecular region at the leading edge. Instead there is a regime, which has been called near free molecular, which extends from just upstream to some distance downstream of the leading edge. This regime can be described in terms of two relevant mean free paths as proposed by Hamel and Cooper[34] in the abstract of their paper which is to be published. Those molecules which strike the surface and are then re-emitted, having lost part or all of their directed velocity, have a considerably shorter mean free path, λ_b, than the free stream molecules, λ_f. The ratio of λ_f to λ_b is approximately the speed ratio S_∞ so that for high Mach number flows the two mean free paths can be very different. It was demonstrated above that $\lambda_f \simeq \frac{M^2}{Re_\infty}$ and that the downstream limit for this near free molecular flow regime occurs approximately for $\frac{M^2}{Re_{x,\infty}} = .2$. Within this region the body molecules become collision dominated over a distance of a few λ_b.

The detailed experimental study of the near free molecular flow regime was carried out at a Mach number of 5.8 and Reynolds numbers of 160 and 130 per cm. From the several density profiles obtained, contours of constant density around the leading edge have been plotted, figures 29 and 30. These give a detailed macroscopic picture of this flow regime from which several

points have already been noted. In the first place the shock wave becomes thinner as the leading edge is approached and is approximately $3\lambda_\infty$ thick at the leading edge. The peak in the density profile moves closer to the surface as the leading edge is approached and occurs on the surface at the leading edge. From figure 29 and 30, it is concluded that this peak value of density is $1.3 \pm .05\rho_\infty$ and, in so far as the correlation presented in figure 33 is valid, is largely independent of the free stream conditions and surface temperature. In fact the density ratio $\frac{\rho_{max}}{\rho_\infty}$ does not increase much above $1.3 \pm .05$ over the first $10\lambda_\infty$ of the plate.

The most striking feature of both figure 29 and 30 is the disturbance extending for a few λ_∞ upstream over which there is a rapid rise in density as the leading edge is approached. The exact extent of this disturbance is difficult to define but there is a 5% increase in density $3\lambda_\infty$ upstream. It will be noted that the contours of constant density are slightly asymmetric with respect to upper surface of the model and that the peak in the density profiles ahead of the model occurs below the leading edge. This is obviously due to the higher pressure on the lower wedge surface of the model but it is not clear what part the wedge angle plays in determining the upstream disturbance. The present results are in agreement with Hickman's[24]

measurements upstream of a flat plate with a 10° wedge angle. However Joss et al[23] using 20° wedge angles found a 5 to 10% increase in density $5\,\lambda_{\infty}$ upstream. In addition this data shows a slight overcompression at the leading edge, and there appears to be a local flow field dominated by the nose of the model which is not observed in the present results. Further experiments will be needed to examine the influence of the wedge angle in more detail.

For the present experiments it is important that the lower wedge surface does not influence the flow over the upper surface of the model. All the tests performed to determine the affect of placing a drift tube close to the leading edge (Appendix II) yielded negative results. Although the drift tube was small this is a good indication that molecules reflected from the lower surface do not influence the flow over the upper surface for a 15° wedge angle. In addition Hickman performed tests with thin metal foil stretched across the flow. The upstream disturbance was similar to that for the flat plate with a 10° wedge angle. These tests are important since they show that the absence of free molecular flow at the leading edge and the upstream disturbance are not due only to lower wedge face of the model.

4.4.2 The merged Regime

Proceeding with the flow field development downstream of the near free molecular flow regime the first continuum regime is the merged layer. As shown above the upstream limit is given approximately by $M^2 / Re_{x,\infty} \simeq .2$ although it is not known how this condition depends on T_w / T_o. Mc Croskey et al defined the downstream limit as the point at which a distinct inviscid layer developes between the shock wave and the viscous layer adjacent to the plate. This was shown to occur for a value of the rarefaction parameter $\bar{V}_\infty$ between .15 and .2. While this definition is justified by the fact that the physical process occurring is the merging of the shock wave and viscous layer it is not obvious from flow field profiles when an inviscid region appears. Due to the varying shock strength over the forward part of the model the inviscid layer will be rotational and there will be an almost linear density gradient across it. Therefore the inviscid layer only appears as a change in the density gradient and for the present profiles merging appears to occur for $\bar{V}_\infty$ between .15 and .17. This is within the limits given by Mc Croskey et al and defines the downstream limit with sufficient accuracy.

There are several effects associated with merging some of which have already been noted. For $\bar{V}_\infty$ between .15 and .2 there

is a sudden increase in the ratio of the shock wave thickness to shock layer thickness which correlates well with $\bar{V}_\infty$ up to a value of 1. It was also noted from figure 34 that for a similar value of $\bar{V}_\infty$, corresponding to $\chi_\infty \triangleq 8$, the surface pressure dropped below the value predicted by 1st order weak interaction theory. There was no region of strong interaction for the present Mach 6 flows.

The most noticeable effect of merging is the decrease in the shock strength below the value predicted by the Rankine - Hugonoit shock relations for the free stream Mach number and measured shock angle. Figure 33 shows the shock strength plotted against $M C^* / Re_{x,\infty}$ for a wide range of conditions. This shows the remarkable result that this simple parameter, based mainly on free stream conditions, correlates the shock strength over most of the merged regime and the transition regime nearer the leading edge. The present experiment has shown that increasing T_w / T_o leads to a thicker shock layer and hence larger shock angles. In fact the shock shape over the merged regime can be correlated against $\frac{M}{Re_{x,w}} (\frac{T}{T_w})^{\frac{1}{2}}$ which is the same as $\frac{M^2}{Re_{x,\infty}} (\frac{T_w}{T_o})^{\frac{1}{2}}$. Therefore some similar dependence of the shock strength on the ratio (T_w / T_o) would be expected. From the data presented, which covers the range of T_w / T_o from .11 to 1, this is clearly not the case. The weak effect of the surface temperature can be

taken account of by the Chapman - Rubesin constant based on Eckert's reference temperature T^*. For the present results C^* only varies from .91 to .98 while Mc Croskey et al[17] used a value of .72 because of the higher stagnation temperature. Therefore it appears that the shock strength depends mainly on $M\,C^*\,/\,Re_{x,\infty}$, which can be interpreted as a Knudsen number λ_∞/X, and only weakly on the surface conditions.

Due to this apparently simple behaviour of the shock strength it is tempting to argue that the collision processes leading to the formation of the shock wave are largely uncoupled from the development of the viscous layer. This obviously cannot be the case since the shock wave exists because of the displacement effect of the viscous layer which in turn is influenced by the shock wave. It is therefore necessary to consider in detail the reasons for the reduction in shock strength as the leading edge is approached. Shorenstein and Probstein[29] have shown this is due to finite transport effects behind the shock which were of two forms. The most important resulted from the finite thickness of the shock. This led to a reduction in tangential velocity below the Rankine - Hugonoit value, by an amount proportional to the shear stress at the interface between the back of the shock and the viscous layer. In addition the temperature was reduced by an amount proportional to the heat

flux at the interface. The second but smaller form of transport effect is associated with the curvature of a finite thickness shock which leads to a lateral transport in mass, momentum and energy and hence alters the straight shock values of stress and heat flux. Slip velocity and temperature jump at the surface also cause futher modifications of the stresses at the interface between the shock and viscous layer. Therefore the shock strength must be closely coupled to the growth of the viscous layer.

The above discussion shows that the merged layer arises from the fact that the viscous effects extend from the surface to the shock wave, which only exists as a result of collisions between the free stream molecules and the slower moving molecules in the viscous layer. As the shock layer thickens the gradients in the outer part of the viscous layer become smaller until at the downstream end of the merged regime they are negligible. Then the effects of viscosity can be considered to be confined to a region adjacent to the surface, i.e. a boundary layer, and there will be no modification of the shock strength by transport effects at the downstream edge of the shock wave. At present the significance of the parameter $M C^{*} / Re_{x,\infty}$ to the development of the shock wave is not understood. The fact that $M / Re_{x,\infty} \sim \lambda_{\infty} / X$ suggests that λ_{∞} is important in the shock wave formation, as might be expected. However in view of the above discussion

and the fact that the correlation holds for more than $100\lambda_\infty$ downstream of the leading edge this interpretation should not be pressed too far.

4.5 Schematic Representation of Flow Field

The various flow regimes have been discussed in detail and can be used as a model to compare with theoretical studies of this problem. For this it will be helpful to refer to the diagramatic representation of the flow presented in figure 37, for $T_w / T_o = .42$. The inner edge of the shock wave is taken as the position of the peak in the density profiles while the outer edge is where the density is 5% above the free stream value. This avoids the difficulties arising at the leading edge from using any particular definition of the shock wave.

The initial disturbance to the free stream occurs upstream of the leading edge. This disturbance developes so that just downstream of the leading edge there is a thick shock wave with a small viscous region between it and the surface. Through this near free molecular regime the shock continues to thicken while the viscous layer is confined to a wedge like region close to the surface. The density profiles for this regime show a gradual rise to a peak value close to the surface and then a rapid decrease as the surface is approached. (For a cold wall

the results available suggest that this rapid decrease in density would not occur and the peak value in the density profile could coincide with the surface). The density gradient in the viscous layer is larger than those in the shock wave and it is possible that the Schlieren photographs of Nagamatsu et al[8] were detecting this gradient and not the shock wave.

Continuum flow is established a few λ_f downstream of the leading edge with the establishment of the merged layer. In this regime the shock strength increases steadily to its Rankine - Hugonoit value at the downstream limit and at the same time the shock wave becomes slightly thinner. The density profile shows the increasing gradients in the shock wave and the rapidly decreasing ratio of shock thickness to shock layer thickness.

Downstream of the merged layer the density profiles show a distinct invicid layer between the shock wave and boundary layer. The density rise through the shock wave is now very rapid and obeys the Rankine - Hugonoit shock relations. For the present M = 6 flows this region has been shown to be a weak interaction regime.

4.6 Comparison of Recent Theoretical Studies with the Flow Field Model

The most significant point to emerge from this experimental

study is the existence of a near free molecular regime extending a few dynamic mean free paths from the leading edge. At high Mach numbers this regime covers a distance $O(100\lambda_\infty)$ and continuum flow is only established for $\frac{M^2}{Re_{x,\infty}} < .2$. Therefore theoretical studies based on the Navier - Stokes equations will only be valid downstream of this and the Boltzmann equation, or some approximation to it, must be used for the near free molecular flow regime.

Four recent theoretical studies typical of the different approaches to this problem are now discussed in terms of this experimental flow field model.

4.6.1 Shock Wave and Viscous Layer Considered Separately

The most recent example of this type of approach is that of Shorenstein and Probstein[29] which has developed from several earlier studies by Oguchi[14][15][28] and Pan and Probstein[16]. The Navier - Stokes equations are used and the assumption of local similarity of the viscous layer is made. As in conventional boundary layer theory the normal pressure gradients is neglected as small but this was based on an estimate by Oguchi[28] for a highly cooled wall. Unfortunately, Crude estimates for the static pressure behind the shock wave, using the approximate calculation procedure of Appendix II, did not support this

assumption, even for the limitation of a cold wall.

Shorenstein and Probstein obtained solutions for the shock wave and viscous layer separately. Then for the zero order solution, the values and normal gradients of the velocity and state variables behind the shock wave were matched to the corresponding viscous layer quantities at the interface between them. Modifications were applied to the jump conditions across the shock for the finite transport effects behind the shock which were discussed in connection with the flow field model. First order corrections were then applied for the effects of shock curvature and velocity slip at the surface. These caused appreciable reductions in the shock strength, surface pressures, skin friction and heat transfer.

One result of this study was a series of correlation formulae which could be expressed in terms of a parameter $\beta = M_\infty^2 C_\infty / Re_{x,\infty} \cdot \sqrt{T_w / T_o}$. As $M_\infty^2 / Re_{\infty,}$ is essentially a dynamic mean free path the formulae for shock shape and shock strength were stated to be valid for $\beta < 1$, i.e. to within one dynamic mean free path of the leading edge.

In figure 28 the predicted shock shape is compared with numerous experimental data most of which are for a cold wall. As far as the scatter in these data allows, the predicted values

of Y_p / X are approximately 25% low. Of greater interest is the comparison of the shock strength, calculated for the experimental conditions of Mc Croskey et al[17], with the experimental results presented in figure 33. The good agreement for values of $M C^* / Re_{x,\infty} < .01$ is encouraging and therefore the present Mach six data is compared with the correlation formula in figure 38. At the downstream limit of the merged regime the Rankine - Hugonoit value of the shock strength is strongly dependent on the Mach number. The parameter C_ρ is independent of the Mach number at this limit allowing a better comparison between the present Mach 6 data and the calculations of Shorenstein and Probstein. For $T_w / T_o = .11$ there is good agreement for values of $\beta < .07$ which corresponds to $M^2 / Re_{x,\infty} < .23$ in reasonable agreemont with the condition for continuum flow. Therefore this approach, in which the transport effects behind the shock wave are allowed for can give an accurate description of the flow in the merged regime for $T_w / T_o << 1$. However, for a cold wall the condition for continuum flow is $\beta < O(.1)$ and not $O(1)$ as suggested by Shorenstein and Probstein. For $1. < \beta < 1$ the assumption of continuum flow breaks down and the correlation formula is not valid. As might be expected for $T_w / T_o = .42$ the measured shock strengths are higher than predicted and the assumptions leading to the neglect of the normal pressure gradient in the viscous layer

should be re-examined.

4.6.2 Solution to Equations valid for the whole Shock Layer

The other theoretical studies considered here can be grouped under this heading. The first is based on the Navier - Stokes equations and is therefore only valid for continuum flow while the remaining two are based on the Boltzmann equation.

(a) Uniformly Valid Expansion of the Navier Stokes Equation

The study by Rudman and Rubin[31] is taken as an example of this technique although Laurmann[30] and Garvine[32] have made similar studies. Rudman and Rubin[31] made no assumptions concerning the existence of a merged shock or boundary layer but assumed only that the disturbed region was relatively thin. In order to estimate the magnitude of the various terms in the governing Navier - Stokes equations all the variables were nondimensionalised with respect to local reference conditions. Linear expansions of these variables in terms of a small parameter ϵ, were assumed to be valid. By retaining only the important terms for various regions of the flow, a set of equations was obtained which was valid throughout the continuum flow field. This approach has obvious advantages over the method of matching solutions discussed above.

Rudman and Rubin[31] used a finite difference scheme to solve these equations and therefore initial conditions are required at the upstream limit of the continuum flow regime. The difficulties of applying these conditions has been commented on by Garvine[32] but these have largely been ignored by Rudman and Rubin. They noted that the characteristic length in the flow direction was approximately M_∞ times that for the direction normal to the flow. This implies that a dynamic mean free path is important in the flow direction, and yet the flow is assumed to be continuum to within a few static mean free paths of the leading edge. They then proceed to specify the initial conditions for their finite difference scheme at the leading edge. Clearly these initial conditions will not be valid for the modified Navier-Stokes equations as the experimental flow field model shows that continuum flow is not established until a few dynamic mean free paths downstream of the leading edge.

The predicted shock strength for M = 25 is shown in figure 33. While the actual values are high the variation in shock strength follows the experimental data. It is also noted that the experimental data do not show any appreciable rise in shock strength over the first $10\lambda_\infty$ of the plate. This suggests that the high values of the predicted shock strength are due to the incorrect assumption that continuum flow is established within

a few static mean free paths of the leading edge which causes too rapid a rise in the shock strength.

It has also been observed that this theory predicts a shock layer growth such that Y_p / X is virtually constant and equal to .7, which does not agree with any experimental data. Finally a compression wave was predicted inside the merged layer but there is no evidence of this from the density profiles at $M = 6$.

This approach to the problem by Rudman and Rubin[31] is attractive in that no assumptions are made about a shock wave or viscous layer. It predicts a large pressure gradient across the shock layer close to the leading edge which was ignored by Shorenstein and Probstein[29]. However, an accurate description of the flow field will not be obtained until the correct initial conditions can be applied.

(b) Discrete Ordinate Solutions to the BGK Approximation of the Boltzmann Equation

Recently Huang and Hwang[33B] have used a discrete ordinate method to obtain solutions to the B.G.K. approximation of the Boltzmann Equation. The study covered flow at Mach 5 and 10 and was an extension of an earlier paper by Huang and Hartley[33A]

for M = 1.5. This earlier study showed density profiles which were in good qualatative agreement with the present experimental results at Mach 6. Quantative agreement was poor and this was thought to be due to the low Mach number but the Mach 5 and 10 results show even less agreement. The shock strength shows no agreement with experiment, figure 33, and the shock layer thickness Y_p is only 15 - 20 λ_∞ at a position of 700 λ_∞ from the leading edge.

All the boundary conditions and initial conditions used were reasonable and it must therefore be concluded that this particular discrete ordinate method is not suitable for studying the near free molecular flow regime.

(c) Monte Carlo Direct Simulation Technique

A monte carlo technique which generates solutions to the Boltzmann equation has recently been used by Vogenitz et al[81] to study the flow near the leading edge of a sharp flat plate. The technique consists of following, by digital computation, the motion of a representative set of molecules flowing past the body while collisions are computed by statistical sampling. Flow field properties and conditions at the surface are given for a monatomic gas using several different molecular models.

Particularly interesting are the computed density profiles for hot and cold walls which are compare with the experimental profiles in figure 39. There is good agreement on general shape even to the extent of predicting a sharp increase in density within a few mean free paths of the wall for the cold wall case. The difference in the magnitude of ρ/ρ_∞ are due partly to difference in X but mainly to differences in T_w / T_o and a more direct comparison would show better agreement. The shock strength, figure 33, is in excellent agreement with all the experimental data. Difficulties were found in trying to compare the shock shape with the experimental values of Y_p / X. For $T_w \simeq T_o$ there was reasonable agreement while for $T_w = .08\ T_o$ the Y_p / X appears to decrease as the leading edge is approached. However it is difficult to take values off the very small graphs presented and therefore this data is not plotted on figure 28.

This good agreement between the theory and that experimental data from the present experiments as published in reference 74 has already been discussed by Vogenitz et al. Since publishing these results the flow around the leading edge has been studied in detail. The disturbance upstream of the leading edge is also predicted and it is shown that a normal leading edge of thickness t could influence the flow over a length l of the plate, given by $l = O(2M \cdot t)$. Calculations have also shown

that for a given wedge angle an edge thickness is reached below which reflections from the lower surface overshadow the reflection of molecules from the leading edge. This could explain the differences noted between the results of Joss et al, for a 20° wedge angle, and the present results for a 15° wedge angle.

Vogenitz et al also discuss the influence of the gas - surface interaction law and the effect of finite plate lengths and demonstrates that this is a very satisfactory approach to rarefied gas flow problems.

In the summary of this discussion of theoretical studies the Monte Carlo solution of Vogenitz et al[76] is complementary to that of Shorenstein and Probstein[29]. The two together give quite an accurate description of the near free molecular and merged regimes for a cold wall. In contrast the two methods which use finite difference techniques lead to unexpected discrepancies particularly that of Huang and Hwang[33B] which should be re-examined to see if the procedure used is valid.

CONCLUSIONS

The extensive measurements presented here establish the electron beam fluorescence technique as a means of making local density measurements with a high degree of accuracy. Measurements can be made throughout the flow field even close to the surface and the leading edge of the model without appreciably disturbing the flow. It should be noted that to obtain reliable measurements to within .25 mm of the surface it is necessary to eliminate the flow through the drift tube as described in Chapter 3.

Quenching of the fluorescence was shown to be appreciable above a density of 7×10^{-7} grams/cm^3 and decreased with decreasing temperature. The quenching cross section appeared to vary with temperature in a similar way to the conventional collision cross section for viscosity, but the experiments were not conclusive in this respect.

The most important contribution to the study of viscous interaction on flat plates is the new flow field model. This differs significantly from the earlier model of Mc Croskey et al and describes in more detail the flow around the leading edge. The data obtained close to the leading edge could be explained in terms of two effective mean free paths as proposed by Hamel and Cooper. These are the mean free path for the

collision of an emitted or body molecule with a free stream molecule, λ_b, and the mean free path for the collision of a free stream molecule with a body molecule, λ_f. $\lambda_f \sim \lambda_b S_\infty$ and can be regarded as a dynamic mean free path. Continuum flow is established several λ_f downstream of the leading edge but over this distance the body molecules become collision dominated over a distance of a few λ_b. This regime is therefore termed near free molecular and its downstream limit is given approximately by $M^2 / Re_{x,\infty} = .2$.

The upstream limit of the near free molecular regime is the first detectable disturbance to the free stream flow which occurs a few free stream mean free paths upstream of the leading edge. It is not known how the wedge angle of the model influences this upstream disturbance but for the present 15^o wedge angle, the density $3\lambda_\infty$ upstream of the leading edge is 5% above the free stream value.

The condition for continuum flow is given approximately by $M^2 / Re_{x,\infty} \leq .2$ which determines the upstream limit of the merged layer. In agreement with Mc Croskey et al the downstream limit for the present data is given by $\bar{V}_\infty = .15$ to $.17$. Finally at Mach 6 the flow is shown to proceed directly from a merged to a weak interaction regime.

The general features of the shock layer such as shock shape, thickness and strength can be correlated reasonably well. If the maximum slope definition of the shock wave is used the shock shape for all the Mach 6 data correlates well against $M_\infty / Re_{x,\infty} (T_w / T_o)^{\frac{1}{2}}$ for values of this parameter up to .1. This correlation does not appear to hold over a wide range of Mach numbers although there is a large amount of scatter in the available data. The effect of increasing the surface temperature is to increase the shock layer thickness and shock angle.

In agreement with earlier investigations the ratio of shock thickness to shock layer thickness for the present data increases markedly as the shock wave and boundary layer merge. This ratio correlates well with $\bar{V}_\infty$ for values of this parameter up to 1. For larger values the correlation breaks down and for a given $\bar{V}_\infty$ there appears to be a dependence on the Mach number.

Over both the merged and near free molecular regimes the shock strength correlates against $M_\infty C^* / Re_{x,\infty}$ for a wide range of M_∞ and $Re_{x,\infty}$. It is largely independent of the wall temperature in spite of the dependence of the shock shape on $(T_w / T_o)^{\frac{1}{2}}$.

The temperature jump, within a few dynamic mean free paths of the leading edge, can be positive or negative depending on

the value of T_w / T_o.

Comparing the present data and flow model with recent theoretical studies reveals a number of discrepancies. However, for the near free molecular regime the numerical calculations of Vogenitz et al[8] are in close agreement with the present experimental results. Provided $T_w << T_o$, the results of Shorenstein and Probstein[29] for the merged regime show reasonable agreement with experimental data for Mach numbers between 6 and 25. This approach is not valid for higher wall temperatures but the data provided here will provide a reliable basis for further studies of the merged layer.

The flow over flat plates at high speeds and low Reynolds numbers can now be described with some accuracy. However the results presented here reveal a number of problems needing further investigation. One is the effect of the model wedge angle on the disturbance upstream of the leading edge. It has also been shown that the effect of the trailing edge can extend a considerable distance upstream. Several investigations have noted the reduction in surface pressure associated with the trailing edge effect but there is still need for quantitative flow field measurements to show how the disturbance propagates upstream through the boundary layer. These two experiments would be a logical extension of the present work for which the electron beam probe is well suited.

APPENDIX I

Calibration of Nozzles

The nozzles used for the experiment which were built at the N.P.L., were contoured to give a nominal Mach 6 flow. They were electroformed from copper with an inner and outer wall to allow liquid nitrogen to be circulated through them. Cooling the nozzle walls with liquid nitrogen greatly reduces the boundary layer thickness and increases the isentropic core size. Consequently the Mach number was very sensitive to the degree of cooling and varied by as much as 2% from one run to the next.

In view of these variations in the free stream conditions it was not possible to perform a single calibration of the nozzle in terms of the stagnation conditions. However, pitot traverses were performed to establish the isentropic core size and the Mach number gradients in the flow. Lateral traverses were made at several axial stations and a detailed traverse along the axis of the nozzle was extended as far upstream as possible to confirm that there were no shock waves in the nozzle flow.

Two nozzles were used in the experiments since the original one was too small to study the transition from the merged to the weak interaction regime. Table AI.1 summarises the flow conditions acheivable in each nozzle. The Reynolds number could be

increased by increasing the stagnation pressure but at the same time the test chamber pressure becomes greater than the free stream static pressure. At the higher stagnation pressures an oblique shock wave is therefore produced at the edge of the nozzle the strength of which depends on the pressure recovery needed. Sufficient traverses were performed to determine the position of this shock wave so that the model could be positioned to avoid it. It was also established that the free stream conditions were not sensitive to the tank pressure, that is they were not affected by the strength of this oblique shock.

Only typical results are presented here in figure AI.1 which shows the core size and lateral Mach number gradients at the exit plane of the larger nozzle. Similar traverses for the smaller nozzle show that the core varies from 4 cm to 6 cm diameter for the range of stagnation pressures, 40 - 120 mm Hg. The axial Mach number gradients, without the model in the flow, were .003 per cm for a stagnation pressure of 40 mm Hg increasing to .008 per cm for a stagnation pressure of 120 mm Hg. The corresponding lateral gradients were .01 and .04 per cm.

Flow Angularity

When discussing the measurements made with the small nozzle it was suggested that the blockage effect of the model was

causing the flow off the axis of the nozzle to be inclined slightly to the axis. The effect of this on the flat plate studies would be to effectively reduce the shock wave angle by approximately the same amount as the flow angularity. As the shock wave angle was small, 15^{o} approximately, small changes in shock angle cause considerable changes in shock strength making it difficult to determine the transition from the merged to the weak interaction regime. Therefore this part of the study was carried out in the larger nozzle where the blockage effect should be smaller.

A simple yaw meter was constructed by mounting three tubes one above the other as shown in figure AI.2. The middle one was connected to a thermistor gauge[72] to measure the pitot pressure. The ends of the outer two were cut at 45^{o} while their free ends were connected to a differential pressure transducer.

This meter was calibrated by yawing it about the axis of the nozzle while recording the output of the pressure transducer. The yaw meter was then inverted and another calibration performed confirming, as shown in figure AI.2, that the tubes are symmetrical. The zero error of $.3^{o}$ was due to a zero error in setting up the incidence gear used for the calibration. A sensitivity of better than 1 mv per degree was obtained so that difference of $.1^{o}$ could be measured with ease.

As it is known that the model can influence the nozzle flow yaw meter traverses were performed with the model in place. A series of axial and lateral traverses were made in the flow approaching the shock layer on the model. There was a slight ambiguity in interpreting the results since the yaw meter also responds to the lateral gradients in the flow. However, it could be concluded that the flow angularity was at the most $.24^{\circ}$ which would cause only a 2 or 3% reduction in shock strength.

APPENDIX II

Probe Interference

The Interaction of an Electron Beam Probe with the Flow

In practice no measurement can be made without disturbing in some way the system on which the measurement is performed. Therefore in interpreting experimental data some consideration must be given to the interaction of the probe with the system. This is particularly so in rarefied gas flows and mention has already been made of the uncertainties in pitot tube and hot wire measurements. However an electron beam probe offers a way of making local measurements in rarefied flows without appreciably disturbing the flow. This is due to the fact that in an elastic collision which scatters the electron through an angle θ only a fraction of the energy is transfered to the molecules, given by

$$2 (1 - \cos \theta) \, m/M$$

As the collision cross section is only appreciable for small θ and the ratio of the mass of the electron to that of the molecule is small the energy transfered is small even for 100 KeV electrons. For an elastic collision with a nitrogen molecule there is no significant change in the velocity or direction of the molecule so the flow will not be disturbed to any great extent.

There are several inelastic collisions which could occur between an electron and a nitrogen molecule. Muntz[1] has discussed these and the most important is the excitation of the $N_2^+ B^2\Sigma$ states which are 18.3 eV above the ground state. During this excitation the molecules are ionized and the secondary electrons emitted have energies ranging from zero to a few hundred electron volts. If a large proportion of the molecules in the vacinity of the beam were ionized in this way, the flow field would be appreciably altered. However an example shows that this is not the case. In a typical situation the beam current might be 1 mA and the beam diameter 1 mm. If the density of the gas is 5×10^{-7} grams per cm^3 then, making reasonable assumptions about the collision cross sections, it can be shown that in the order of 10^{-5} of the molecules in the vicinity of the beam collide with an electron. Further this excitation of the molecules is confined to the relatively small area traversed by the beam. Therefore the passage of the beam through the gas should not appreciably disturb the flow.

The Affect of the Drift Tube

The possible arrangement of the electron beam for studying the growth of the shock layer over the flat plate model has been discussed in Chapter 3. It is convenient to fire the

electrons through a hole in the model so that the beam is perpendicular to the surface of the model. However since the flat plate model is a wedge with one face parallel to the flow the pressure on the underside of the model will be greater than that on the upper surface. Therefore some gas must flow through this hole and disturb the shock layer. The alternative arrangement is to insert a small tube, referred to as a 'drift' tube, between the model and the electron gun, figure A2.1. In this situation the pressure on the upper surface of the model is considerably greater than the pressure in the electron gun so that some gas must flow down the drift tube into the gun. In addition if the drift tube is placed near the leading edge of the model it could influence the flow over the upper surface.

To determine the magnitude of these various effects preliminary experiments were performed with simple uncooled copper flat plates and wedges. The wedge angle on all models was 15° and a series of 1 mm diameter holes was drilled through them at intervals along their centre lines. During a test all but one of these holes was sealed off and the electron beam was aimed through the remaining one as in figure A2.1. The procedure for aligning the model, electron beam and optics is dealt with in Chapter 3.

These initial tests were performed at a Mach number of

6.41 and a Reynolds number of 410 per cm. Density profiles through the shock layer were obtained for several different axial stations on each model by moving it so that different holes were aligned with the beam. At each station measurements were performed with and without the drift tube in place. Typical profiles for the flat plate and wedge are shown in figures A2.2 and A2.3 respectively. The flat plate profiles show that without the drift tube there is a sharp increase in density as the surface of the model is approached which is not observed when the drift tube is in place. Further the shock strength is higher for the case in which the drift tube is missing and it did not decrease in the way expected as the leading edge was approached, figure A2.4. These results clearly show that without the drift tube the gas flowing through the hole in the model from the underside seriously disturbs the shock layer, particularly near the leading edge. In the case of the wedge the pressure on the upper and lower surfaces is the same provided the model is at zero incidence. Therefore there would be no flow through the hole in the model so that the density profile obtained without the drift tube should be reliable. When the drift tube was used the profile obtained, figure A2.3, showed that the density near the surface was lowered by about 10%. Obviously the flow of gas into the drift tube is sufficient to appreciably

disturb the shock layer.

These preliminary results showed that the flow of gas either way through the hole in the model must be carefully avoided if reliable results are required close to the surface of the model. To do this the drift tube was re-designed as shown in figure 13. The tube was divided into two parts by a small cavity to which nitrogen could be supplied at a controlled rate. A pressure sensing thermistor[72], calibrated against a McLeod gauge, was used to monitor the pressure in this cavity and by adjusting the rate at which nitrogen was supplied the pressure in the cavity could be maintained equal to that on the surface of the model. Thus any flow through the hole in the model surface was completely eliminated.

To determine how sensitive the flow was to gas injected into or removed from the bottom of the shock layer density profiles were obtained .62 cm from the leading edge for different pressures in the drift tube cavity. Figure A2.5 shows two extreme cases from which it is concluded that injecting gas into the bottom of the shock layer has a far more pronounced effect than the loss of gas down the drift tube. However if accurate results are required close to the surface the pressure in the drift tube cavity must be maintained equal to that on the surface of the model to within $\pm$ 10%. This pressure balancing was used

in all further measurements and the results are thought to be reliable to within .025 cm of the surface.

As it is essential to use the drift tube for accurate work extensive tests were performed to see if the tube fixed to the underside of the model influenced the flow over the upper surface. The foremost station at which measurements were made was .175 cm from the leading edge when the front of the drift tube was only .11 cm from this edge. Three different types of measurements were made, each with and without the drift tube in this foremost position. Initially pitot traverses were made through the shock layer when the results shown in figure A2.6 were obtained. A thermistor gauge[72] was used to measure the pitot pressure which limited the accuracy of the measurements at the highest pressures. For the conditions of the test, $M = 6.41$ and $Re/cm = 410$, this pressure was approximately 3 mm Hg. At these pressure levels the thermistor is not very sensitive to pressure limiting the reproducability to $\pm$ 3%. Within this accuracy no influence of the drift tube could be detected.

The other tests were carried out under the more rarefied conditions acheivable with the larger nozzle, see Table A1.1. The free stream mean free path was as large as .62 mm so that the foremost measuring station was approximately 3, free stream,

mean free paths from the leading edge. For these conditions the surface pressure was measured to within .313 mm of the leading edge. To do this hypodermic tubes were pushed into the holes in the model through which the beam normally passed and sealed with araldite. These tubes were connected to a bank of thermistor gauges[72] and the surface pressure recorded with and without a drift tube opposite the foremost hole in the model. Within the experimental scatter of the data, $\pm$ .5 Hg, there was very little difference in the two sets of measurements, figure A2.7.

Finally a much more conclusive test was devised. In investigating the flow field around the leading edge of the model it was found that there was an appreciable disturbance as far as 5 mean free paths upstream of the leading edge. Further by correct masking of the optics it was possible to determine the density profile across the leading edge approximately one mean free path upstream of the leading edge. This was done with and without a dummy drift tube opposite the foremost hole in the model. As can be seen from figure A2.8 the density profile below the leading edge is considerably affected by the dummy drift tube but there is no detectable change in the profile above the leading edge.

These three tests conclusively show that the technique can be used to within .175 cm of the leading edge without causing any appreciable disturbance to the flow over the top surface of the model.

The Interaction of a Small Pitot Probe with the Flow

Pitot probes have been used extensively in aerodynamics to measure impact pressures. In subsonic flow such a probe measures the stagnation pressure while for supersonic flow a normal shock is produced in front of the probe and the probe records the stagnation pressure behind this shock. In either case if the static pressure is known the Mach number can be calculated. However if the density is reduced to the extent that the Reynolds number based on probe diameter becomes small, of the order of 100, then viscous effects modify the pressure recorded by the pitot tube. For open ended tubes, as the Reynolds number based on probe diameter is reduced, the measured pressure initially drops below the ideal pitot pressure and then rapidly increases[82]. Many investigations[82] have shown that for uniform flow this variation with Reynolds number is well correlated by $Re_{2D}\ (\rho_2/\rho_\infty)^{\frac{1}{2}}$ where D is the external diameter of the probe.

For boundary layer measurements it is usually necessary

to use a small probe diameter to obtain good spatial resolution and minimise the disturbance to the shock layer. If quantative data are required in such a situation there are two problems to be overcome. In the first instance, for a shock layer the viscous effects will not be the same as for a uniform flow due to the shear produced in the layer. Therefore, although a small pitot tube could be calibrated against a larger tube in a uniform flow, the correlation against $Re_{2D}\ (\rho_2/\rho_\infty)^{\frac{1}{2}}$ would not be valid for the shock layer. The second problem is the disturbance to the shock layer caused by the presence of the probe. This would be expected to be appreciable near the surface of the model or close to the leading edge where the probe dimensions are comparable to the shock layer thickness. It is necessary to determine the conditions under which such affects are important before attempting to use pitot tube data in shock layer calculations. Such calculations would involve an iterative technique making use of pitot tube, electron beam and possibly hot wire measurements in a similar manner to McCrosky[73]. While this thesis contains insufficient data to carry out these calculations, tests were performed to determine the conditions under which reliable results could be obtained.

A small pitot tube was traversed through the shock layer while monitoring the surface pressure. The tube consisted of

a flattened hypodermic tube .75 mm high by 1 mm wide and the surface pressure was measured using the bank of thermistor gauges. For each axial traverse the pressure was monitored at an axial station directly beneath the tip of the pitot tube and at several stations upstream. The measured impact pressures are shown in figure A2.9. from which qualatative conclusions can immediately be drawn. As the leading edge is approached the shock strength decreases and the ratio of shock wave thickness to shock layer thickness increases as observed by several investigators. In figures A2.10 and A2.11 the surface pressure at each axial station is given as a function of the height of the pitot tube above the surface of the model. For the traverse 1.91 cm from the leading edge, figure A2.10 as the pitot tube moved into the shock layer the surface pressure directly beneath it steadily increased. However upstream of the pitot tube there is no change in the surface pressure until the tube is close to the surface when a small increase in pressure was recorded. In contrast for the traverse near the leading edge, figure A2.11, there was an increase in surface pressure both directly beneath the tube and upstream of it as the tube moved into the shock layer.

These curves indicate that when the probe is small compared with the shock layer thickness there is no appreciable disturbance

upstream of the probe until the tube is close to the surface as expected. Therefore the measured impact pressure should not be affected to any great extent by the disturbance caused by the probe in the flow except near the surface. However, when the probe size is comparable to the shock layer thickness the present results suggest that the whole flow field is significantly altered. This is in spite of the fact that the flow field is supersonic throughout close to the leading edge.

At the present time there is no way of estimating the magnitude of the error in the measured impact pressure due to the affect of the probe on the flow. In addition corrections for viscous effects in a shear layer are uncertain but sufficiently far from the leading edge a pitot tube reading might be reliable in the outer parts of the shock layer. Some evidence supporting this can be obtained by using the density ratio across the shock wave and the shock angle determined from electron beam measurements to calculate the pitot pressure behind the shock wave. For the merged regime the term shock wave should not strictly be used but it is used here to denote the region over which the density or pitot pressure rises to a maximum as the shock layer is entered. The value of density or pitot pressure behind the shock is taken to be this maximum value. To calculate the pitot pressure it is necessary

to make several approximations which limit the reliability of the calculations. One of the more serious approximations is that the tangential velocity is assumed to be unchanged on crossing the shock. For the merged layer where the shock is thick there will, in practice, be some reduction in the tangential velocity so that the calculated velocity and local Mach number behind the shock will be high. Transport effects behind the shock have also been neglected although Garvine[83] has shown that they considerably reduce the shock strength. Therefore this assumption might lead to high calculated pitot pressures. Finally the shock curvature has been neglected but measurements have shown that it is small, except near the leading edge, and this error is unlikely to be serious.

Another problem encountered near the leading edge was that the shock angle was difficult to define and depended on the definition used to infer the mean shock position from the density profiles. In the present case the point of maximum slope in the profiles has been used.

Following McCrosky et al[17] the equations of continuity and normal momentum can be combined to give the static pressure behind the shock.

$$P_s = P_\infty + \rho_\infty U_\infty^2 \sin^2 \theta_s \, (1 - \rho_\infty/\rho_s)$$

In addition the equation of state gives the temperature while the continuity equation can be used to calculate the component of normal velocity behind the shock. Assuming that tangential velocity is unchanged across the shock the velocity and hence the Mach number behind the shock can be calculated. To obtain the stagnation pressure behind the shock the total temperature is assumed to be constant, i.e. transport effects behind the shock are neglected. Then

$$\frac{P_{o_s}}{P_{o_\infty}} = \frac{\rho_s}{\rho_\infty}\left(\frac{T}{T_s}\right)^{\frac{1}{\gamma-1}}$$

In the present case $\gamma = 1.4$ so the temperature ratio is raised to the power 2.5. As T_s depends on the measured values of and $\sin^2\theta_s$ the calculated stagnation pressure will be very sensitive to errors in these quantities. Finally the pitot pressure is calculated assuming a normal Rankine-Hugonoit shock is formed in front of the pitot tube. Using this procedure P_{o_s} is probably too high due to the assumption of adiabatic conditions across the shock. However this error is offset by the calculated local Mach number being high which leads to a lower calculated pitot pressure. Obviously a more exact analysis of the various assumptions is necessary before this calculation procedure can be considered as reliable and the values presented here are only regarded as estimates.

The procedure given above has been used to calculate the pitot pressure behind the shock for a wide range of $M_{\infty}/Re_{x,\infty}$. Figure A2.12 shows these values compared with the measured pitot pressure ratio across the shock wave. Corrections to the measurements for viscous effects were calculated using the data published by Schaaf[78] assuming that the correlation with $Re_{2D}(\frac{\rho_2}{\rho_\infty})^{\frac{1}{2}}$ was also valid in the shock layer. The dimensions of the probes were such that the measured values were 2 to 3% low and the corrections for the free stream were similar to those behind the shock wave. Therefore the actual measured ratios have been plotted.

For values of $M_{\infty}/Re_{x,\infty} < .03$ the calculated values are 4% low but the differences increase rapidly for larger $M_{\infty}/Re_{x,\infty}$. This is almost certainly due to the break down of the assumptions in the calculation, in particular shock curvature would be appreciable close to the leading edge. However, while this good agreement could be the result of cancelling errors, it does support the earlier suggestion that a pitot tube gives reliable readings in the outer part of the shock layer sufficiently far from the leading edge. Therefore in this region an interative technique to correct the pitot pressures for the effects of viscosity and shear could yield accurate quantitative results.

APPENDIX III

The Affect of Secondary Electrons on Rotational Temperature Measurements

The electron beam fluorescence technique is now well established as a means of making local density measurements in rarefied flows. In addition, if the spectrum excited by the beam has a rotational fine structure it is theoretically possible to determine the rotational temperature of the gas. Such measurements have been limited to air or nitrogen where it is necessary to measure the relative intensity of the rotational lines in one of the bands of the first negative system of nitrogen. The relative intensities of the lines are proportional to the relative populations of the $B^2\Sigma_u^+$ states of the molecular ion which give rise to the first negative system. The rotational distribution of the unexcited molecules is calculated from this population distribution for the excited ions by using a mathematical model to predict the rotational changes caused by a fast electron colliding with a ground state molecule. Provided the gas is in rotational equilibrium this distribution can be used to define a rotational temperature which in many flows is virtually equal to the translational temperature.

In practice considerable difficulties have been encountered and it has not been possible to make reliable measurements of rotational temperature. The approach most commonly used is that of Muntz[1] but as discussed in Chapter I there are considerable discrepancies between the calculated and true rotational temperature. Smith[57] has shown that excitation by secondary electrons could be responsible while Maquire[58] suggests that preferential quenching of the more highly populated states is important. The present study extends Muntz's theory to include the effect of secondary electrons and shows that the proposed model gives the correct temperature over a wide range of densities.

Muntz's Theory

The accuracy with which the rotational temperature can be determined depends on the accuracy of the theoretical description of the excitation and emission process as well as the accuracy of the line intensity measurements. When a beam of moderate energy electrons is passed through low density nitrogen the most prominent fluorescence is from the first negative system of N_2^+. This arises from transitions between the $B^2\Sigma_u^+$ states and the ground molecular ion states $X^2\Sigma_g^+$. Muntz approached the problem by considering the possible ways in which the $B^2\Sigma_u^+$ states

could be excited and then used order of magnitude arguements to eliminate those which were negligible.

Cascade Population of $N_2^+ B^2\Sigma$

The population of the $B^2\Sigma$ states by transition from higher levels of N_2^+ would be accompanied by an emission comparable in intensity to that of the the first negative system. No such emission has been observed. In addition the two electronic states of N_2^+ other than $B^2\Sigma$ which have been identified combine only with the ground state $N_2^+ X^1\Sigma$. Therefore cascade population of the $B^2\Sigma$ states is unlikely.

Double Excitation to $N_2^+ B^2\Sigma$

It is possible that a primary electron would excite a ground state molecule to some electronic state of N_2 or N_2^+ and that this state is excited by a second electron to the N_2 $B^2\Sigma$ state. Muntz stated that the most likely mode of double excitation is the excitation of ground state ions to the N_2 $B^2\Sigma$ states. He then used an order of magnitude analysis to show that this process would be between 4×10^{-2} to 4×10^{-5} times as effective as the direct excitation of the N_2 $B^2\Sigma$ states from the ground state molecules.

Excitation by Secondary Electrons

Muntz was unable to give conclusive arguements for the excitation of the N_2^+ $B^2\Sigma$ states by secondary electrons. These secondaries will be produced with an energy distribution from zero to a few hundred electron volts. Those with energies below 3.1 eV cannot produce any excitation. Those with energies greater than 3.1 eV can excite the ground state ions while those with energies greater than 18.7 eV can excite ground state molecules directly to the N_2^+ $B^2\Sigma$ states. Muntz estimated that excitation of the ground state ions could be neglected. However the secondary electrons with energies greater than 18.7 eV would be expected to play a part in exciting the first negative system. The total ionisation cross-section of nitrogen molecules by electrons is a maximum for 100 eV electrons and is 2.87×10^{-16} cm^2. This is approximately an order of magnitude greater than the cross section for 17.5 KeV electrons. Muntz concluded that there are either few secondary electrons with energies greater than 18.7 eV, or that there are a number of such secondaries but the excitation caused by them is similar to the excitation caused by the primary electrons. It is this conclusion which is the weakest point in Muntz's arguements. The relatively slow secondary electrons will not necessarily obey the same laws as the fast primary electrons when exciting the N_2^+ $B^2\Sigma$ states.

The Emission Process

The mean life time of the states giving rise to the 0-0 band of the first negative system is $6.53 \pm .22 \times 10^{-8}$ seconds[84]. Muntz's experiments were limited to number densities of 1.5×10^{16} molecules per cm^3 or less. At this density he estimates that an ion would traverse a mean free path in approximately 2×10^{-7} secs. and concludes that there will be little interference with the electron excited distribution of the $N_2^+ B^2\Sigma$ states. At higher densities an appreciable number of the excited ions will collide with other molecules and give up their energy by a non-radiative process. This quenching was considered when the validity of room temperature calibrations for absolute density measurements was discussed in Chapter II. Figure 12 shows that quenching first becomes appreciable at a number density of 1.5×10^{16} molecules per cm^3 in reasonable agreement with Muntz's estimate above. Therefore his conclusion that the spontaneous emission process giving rise to the first negative bands is not disturbed by gas kinetic collisions is reasonable for the conditions of his measurements.

At higher densities where quenching is appreciable Muntz's arguements will only be altered if the quenching cross section, equation 1.2 Chapter II, is different for each rotational level. Maquire[58] has considered this situation and postulates that

the more highly populated rotational levels are quenched to a greater extent than the states with lower populations. This increases the intensity of the lines arising from the higher rotational quantum states with respect to those from the lower quantum states. Such an effect would lead to the calculated rotational temperatures being too high as observed. However this discrepancy has been found to extend to densities where, from figure 12, quenching is apparently not significant. At this stage the possibility of more than one secondary process which counteract each other cannot be ruled out.

Excitation - Emission Process

The Excitation - Emission process finally assumed by Muntz was direct excitation from the ground state to the $N_2^+ B^2 \Sigma$ state followed by spontaneous emission to the $N_2^+ X^1 \Sigma$ state as illustrated in figure A3.1. Secondary electrons were assumed to play no part or to behave in the same way as the primary electrons. Quenching of the excited states by gas kinetic collisions was not considered. The assumptions involved in this model are reasonable except for those concerning the secondary electrons with energies greater than 18.3 eV.

Calculation of the Rotational Temperature

To predict the relative intensities of the rotational lines of a particular vibrational band in the emission it is necessary to find the relative population distribution in the rotational levels of a particular vibrational level of the N_2^+ $B^2\Sigma$ state due to direct excitation from the N_2 $X^1\Sigma$ state.

Muntz assumed that the $X^1\Sigma$ and $B^2\Sigma$ belong to Hund's case (b), reference 85, and that the high energy electrons bahaved as photons in the excitation process. Therefore if the rotational energy levels are designated by the quantum number K then the selection rules applying are $\Delta K = \pm 1$ and $\Delta K \neq 0$. Following the usual spectroscopic nomenclature the upper state is denoted by K' and the lower state by K''. The upper state K' is populated from two lower rotational levels $K'' = K' - 1$ and $K'' = K' + 1$ giving rise to the R and P branches in the excitation. Therefore the number of molecules per second excited to a given K' level is the sum of such transitions from all the vibrational levels of the lower state. Muntz assumed that the rotational and vibrational eigenfunctions are separable(85) and used the Hönl - London factors for the relative rotational transition probabilities. He further assumed that the rotational distribution in the N_2 $X^1\Sigma$ vibrational levels was a Boltzmann distribution and hence obtained an expression for the number of molecules

per second brought to a given K' level. For the emission the intensity of a given line is proportional to the rate of emission of photons at that wavelength. However the rate of photon emission from a given rotational level, K', must be equal to the rate of excitation to that level so that it is possible to obtain an expression for the relative rotational line intensities. In calculating the rotational temperature from this expression it is convenient to treat low and high vibrational temperatures separately. When Tv is low, less than 800° K, there is no appreciable excitation of the vibrational levels of N_2 $X^1\Sigma$ other than $V_1'' = 0$. Then the relative line intensities are given by

$$\frac{[I(K', K_2'')]_{v'v_2''}}{G_p 2K'} = \chi e^{-B_{v_1''}K'(K+1)hc/kT_R} \quad \ldots(A3.1)$$

where $$G_p = \left[\frac{(K'+1)e^{-2\phi(K'+1)/T_R} + K'e^{2\phi K'/T_R}}{2K'+1}\right] \quad \ldots(A3.2)$$

and $\phi = B_{v_1''}\, hc/k$

χ = a constant for a given v'.

Therefore if $\log_e$ of the left hand side of equation (A3.1) is plotted against $K'(K'+1)$ a straight line should result the slope of which is ϕ / T_R. As G_p is a function of T_R it is

necessary to assume an appropriate value of T_R and then calculate the correct value by iteration. G_p is small for most temperatures and two or three iterations are suffieient to obtain a reliable value of T_R.

At higher Vibrational Temperatures, $T_v > 800^\circ$ K, there is significant excitation of the upper vibrational levels of $N^2X^1\Sigma$. Therefore the total rate of excitation to a given K' level is the sum of the contributions from each of these vibrational levels. However Muntz showed that except for very high vibrational temperatures the contribtion from levels other than $V_1'' = 0$ is small. Further the rotational constant for the lower state $B_{V_1''}$ shows only a very weak dependance on V_1''. In view of this it is possible to use an effective rotational constant which is an average value determined by weighting the $B_{V_1''}$ in the average according to the product of the Frank-Condon factor and relative population for each vibrational level. Muntz showed that the error in this procedure was not significant even for a vibrational temperature of $4{,}000^\circ$ K.

Secondary Electron Excitation

Muntz's theory for excitation by fast primary electrons has been presented in some detail. The number of collisions between the primary electrons and molecules leading to the

excitation of the $B^2\Sigma_u^+$ states is proportional to the product of the gas density and primary beam current, i.e. $n\, i_p$. As each collision produces a secondary electron the number of secondaries in the vicinity of the primary beam will also be approximately proportional to $n\, i_p$. This approximation should be good for secondaries with energies in excess of 18.7 eV. However the low energy secondaries might be concentrated towards the centre of the beam because of the slower moving positive ions produced there. This is not important for the present arguement since they will play no significant part in the excitation of the nitrogen molecules. Some of the secondaries with energies in excess of 18.7 eV will excite ground state molecules to the $B^2\Sigma_u^+$ states. The cross sections for these transitions are unknown, but since they are between two Σ states, transitions for which ΔK would be even are rigorously forbidden[85] by the quantum selection rules. However, since the secondaries are of relatively low energy, transitions for which ΔK is odd are not rigorously forbidden. Thus in addition to $\Delta K = \pm 1$, allowed for the primaries, transitions for which $\Delta K = \pm 3, \pm 5 \ldots$ could also occur. The cross section, σ, for each transition will depend on the relative velocity of the electron and molecule as well as ΔK. As the electron velocity is much higher than the molecular velocity the relative velocity can be taken to be

that of the electron. Then, if f(v) is the velocity distribution function for the secondaries, the rate of excitation of a particular upper state K' by secondaries is given by

$$R = B \cdot n \sum_{V''=0,1,\cdots} \sum_{\Delta K=\pm 1,\pm 3,\cdots} \left[\int_{v} f(v)\, \sigma(K', K'' v)\, N_{K''}\, dv \right] \qquad \ldots(A3.3)$$

where B is a constant and $N_{K''}$ is the population of the K'' state.

For vibrational temperatures less than about 800° K most of the molecules are in the ground vibrational state and the summation over the vibrational levels in equation (A3.3) is not required. If also the gas is in rotational equilibrium the population distribution of the rotational levels will be Mazwellian and can be written as a function of K''. Further, for each transition, K'' can be written in terms of K' so that for low vibrational temperatures equation (A3.3) can be expressed in the form

$$R = B \cdot n\, F(K', T_R) \qquad \ldots(A3.4)$$

It is probable that the excitation cross-section $\sigma(K', K'', V)$ near the threshold energy would depend on the vibrational level from which the transition arises. Therefore once there is significant vibrational excitation ($T_v > 800°$ K), R

would be a function of T_v as well. However it is known that since the equilibrium internuclear distances of N_2 $X^1\Sigma$ and N_2^+ $B^2\Sigma$ are similar the Frank-Condon factors other than q(0,0) q(1,1) and q(2,2) are all comparatively small. Although the Frank-Condon factors will not be valid for the secondaries the vibrational transition probabilities should behave in a similar way. Therefore for a given band, say the 0-0 band, these probabilities should also be small for all except the 0-0 transition. Thus, the contribution to the rate of excitation of a given K' state from vibrational levels $v'' = 1,2 \ldots$ should be small except at very high vibrational temperatures. Therefore R should only be a weak function of T_v and the correction procedure given below should be reasonable for values of T_v somewhat greater than 800° K. The exact upper limit has yet to be determined.

The arguement briefly presented above for the secondary electrons is analogous to that given by Muntz for excitation by the primaries. However, the number of secondaries is not constant but proportional to the number density of the gas. Therefore following Muntz's arguement, adding the contribution from the primary and secondary electrons will lead to a modified form of equation (A3.1).

$$\frac{(I(K', K_2''))_{v', V_2''}}{2K'(G_p + nG_s)} \propto \ell^{(-\phi K'(K'+1)/T_R)} \quad \ldots(A3.4)$$

G_s is the function for secondary electrons corresponding to G_p given by Muntz for the primary electrons. The form of the term $n\,G_s(K', T_R)$ shows that the effects of n and T_R on the secondary electron excitation can be studied independently. In particular, it is immediately evident that as n tends to zero equation (A3.4) reduces to equation (A3.1), Muntz result, so that his theory should be more accurate at low densities. This is supported by the measurements of several investigators(48)(54)(55).

Equation (A3.4) is expressed in a more useful form by normalising the line intensities with respect to that of any given line in the same band. It is convenient to choose the third line for the normalising value, since at low temperatures this is one of the more intense lines and as a detailed consideration of forbidden transitions shows, the effect of secondaries on it is small except at high rotational temperatures.

Thus.

$$\frac{I(K')}{I(3)} \equiv f(K', T_R) \quad \frac{1 + n\,G(K', T_R)}{1 + n\,G(3, T_R)} \quad \ldots(A3.5)$$

where $G = G_s / G_p$

and $$f(K', T_R) = \frac{K' G_p(K', T_R) \, e^{-\emptyset K'(K'+1) / T_R}}{3 G_p(3, T_R) \, e^{-12\emptyset / T_R}} \quad \ldots (A3.6)$$

For low number densities, less than about 3×10^{15} molecules per cm^3, $n G(3, T_R)$ will be small so that

$$\frac{I(K')}{I(3)} = f(K', T_R) \left\{ 1 + n \left[G(K', T_R) - G(3, T_R) \right] \right\} \quad \ldots (A3.7)$$

Experimental Corroboration

To verify the validity of equation (A3.4) the experimental data of Ashkenas[54] is used as he has carefully measured the rotational temperature of a slowly flowing stream of nitrogen under conditions where the gas is undoubtedly in rotational equilibrium. From the data provided $I(K') / I(3)$ was plotted against n for the first fifteen lines at two temperatures, 77.8° K and 289° K. Typical plots are shown in figure A3.2 and in all cases the ratio $I(K') / I(3)$ tends to the predicted limit, $f(K', T_R)$, as n tends to zero. For $K' = 4$ the ratio $I(K') / I(3)$ does not vary greatly since the effect of secondaries is similar for both lines. From equation (A3.5), it is evident that if $G(K', T_R)$ is greater than $G(3, T_R)$, the ratio, $I(K') /$

I(3), will initially increase with n and then tend to a constant value when n $G(3, T_R)$ becomes large compared to unity. At 77.8° K, the factor $G(3, T_R)$ was found to be 1.05×10^{-16} cm^3 $molecules^{-1}$ while $G(15, T_R)$ was 23.2×10^{-16} cm^3 $molecules^{-1}$. Therefore for number densities larger than about 3×10^{16} the ratio I(15) / I(3) should be almost independant of n as is clearly seen in figure A3.2.

For small values of n, equation (A3.7) shows that I(K') / I(3) varies linearly with n. Therefore values of $G(K', T_R) - G(3, T_R)$ were obtained from the slopes of the curves as n tends to zero. However, $G(3, T_R)$ could only be determined by an iterative method by varying it systematically and calculating the rotational temperature for several different densities, For one particular value of $G(3, T_R)$ the calculated temperatures agreed with those indicated by the thermocouple for the whole range of densities. The values obtained at 77.8° K are given in figure A3.3 where they are compared with the value given by Muntz's theory. If the left hand side of equation (A3.4) was plotted against K' (K'+1) a good straight line was obtained, figure A3.4. Varying the number of lines used to calculate T_R between 11 and 15 caused the calculated value to vary by no more than $\pm$ 2%. Similar results were obtained for the room temperature measurements, figure A3.5, and the actual values

of $G(K', T_R)$ for both temperatures are given in table A3.1.

If the secondary electrons, in the vacinity of the primary electron beam, are influenced to any great extent by the gas flow the correction factors obtained above would not apply for high speed flows. In fact Petrie[86] has made measurements in a Mach 11 nozzle which show that the gas flow causes a slight asymmetry in the halo produced by the secondary electrons. Therefore for high speed flows the slit should be perpendicular to the beam, as in Ashkena's experiment, so that the measurements are not sensitive to small changes in the halo position. To confirm that the values of $G(K' T_R)$ for a slowly flowing stream are also valid for high speed flows they were used to reduce the data given in reference 53 for a Mach 3.92 flow. The values obtained were virtually independent of the number of lines used and agree well with the calculated free stream static temperature of 73.4° K, see figure A3.3. Similar data was provided by A.E.D.C.[87] and although details of the flow geometry were not given, the free stream static temperature was estimated as $75 \pm 5^{\circ}$ K. A value of 78° K was obtained from the rotational spectra provided. Finally the free jet data of Maquire[58] at a static temperature of 80° K is also shown.

Concluding Remarks

It is concluded that the secondary electrons play an important part in the excitation of the $B^2\Sigma_u^+$ states of N_2^+. When the effect of the secondaries is taken into account as indicated above the correct rotational temperature can be calculated. For this the values of $G(K', T_R)$ given in table (A3.1) can be used provided a similar optical system to that in reference 54 is used. At high densities further consideration must be given to quenching since the intensity of the 0-0 band does not increase as n^2 as equation (A3.4) predicts for large n. However, from the results presented in figure A3.5 it appears that any preferential quenching of the more highly populated levels[58] is not as important as the effect of secondary electrons.

The most serious limitation, at the present time, is that values of $G(K', T_R)$ can only be obtained at two temperatures, 77.8° K and 289°K. All that can be done is to give a qualitative description of the way in which the effect of secondary electrons varies with rotational temperature and to suggest an empirical relation for this. Figure A3.6 is a schematic diagram showing transitions from the $X^1\Sigma^+$, rotational states to the $B^2\Sigma_u^+$ states at two different rotational temperatures. If we consider the excitation to say the $K' = 10$ level then the allowed transitions, $\Delta K \pm 1$, arise from the $K'' = 9$ and 11 states. At

rotational temperatures near room temperature the population of these two levels is not greatly different from the population of the lower K'' states. The forbidden transitions $\Delta K = \pm 3, \pm 5, \ldots$ will occur from levels 7, 5, 3, 1, 13, 15, ... but are relatively few due to the small cross sections for such transitions. However at lower rotational temperatures the population of the higher rotational states is much less than that of the lower states as indicated in part (b) of figure A3.B. Therefore the population of the states from which the allowed transitions arise is very much less than the population of the states from which the forbidden transitions arise. This will have the effect of making the secondary electrons relatively more important, for the higher K' levels, as the rotational temperature is lowered. At high rotational levels the lines of highest intensities occur for higher values of K'. Therefore as the rotational temperature is increased to several hundred degrees, 500 to 1,000° K, a similar arguement to that above shows that secondary electron excitation becomes relatively more important for the lower K' levels. Thus, if Muntz's theory is used the effect of the secondary electrons is to make the calculated temperatures too high at low temperatures and too low at high temperatures as is in fact observed[53][54][55].

The function $G_s(K', T_R)$ is the sum of a series of terms

involving an unknown collision cross section. However it would be expected to have a similar form to G_p. i.e.

$$G_s(K', T_R) = F_1(K') e^{f_1(K')/T_R} + F_2(K') e^{-f_2(K')/T_R}$$

where F_1, F_2, f_1, and f_2 are unknown constants for a given K'. By the correct choice of these constants the required behaviour of $G(K', T_R)$ can be obtained. Once experimental data is available for two temperatures other than 77.8 and 289° K it will be possible to test the validity of this expression.

REFERENCES

1. Muntz, E.P. "Measurement of Rotational Temperature, Vibrational Temperature and Molecule Concentration in Non-radiating Flows of Low Density Nitrogen". U.T.I.A. Report No. 71.

2. Becker, J.V. "Results and Recent Hypersonic and Unsteady Flow Research at the Langley Aeronautical Laboratory". J App. Phys. Vol. 21 No. 7 p. 622 (1950).

3. Bertram, M.H. "Boundary - Layer Displacement Effects in Air at Mach Numbers of 6.8 and 9.6". N.A.S.A. TR R-22.

4. Bertram, M.H. Blackstock, T.A. "Some Simple Solutions to the Problem of Predicting Boundary - Layer Self - Induced Pressures". NASA TN D-798.

5. Lees, L Probstein, R.F. "Hypersonic Viscous Flow over a Flat Plate", Rept. No. 195. Dept. of Aero. Eng. Princeton Univ.

6. Hayes, W.D. Probstein. R.F. "Hypersonic Flow Theory". Academic Press N.Y 1959.

7. Schaaf, S.A. Hurlburt, F.C. Talbor, L and Aroesty, J "Viscous Interaction Experiments at Low Reynolds Numbers". J ARS Vol. 29 No. 7 p. 527 (1959).

8. Nagamatsu, H.T. and Sheer, R.E. Jr. "Hypersonic Shock Wave Boundary Layer Interaction with Leading Edge Slip", J ARS Vol. 30 No. 5 p. 454 (1960).

9. Nagamatsu, H.T. Weil, J.A. and Sheer, R.E. Jr. "Heat Transfer to a Flat plate in High Temperature Rarefied Ultra-high Mach Number Flow", J ARS Vol. 32 No. 4 p. 533 (1962).

10. Vidal, R.J. and Wittliff, C.E. "Hypersonic Flow about Blunt and Slender Bodies". Rarefied Gas Dynamics (Ed Laurmann). Vol II pp. 343-378. Academic Press N.Y. (1963).

11. Talbot, L. "Criterion for Slip near the Leading Edge of a Flat Plate in Hypersonic Flow". J. AIAA Vol. 1

No. 5 pp. 1169-1171 (1963).

12. Chaun, R.L. and Waiter, S.A. "Experimental Study of Hypersonic Rarefied Flow near the Leading Edge of a Thin Flat Plate". Rarefied Gas Dynamics (Ed Laurmann) Vol, II pp. 328 - 342, Academic Press N.Y. (1963).

13. Laurmann, J.A. "Structure of the Boundary Layer at the Leading Edge of a Flat Plate in Hypersonic Slip Flow". J. AIAA Vol. 2 No. 9 p. 1655 (1964).

14. Oguchi, H. "The Sharp Leading Edge Problem in Hypersonic Flow", Rarefied Gas Dynamics (Ed Talbot) p. 501, Academic Press N.Y. (1961).

15. Oguchi, H. "Leading Edge Slip Effects in Rarefied Hypersonic Flow", Rarefied Gas Dynamics (Ed Laurmann) Vol II p. 181 Academic Press N.Y. 1963.

16. Pan, Y.S. Probstein, R.F. "Rarefied Flow Transition at a Leading Edge". Mass. Inst. Tech Fluid Mech. Lab. Report 64-8 1964.

17. McCroskey, W.J. Bogdonoff, S.M. and McDougall, J.G. "An Experimental Model for the Sharp Flat Plate in Rarefied Hypersonic Flow", J AIAA Vol. 4 No. 9 p. 1580 (1966).

18. Becker, M and Boylan, D.E. "Experimental Flow Field Investigations near the Sharp Leading Edge of a Cooled Flat Plate in a Hypervelocity, Low Density Flow". Rarefied Gas Dynamics (Ed Brundin) Vol. II p. 993 Academic Press (1966).

19. Potter, J.L. Kinslow, M and Boylan, D.E. "An Influence of the Orifice on Measured Pressures in Rarefied Flow". Rarefied Gas Dynamics (Ed de Leeuw) Vol. II p. 175 Academic Press N.Y. 1966.

20. Bartz, J.A. and Videl, R.J. "Experimental Study of Pseudo Transpiration at an Orifice in Rarefied Flow". AFOSR 68-1927.

21. Harbour, P.J. and Lewis, J.H. "Preliminary Measurements of the Hypersonic Rarefied Flow Field on a Sharp Flat Plate using an Electron Beam Probe. Rarefied Gas Dynamics

(Ed Brundin) Vol. II p. 1031 Academic Press N.Y. (1966).

22. Joss W.W., Vas, I.E. and Bogdonoff, S.M. "Studies of the Leading Edge Effect on the Rarefied Hypersonic Flow over a Flat Plate AIAA Paper No. 68-5 (1968).

23. Joss, W.W. Bogdonoff, S.M. "A Detailed Study of the Flow around the Leading Edge of a Flat Plate in Hypersonic Low Density Flow" Princeton Univ. Internal Memo. 20 (1968).

24. Hickmann, R.S. "Hypersonic Tranistional Flow at the Leading Edge of a Sharp Flat Plate". Sixth Rarefied Gas Dynamics (Ed Trilling and Wachman). To be published.

25. Becker, M "Flat Plate Flow Field and Surface Measurements from Merged Layer into Transition Regime. Sixth Rarefied Gas Dynamics. (Ed Trilling and Wachman). To be published.

26. Nagamatsu, H.T.
Wisler, D.C.
Sheer, R.E. Jr.
"Continuum to Free Molecule Flow in the Vacinity of the Leading Edge of a Flat Plate at Mach Numbers of 19.4 and 24.1". General Electric Report No. 67 - C - 247.

27. Potter, J.L.
"The Transitional Rarefied - Flow Regime". Rarefied Gas Dynamics (Ed Brundin) Vol. II p. 881, Academic Press N.Y. (1966).

28. Oguchi, H.
"Shock Wave and Viscous Layer Structure in a Rarefied Hypersonic Flow near the Leading Edge of a Sharp Flat Plate". I.S.A.S. Report No. 418 Univ. of Tokyo 1967.

29. Shorenstein, M.L.
Probstein, R.F.
"The Hypersonic Leading Edge Problem" AIAA Paper No. 68-4.

30. Laurmann, J.A.
"Preliminary Results of a New Formulation of the Hypersonic Leading Edge Problem" Rarefied Gas Dynamics (Ed Brundin) Vol. II p. 955 Academic Press N.Y. (1966).

31. Rudman, R
Rubin, S.G.
"Hypersonic Viscous Flow over slender Bodies with sharp Leading Edges". AIAA Paper No. 68-3.

32. Garvine, R.W.
"Treatment of the Hypersonic Leading Edge Problem from the Continuum side of Transition". Sixth Rarefied Gas Dynamics (Ed Trilling and Wachman). To be published.

33A. Huang, A.B. and Hartley, D.L.
"Kinetic Theory of the Sharp Leading Edge Problem; I Supersonic Flow". 18th International Astronautical Conference, Belgrade Yugoslavia Sept. 1967.

33B. Huang, A.B. and Hwang
"Kinetic Theory of the Sharp Leading Edge Problem; II Hypersonic Flow" 19th Congress of the International Astronautical Federation N.Y. 1968

34. Hamel, B.B.
Cooper, A.L.
"A First Collision Theory of the Hyperthermal Leading Edge Problem" Sixth Rarefied Gas Dynamics (Ed Trilling and Wachman). To be published.

35. Grun, A.E.
Schopper, E.
"The Investigation of Energy Exchange and Extinction Processes in Gases by Excitation with Fast Particles"
2 Naturforschung 9a pp. 134-147 (1954)
A.E.R.E. Lib/Trans 780.

36. Grun, A.E.
"Some Gas Dynamic and Spectroscopic Observations made on Excited Gas Stream" 2 Naturforsch 9a pp. 833-836 (1954).

37. Grun, A,E.
Schumacher, B.
"The Application of Intensive Corpuscular Rays to the Excitation of Gases". 2. Angew Phys 1954 5. pp. 198-200.

38. Schumacher, B.W.
"The Design of Dynamic Pressure Steges for High - Pressure / High - Vacuum Systems", UTIA Report No. 78 1961.

39. Schumacher, B.W.
"Electron Beam Probe Installation for a Large Wind Tunnel". ORF PRR. 6303 1963.

40. Wada. I.
"Experimental Study of Low Pressure Hypersonic Flow by Using an Electron Beam Densitometer", Rarefied Gas

Dynamics (Ed de Leauw) Vol. II p. 535 Academic Press N.Y. 1965.

41. Schumacher, B.W. Aruja, E. "Measurements of Electron Single - Scattering in Gases". O.R.F. PRR 6406.

42. Schumacher, B.W. Aruja, E. and Falckenberg, H.R. "The Electron Single Scatter Gauge - A New Vacuum Gauge for the Range from 10^{-5} Tor to 1 Tor", ORF PRR. 6501.

43. Schumacher, B.W. Gadamer, E.O. "Electron Beam Probe for Measuring the Local Gas Density in a Wide Field of Observation", Canadian J. Phys. June 1958 p. 659.

44. Gadamer, E.O. "Measurement of the Density Distribution in a Rarefied Gas Glow using the Fluorescence Induced by a Thin Electron Beam", UTIA Report No. 83 (1962).

45. Muntz, E.P. Marsden, D.J. "Electron Excitation Applied to the Experimental Investigation of Rarefied Gas Flows", Rarefied Gas Dynamics (Ed Laurmann) Vol. II p.495 Academic Press N.Y. 1963.

46. Wada, I. "Experimental Study of Hypersonci Low Density Flow by using the Electron Beam Fluorescence Method", Rarefied Gas Dynamics (Ed Brundin) Vol. II p. 1193 Academic Press N.Y. 1967.

47. Harbour, P.J. "Absolute Determination of Flow Parameters in a Low Density Hypersonic Tunnel", Princeton Univ. Internal Memo. 23 (1968).

48. Hickman, R.S. "An Experimental Study of Hypersonic Rarefied Flow over a 10^{o} Cone", Rarefied Gas Dynamics (Ed Brundin) Vol. II p. 1067 Academic Press N.Y. 1962.

49. Ahouse, D.R.
Harbour, P.J. "Flow Field Measurements Upstream of a Blunt Body in a Rarefied Hypersonic Stream", Princeton Univ. Internal Memo. 25 (1968).

50. Butefisch, K "Investigation of Hypersonic Non-Equilibrium Rarefied Gas Flow Around a Circular Cylinder by the Electron Beam Technique". Sixth Rarefied Gas Dynamics (Ed Trilling and Wathmann) To be published.

51. Morrone, P.V. "Rotational Temperature and Density Measurements in Underexpanded Jets and Shock Waves Using an Electron Beam Probe". UTIAS Report No. 113 1966.

52. Rothe, D.E. "Electron Beam Studies of the Diffusive Separation of Helium - Argon mixtures in Free Jets and Shock Waves", UTIAS Report No. 114 1966.

53. Robben. F. Talbot, L. "Some Measurements of Rotational Temperatures in a Low Density Wind Tunnel Using Electron Beam Fluorescence". Univ. of California Report No. As-65.5.

54. Ashkenas, H. "Rotational Temperature Measurements in Electron Beam Excited Nitrogen" Phys of Fluids 10(1967) 2509.

55. Hunter, W.W. "Investigations of Temperature Measurements in 300° K to 1100° K Low Density Air using an Electron Beam Probe", N.A.S.A. TN. D - 4500.

56. Hickman, R.S. "Rotational Temperature Measurements in Nitrogen using an Electron Beam" Univ. of S. California USC AE 104 (1966).

57. Smith, R.B. "N_2 1st Negative Band Broadening due to Electron Beam Excitation". Sixth Rarefied Gas Dynamics (Ed Trilling and Wachman. To be published.

58. Maquire, B.L. "Density Effects on Rotational Temperature Measurements in Nitrogen Using the Electron Beam Excitation Technique". Sixth Rarefied Gas Dynamics (Ed Trilling and Wachman To be published.

59. Bates, D.R. "The Intensity Distribution in the Nitrogen Band Systems Emitted from the Earths Upper Atmosphere". Proc. Roy. Soc. A 196 217 (1949).

60. Muntz, E.P. "The Direct Measurement of Velocity Distribution Functions", Rarefied Gas Dynamics (Ed de Leeuw) Vol. II p. 128 Academic Press N.Y. 1966.

61. Muntz, E.P. "Measurements of Anisotropic Velocity Distribution Functions in Rapid Radial Expansions", Rarefied Gas Dynamics (Ed Brundin) Vol. II p. 1257 Academic Press N.Y. 1967.

62. Willis, D.R.
Hamel, B.B.
"Non Equilibrium Effects in Spherical Expansions of Polyatomic Gases and Gas Mixtures", Rarefied Gas Dynamics (Ed Brundin) Vol. I p. 837 Academic Press N.Y. 1967.

63. Muntz, E.P.
"Molecular Velocity Distribution - Function Measurements in a Flowing Gas", Phys. of Fluids, Vol. 11 No. 1 (1968).

64. Rothe, O.E.
"Flow Visualisation Using a Traversing Electron Beam", AIAA. J. Vol. 3 pp. 1945-1946 (1965).

65. Sebacher, D.I.
Duckett, R.J.
"A Spectrographic Analysis of a 1 - Foot Hypersonic - Arc - Tunnel Airstream using an Electron Beam Probe", NASA Tech. Report R - 214.

66. Haine, M.E.
Einstein, P.A.
"Characteristics of the Hot Cathode Electron Microscope Gun", British Hournal of Applied Physics Vol. 3 p. 40 (1952).

67. Liebmann and Grad.
Proc. of Phy. Soc. B 64 p. 956 (1951).

68. Vas. I.E. and Allegre, J. "The N-4 Hypersonic Low Density Facility and some Preliminary Results on a Sharp Flat Plate", Rarefied Gas Dynamics (Ed Brundin) Vol. II pp. 1015-1030 Academic Press (1966).

69. Muntz, E.P. Abel, S.J. and Maquire, B.L. "The Electron Beam Fluorescence Probe in Experimental Gas Dynamics" I.E.E.E. Trans. on Aerospace, p. 210 (1965).

70. Rogers, E.W.E. Berry, C.J. and Davis, B.M. "Experiments with Cones in Low - Density Flows at Mach numbers near 2". A.R.C. 25 713.

72. Berry, C.J. "Low Pressure Measurements with Thermistors", J Sci. Inst. Vol, 44, 1967.

73. Mc Croskey, W.J. "An Experimental Model for the Sharp Leading Edge Problem in Rarefied Hypersonic Flow". Ph.D. Thesis, Princeton Univ. New Jersey.

74. Metcalf, S.C. Lillicrap, D.C. and Berry, C.J. "A Study of the Effect of Surface Temperature on the Shock - Layer Development over Sharp-Edge Shapes in Low - Reynolds - Number High-Speed Flow", Sixth Rarefied Gas Dynamics (Ed Trilling and Wachman). To be published.

75. Kinslow, M. and Arney, G.D. — Agardograph 119 August 1967.

76. Patterson, G.N. — "Molecular Flow of Gases", Chapman and Hall, London 1956.

77. Shen, S.F. — "A Theory for the Slip - Flow Boundary Conditions over a Surface defined by Arbitrary Gas - Surface Interaction Parameters", Rarefied Gas Dynamics (Ed Brundin) Vol. I p. 623 Academic Press N.Y. 1967.

78. Cercignani, C and Tironi, G. — "Some Applications to the Transition Regime of a New Set of Boundary Conditions for Navier - Stokes Equations", Sixth Rarefied Gas Dynamics (Ed Trilling and Wachman), To be published.

79. Loyalka, S.K. and Ferziger, J.H. — "Model Dependence of the Slip Coefficient", Phys of Fluids, Vol. 10 No. 8 p. 1833 (1967).

80. Loyalka, S.K. and Ferziger, J.H. — "Model Dependence of the Temperature Slip Coefficient", Phys of Fluids, Vol. 11 No. 8 p. 1668 (1968).

81. Vogenitz, F.W. Broadwell, J.E. and Bird, G.A. "Leading Edge Flow by the Monte Carlo Direct Simulation Technique", AIAA 7th Aerospace Sciences Meeting, N.Y. Jan 1969.

82. Schaaf, S.A. "The Pitot Probe in Low-Density Flow", AGARD Report 525 1966.

83. Garvine, R.W. "Shock Wave Transport Effects on Hypersonic Leading Edge Flow", AIAA J. Vol. 4 No. 10 p. 1856 (1966).

84. Bennet, R.G. and Dalby, F.W. "Experimental Determination of the Oscillator Strength of the First Negative Bands of N_2^+", J. Chem. Phys. 31 No. 2 p. 434 (1959).

85. Herzberg, G. "Spectra of Diatomic Molecules" D Van Nostrand and Co. N.Y. (1950).

86. Petrie, S.L. and Boiarski, A.A. "The Electron Beam Diagnostic Technique for Rarefied Flow at Low Static Temperatures", Sixth Rarefied Gas Dynamics (Ed Trilling and Wachman). To be published.

87. Private Communication with Arnold Engineering Development Center.

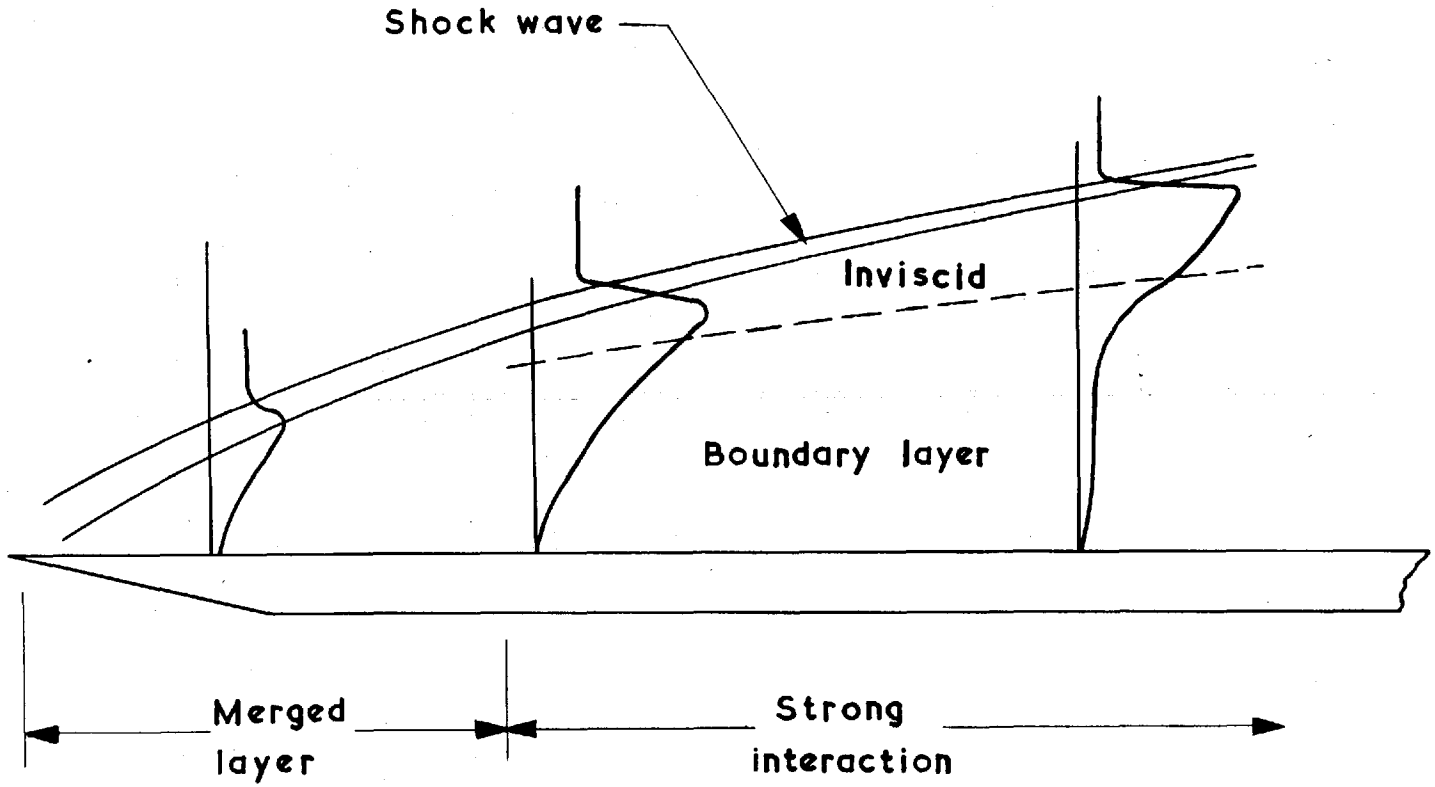

FIG.1. Schematic diagram of flow field and mass flow profiles by McCroskey et al.

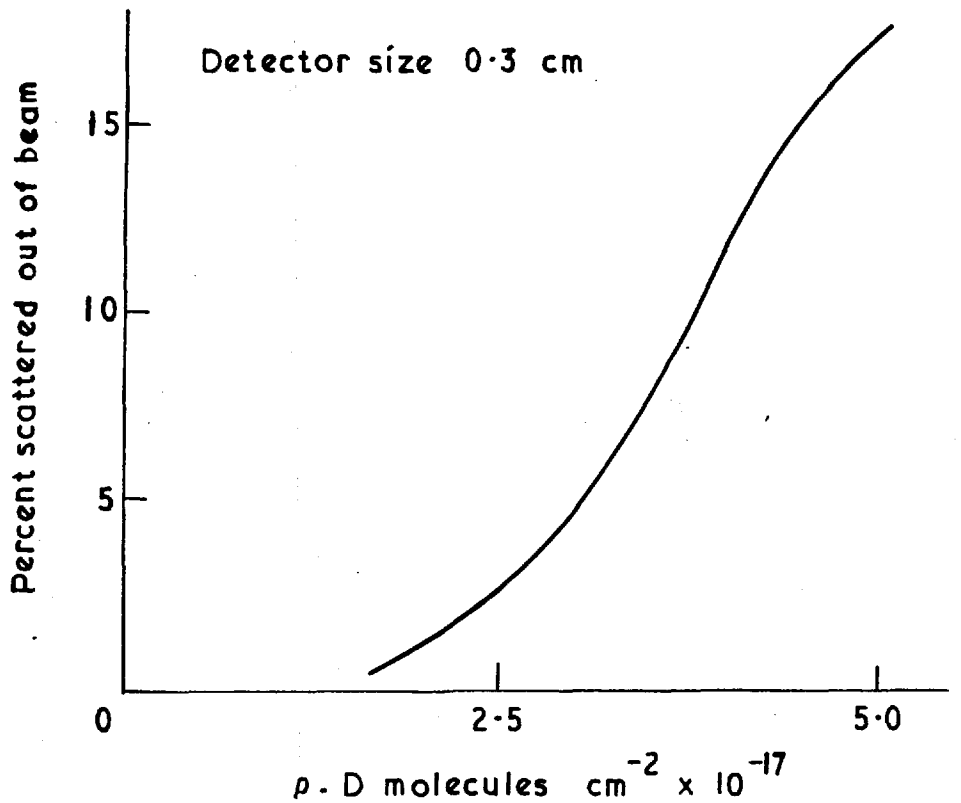

FIG.2 No. of electrons scattered outside of a 0·3 cm dia. detector

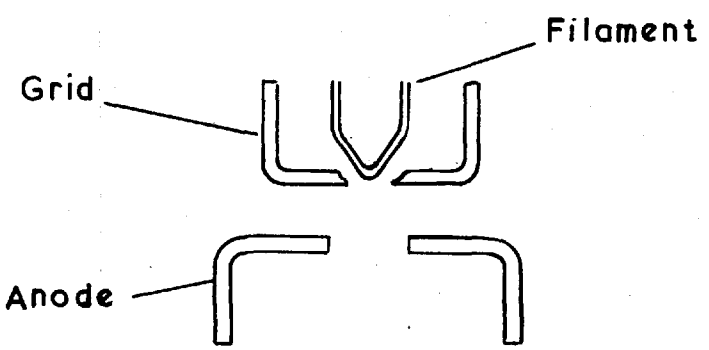

FIG.3. Electrode arrangement in electron microscope gun

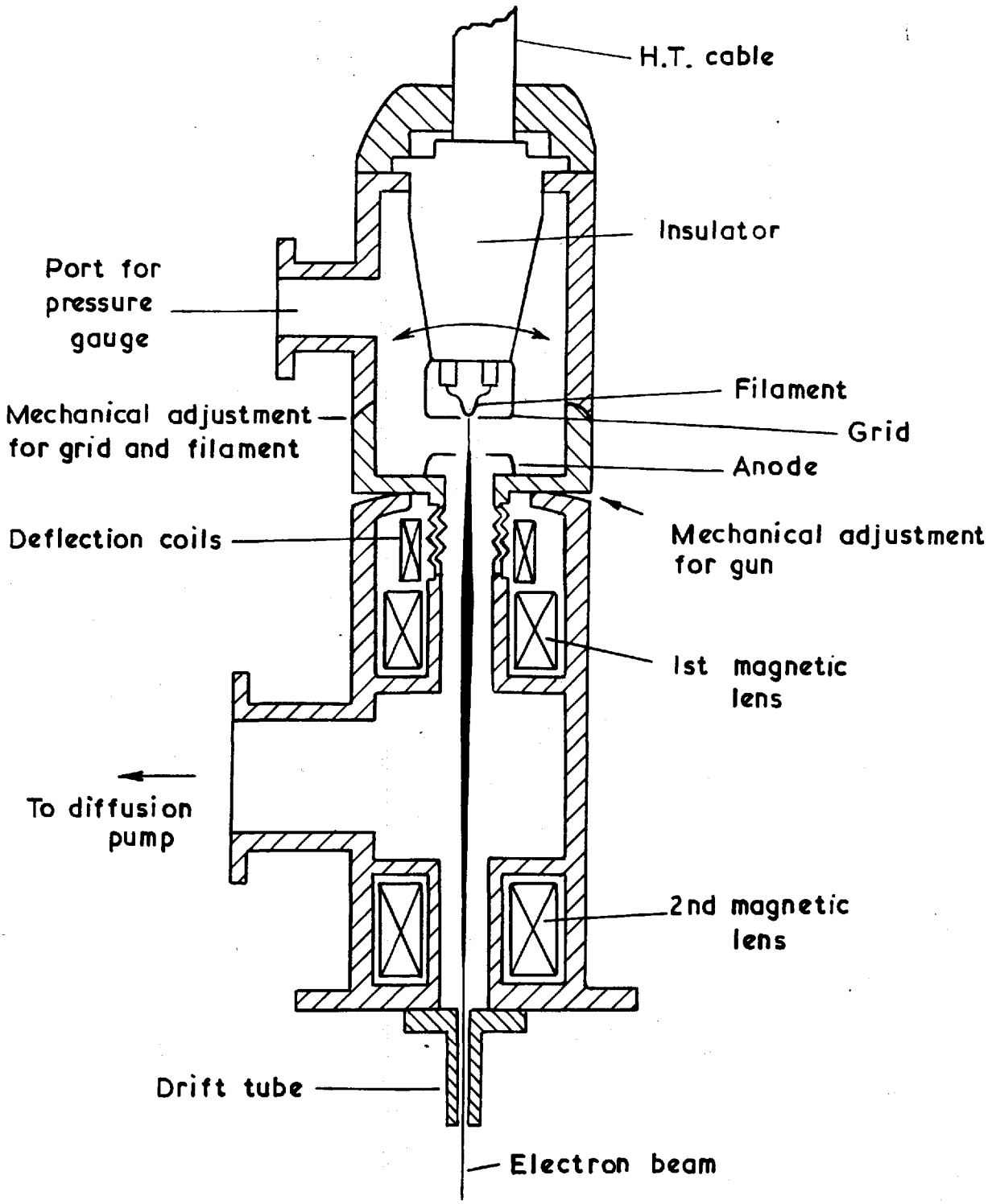

FIG.4 Schematic diagram of electron gun

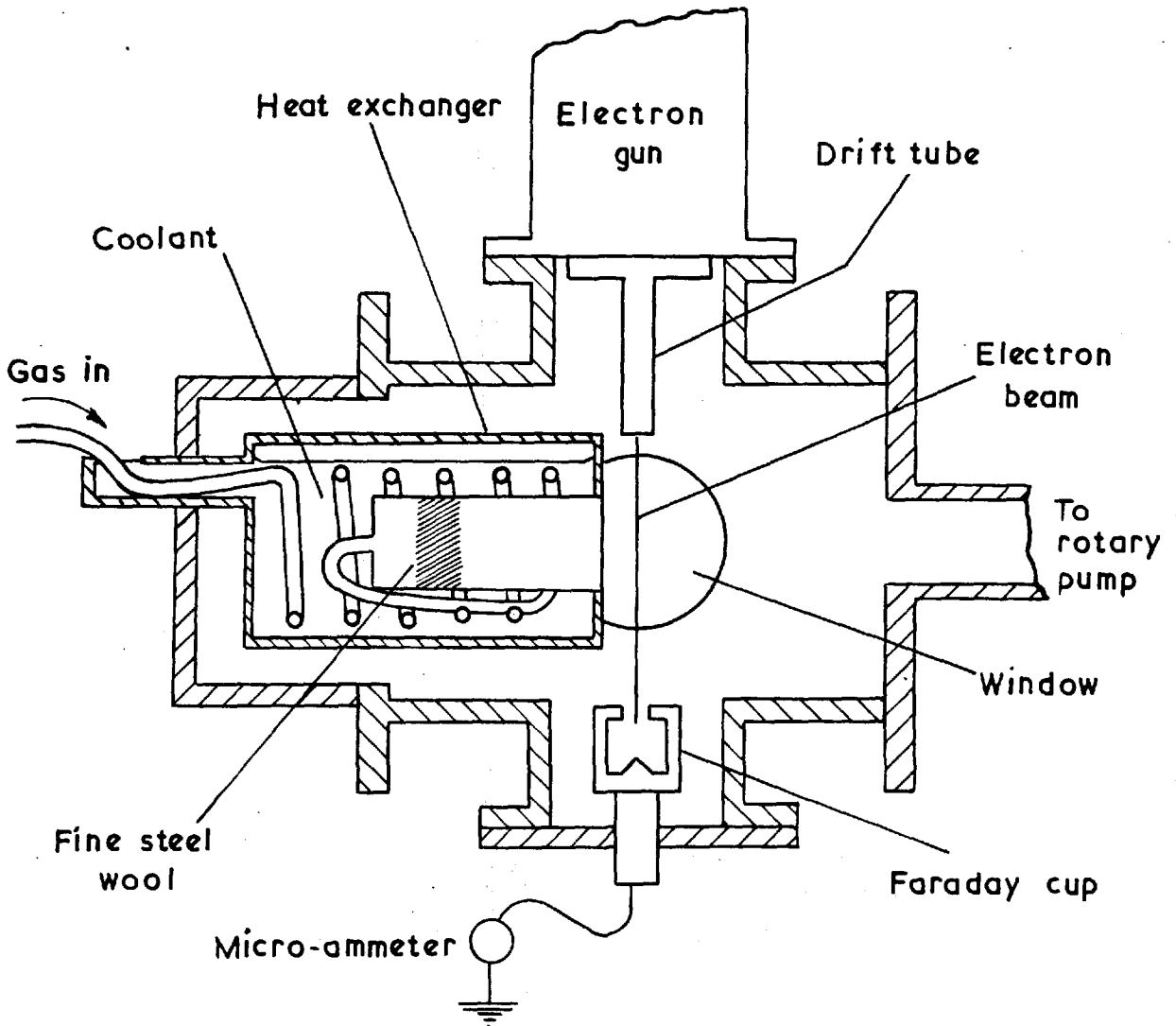

Schematic diagram of small vacuum test chamber

FIG 5

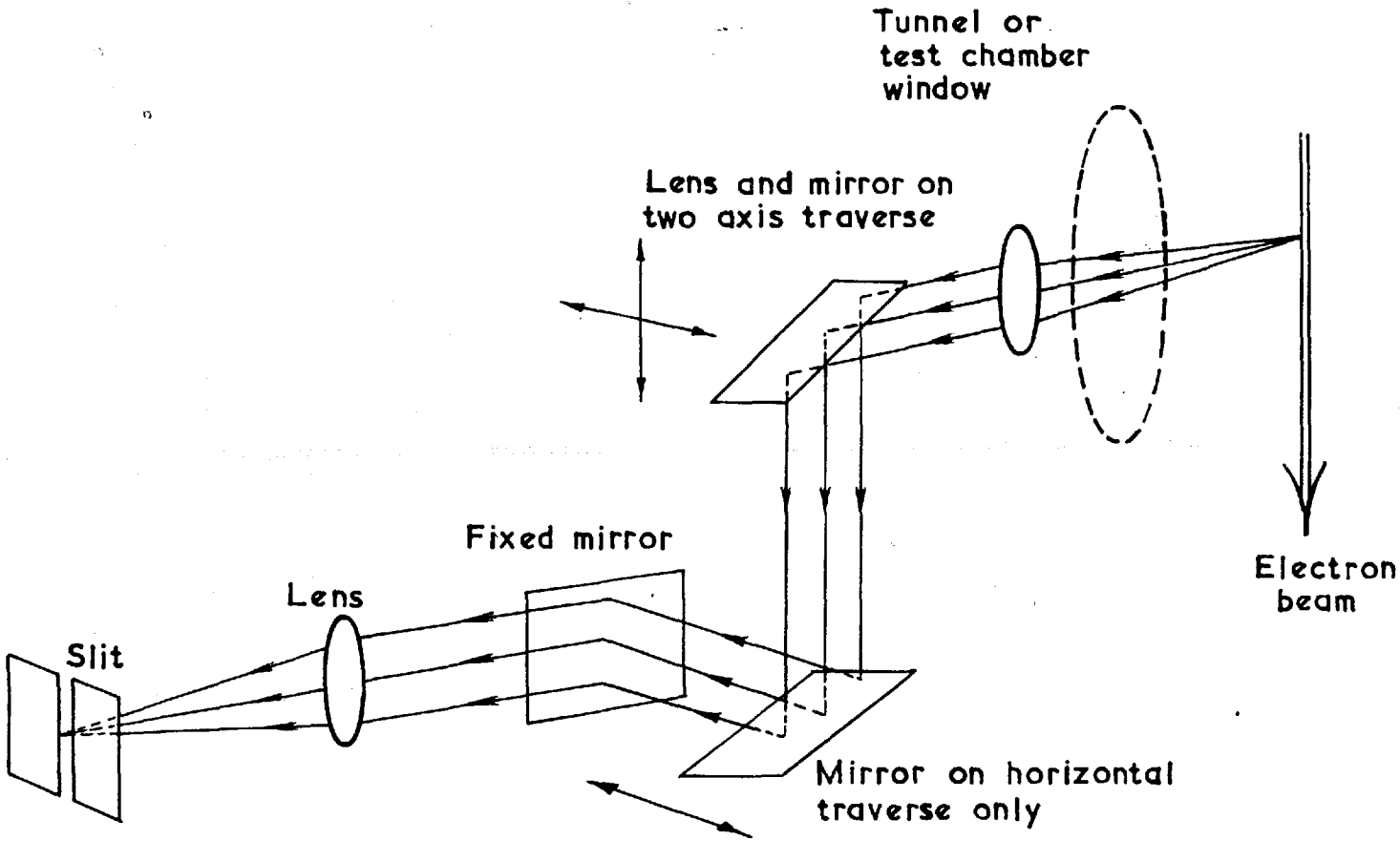

FIG. 6. Schematic diagram of optical system used to observe the beam.

FIG. 7

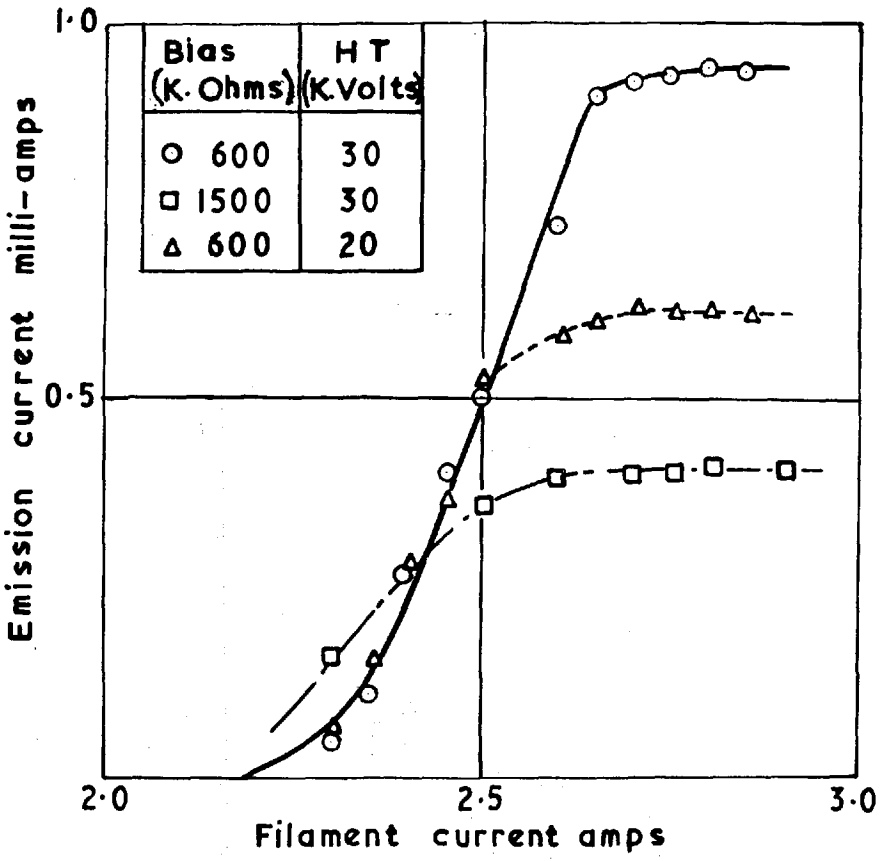

Hairpin filament characteristics

FIG. 8

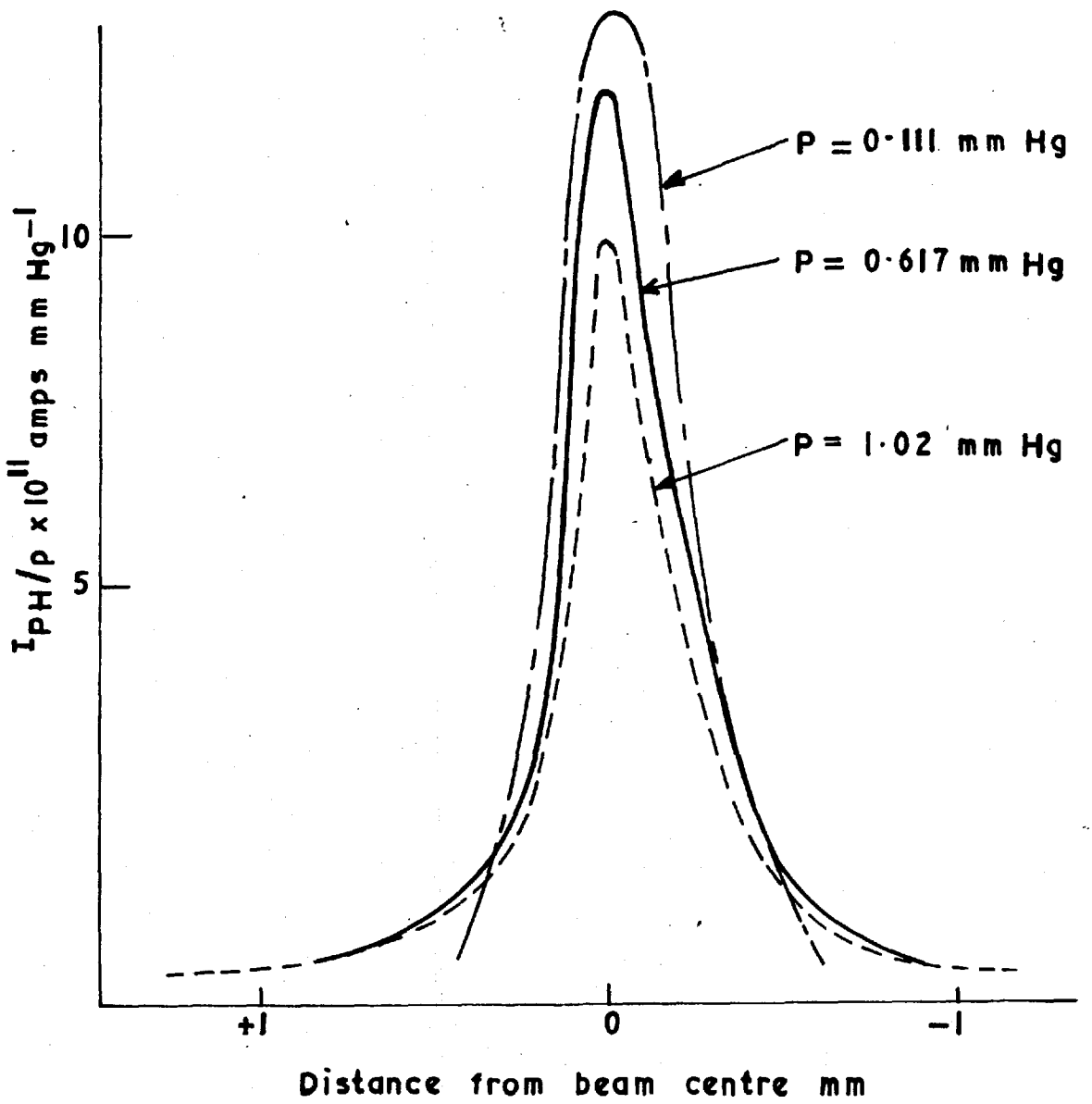

Typical current density profiles of beam

FIG. 9

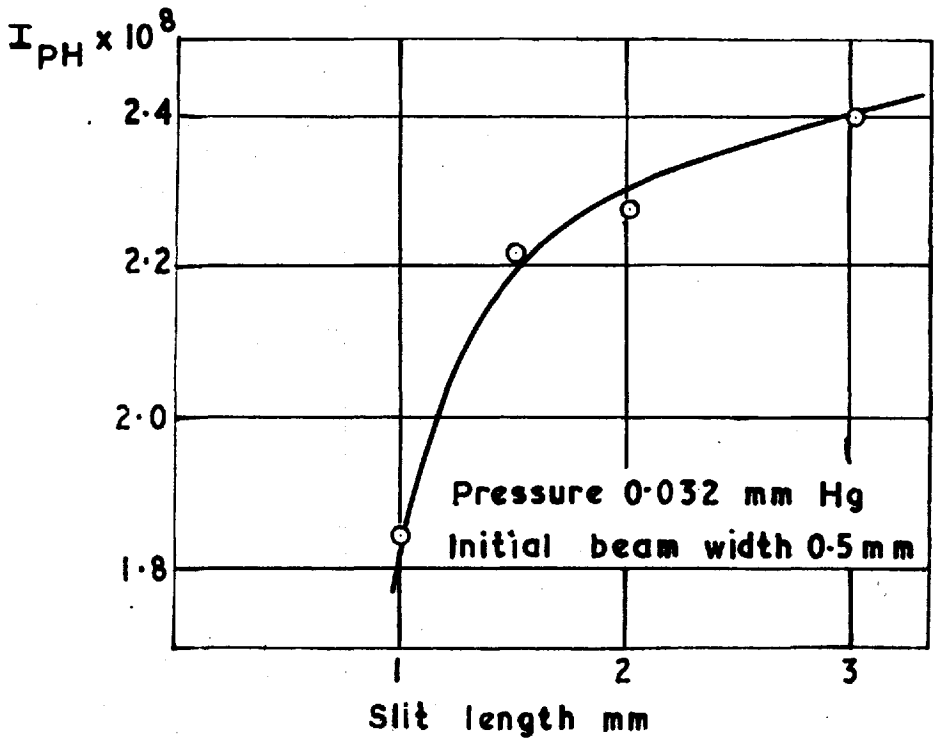

Variation of I_{PH} with slit length

FIG. 10

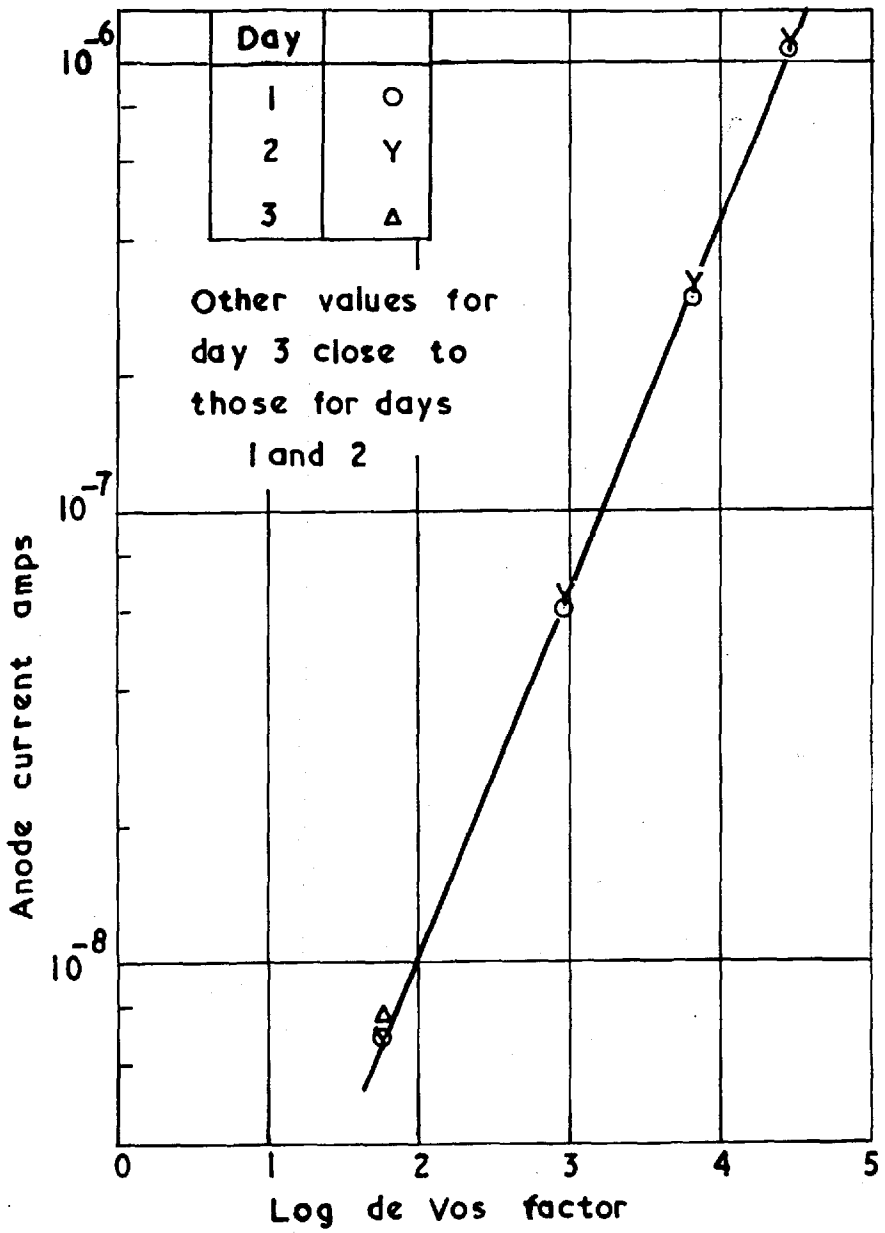

Typical photomultiplier calibration curves

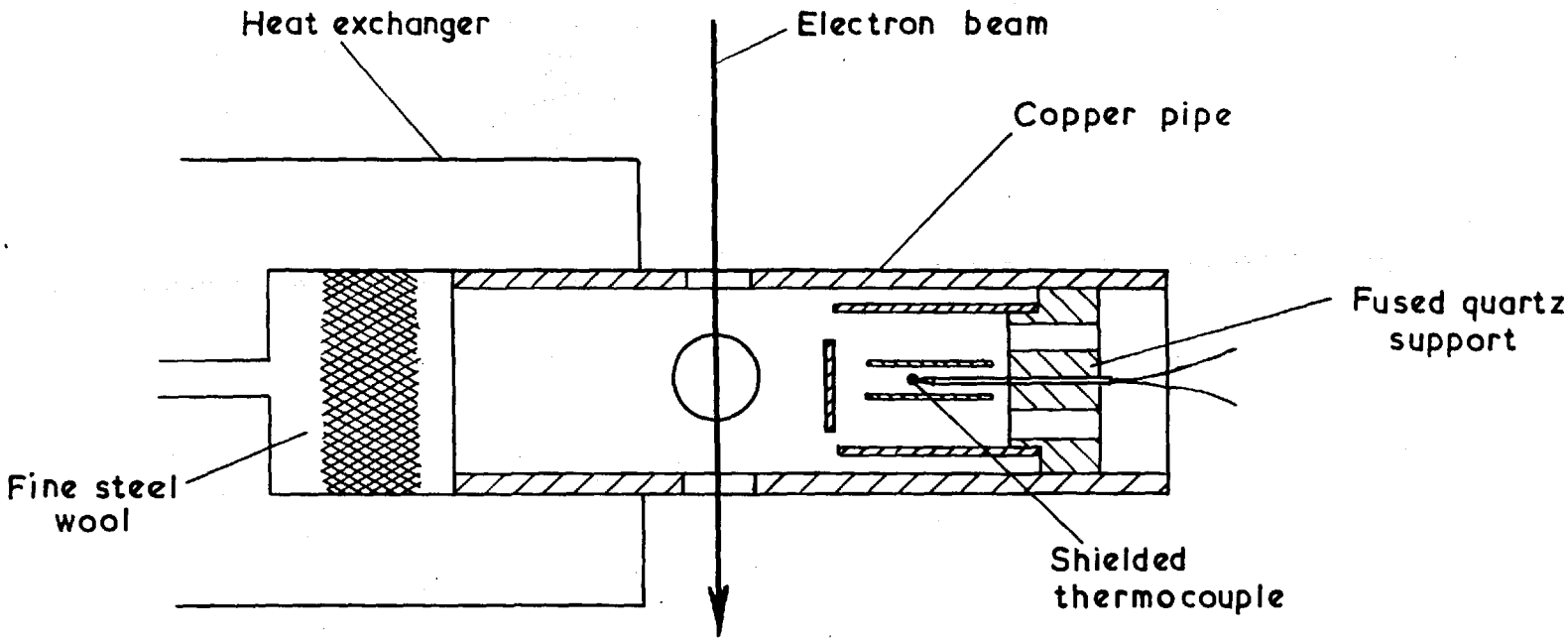

FIG. 11

Arrangement used in test chamber for low temperature work

FIG. 12

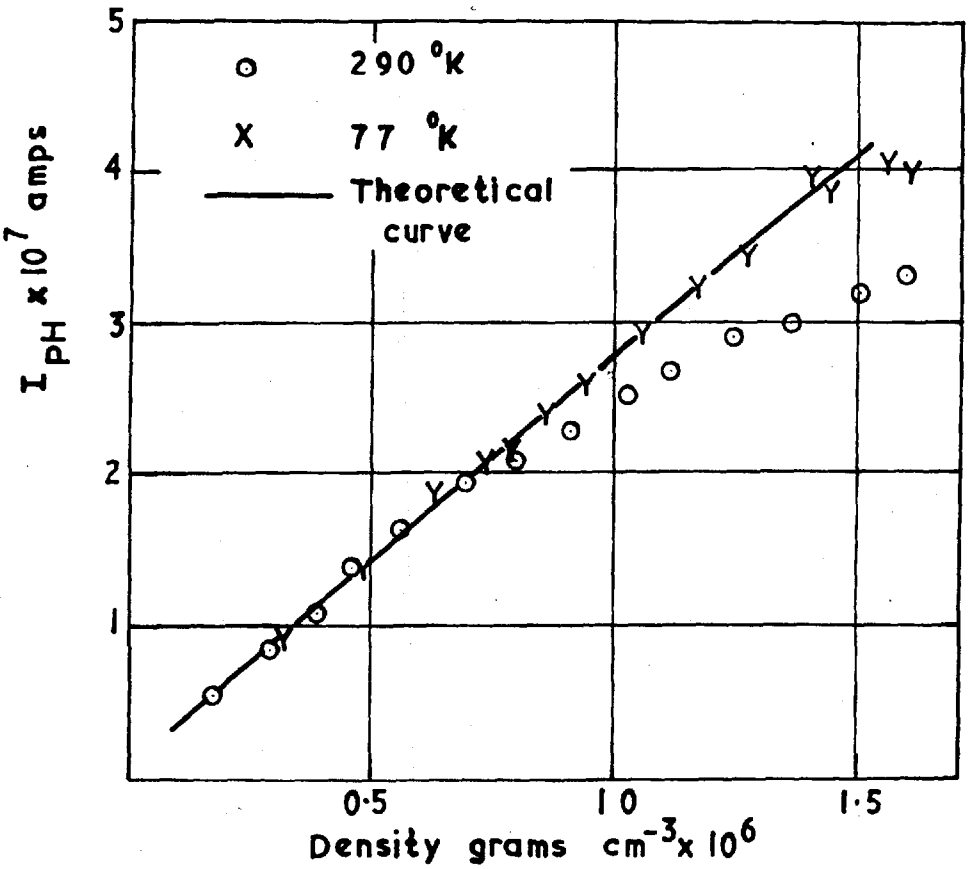

Quenching of the 0 – 0 band of the first negative system of nitrogen

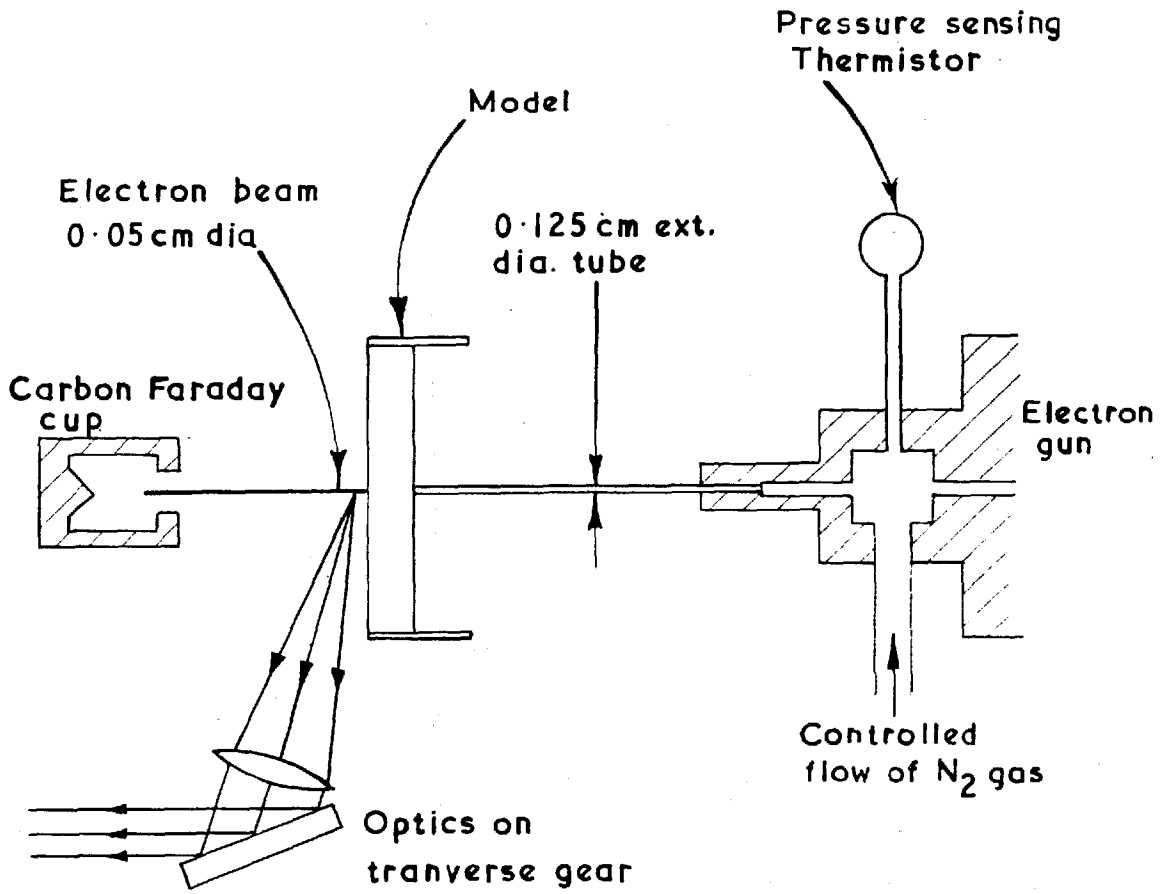

FIG. 13. Electron beam arrangement with modified drift tube.

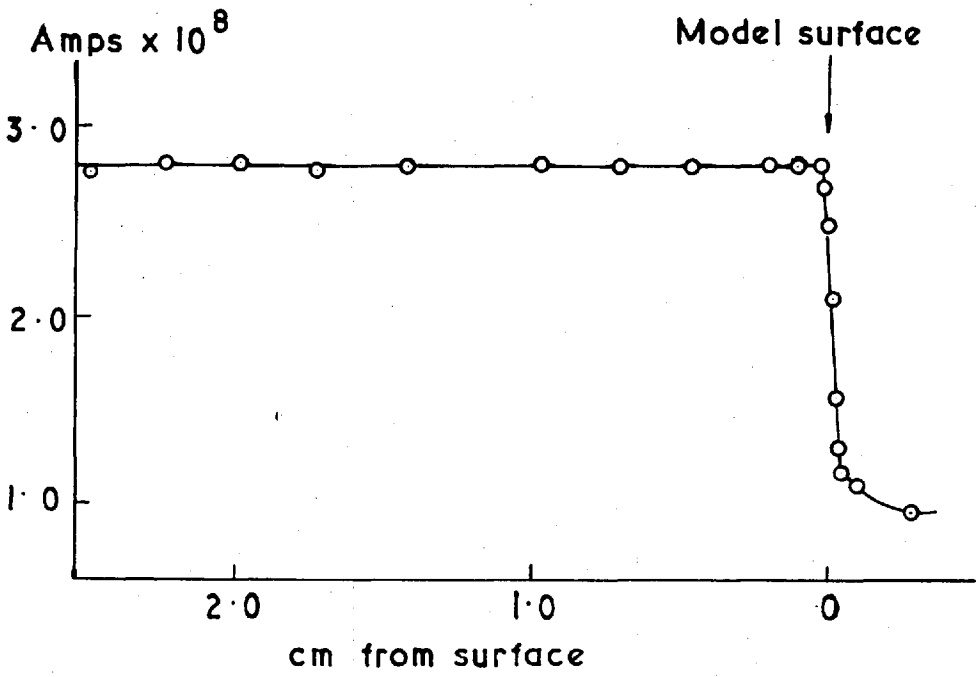

FIG.14. Fluorescent intensity against distance from surface

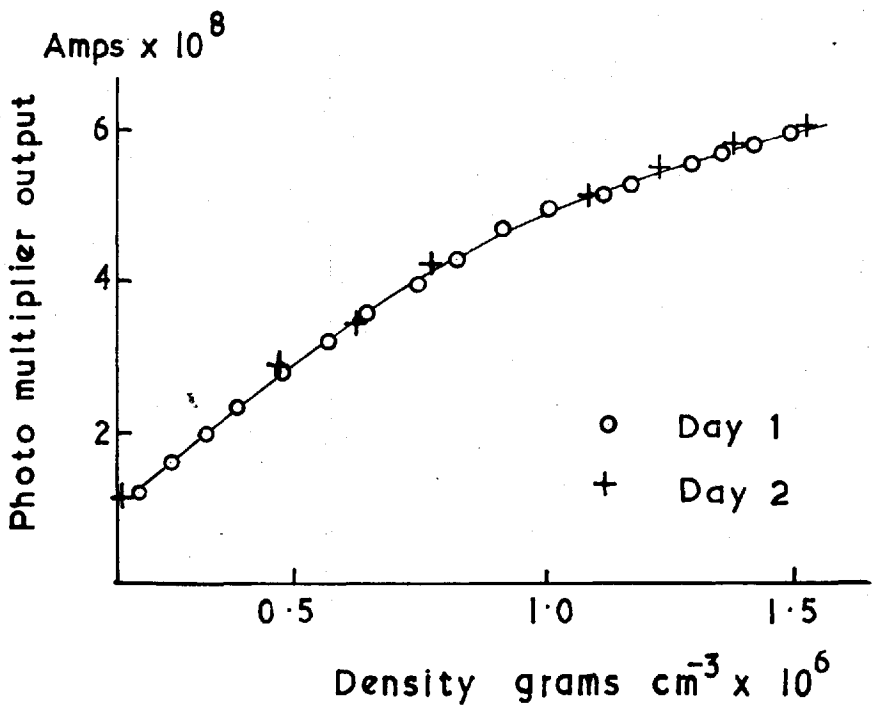

FIG.15 Calibration curve for absolute density measurements.

Side elevation: section through centre line.

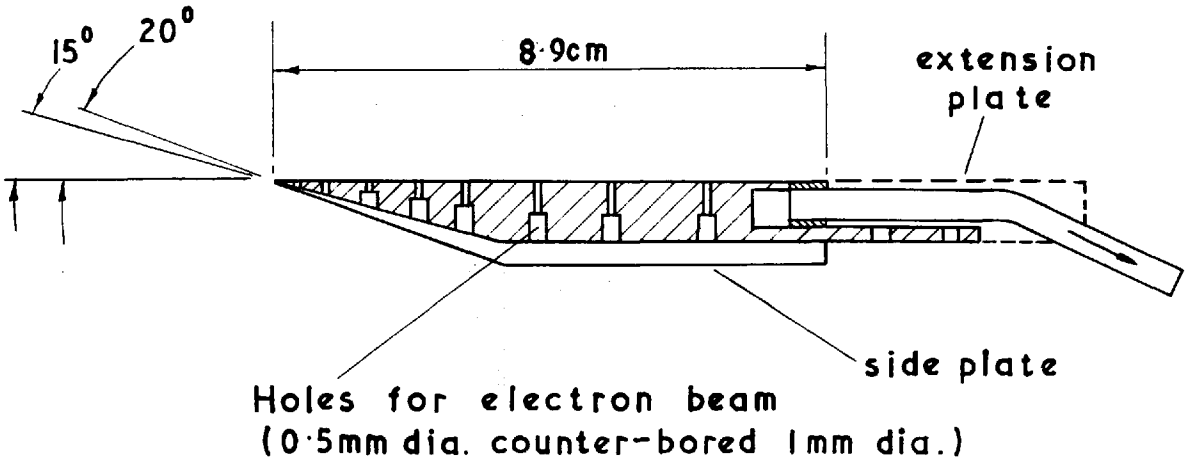

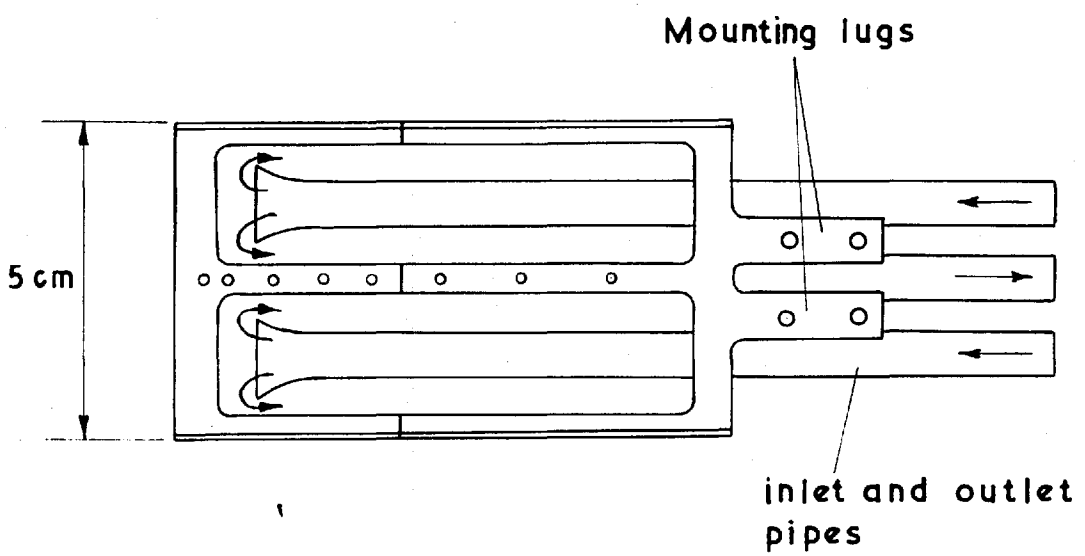

Underside of model: Covers over the cavities removed to show circulation of coolant through them.

FIG. 16 Flat plate model.

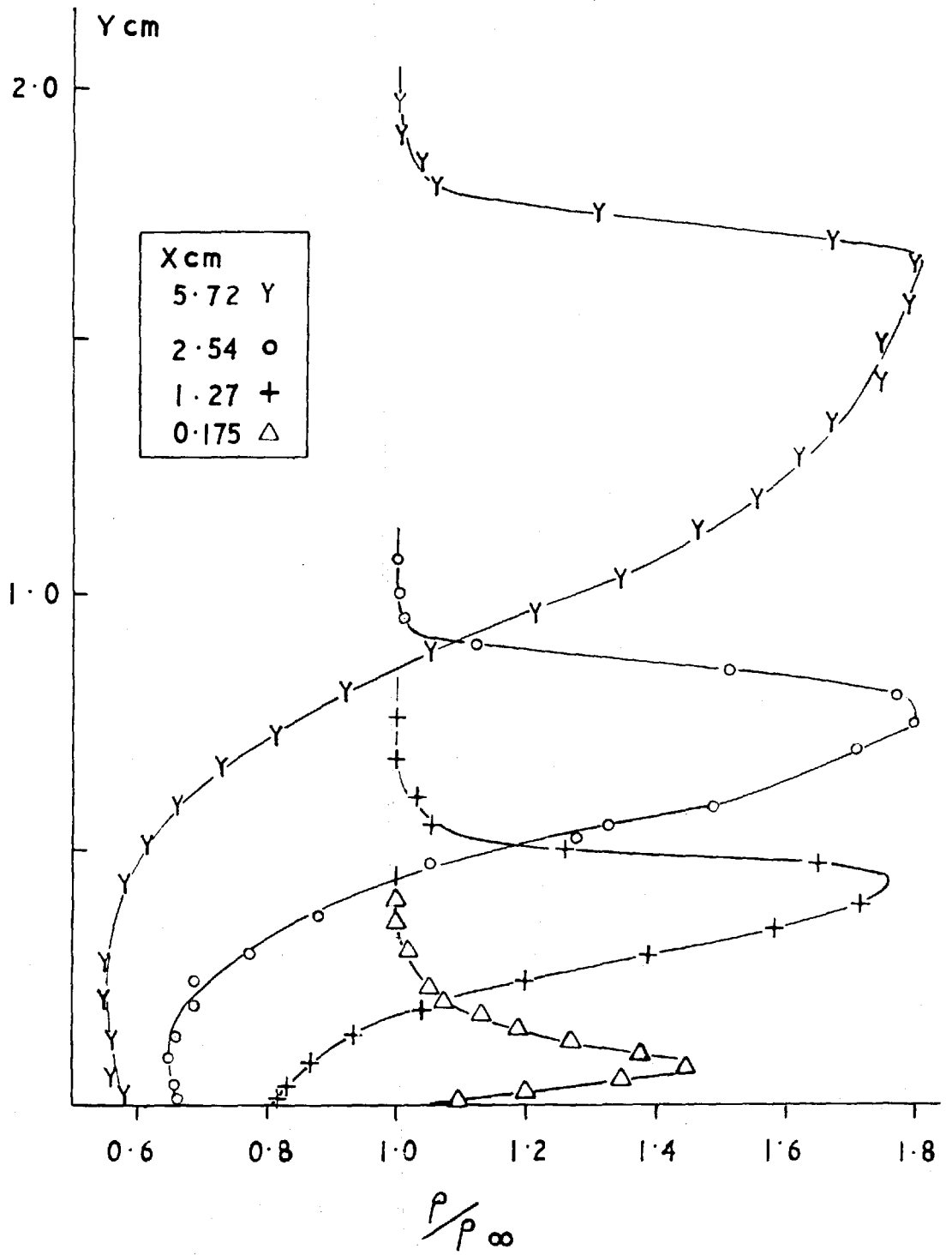

FIG. 17. Typical density profiles through the shock layer: $M = 6{\cdot}6$ $Re_\infty/cm = 650$, Water cooled model.

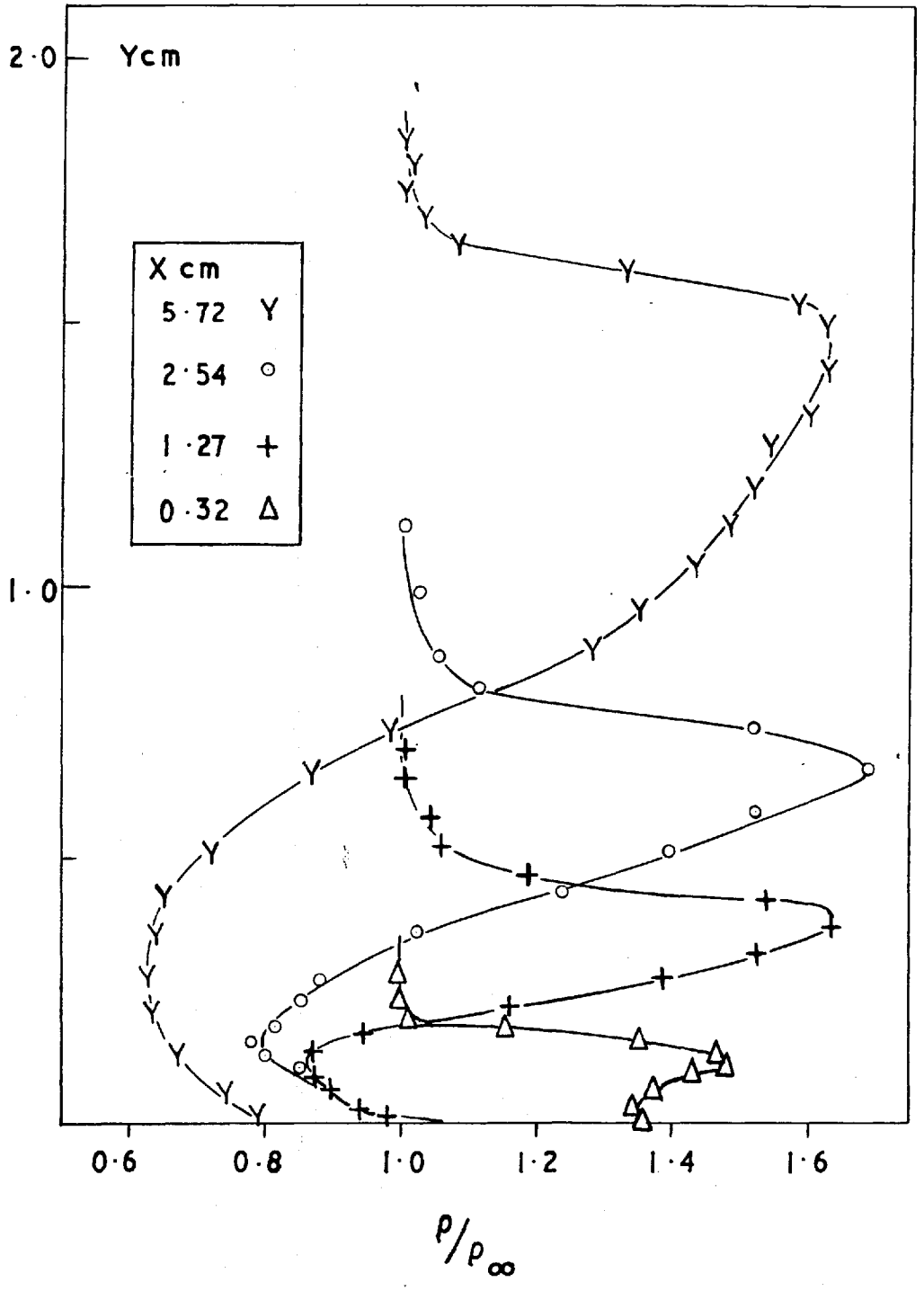

FIG. 18 Typical density profiles through the shock layer: $M = 6 \cdot 6$ $Re_\infty/cm = 650$, liquid nitrogen cooled model.

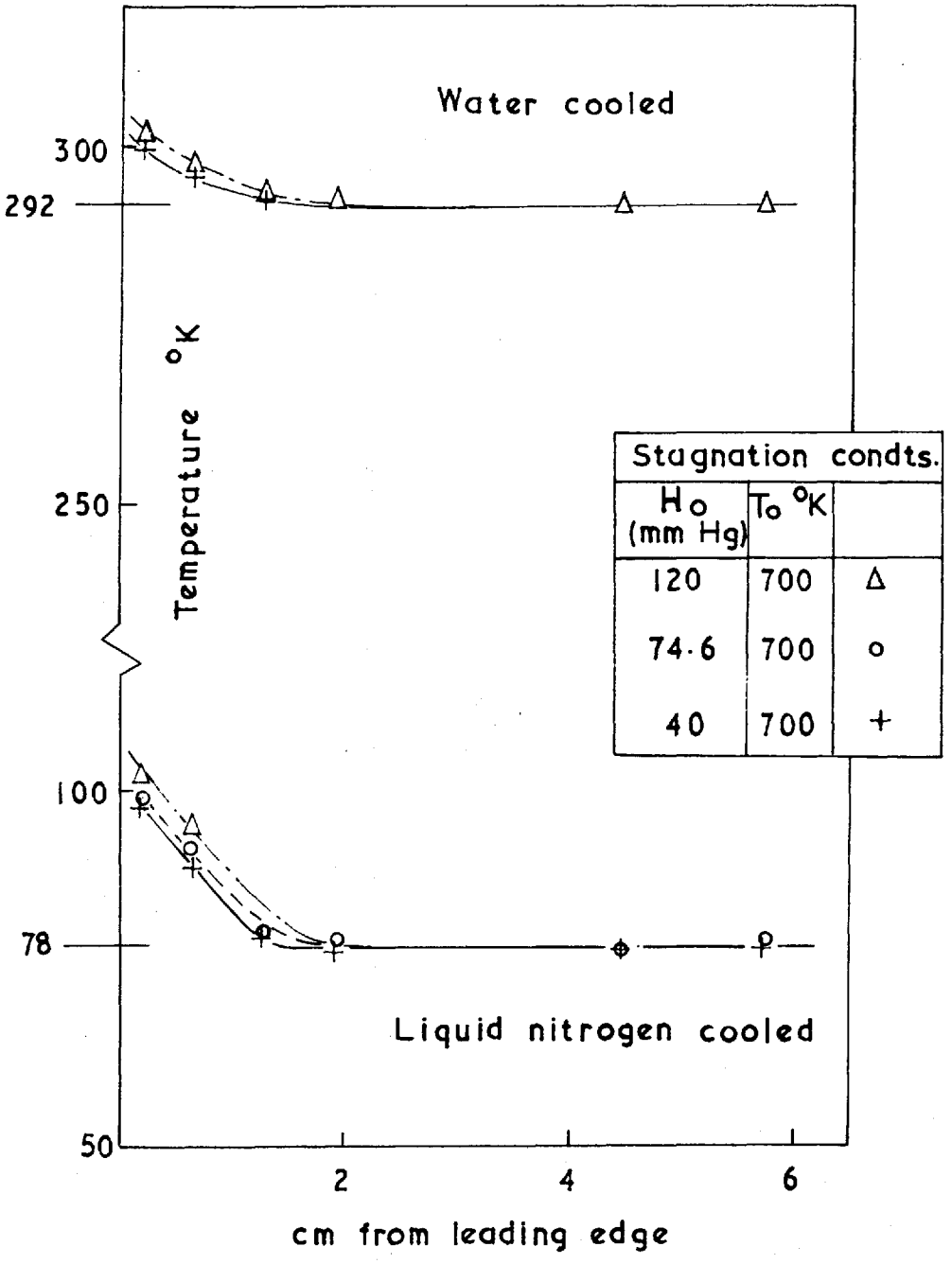

FIG. 19 Measured surface temperature.

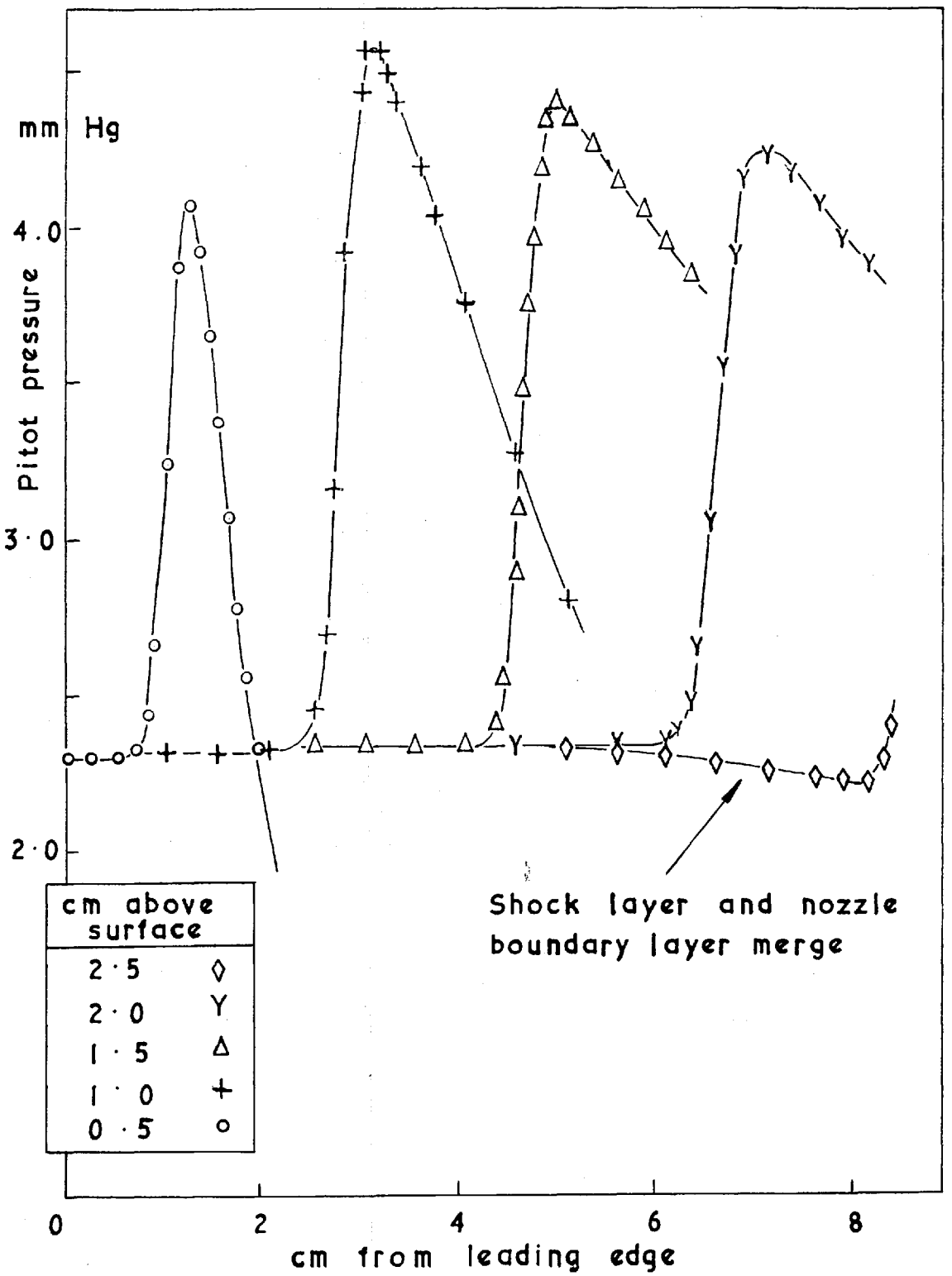

FIG. 20. Axial pitot traverses for water cooled model $M = 6 \cdot 6$ Re_∞/cm 650.

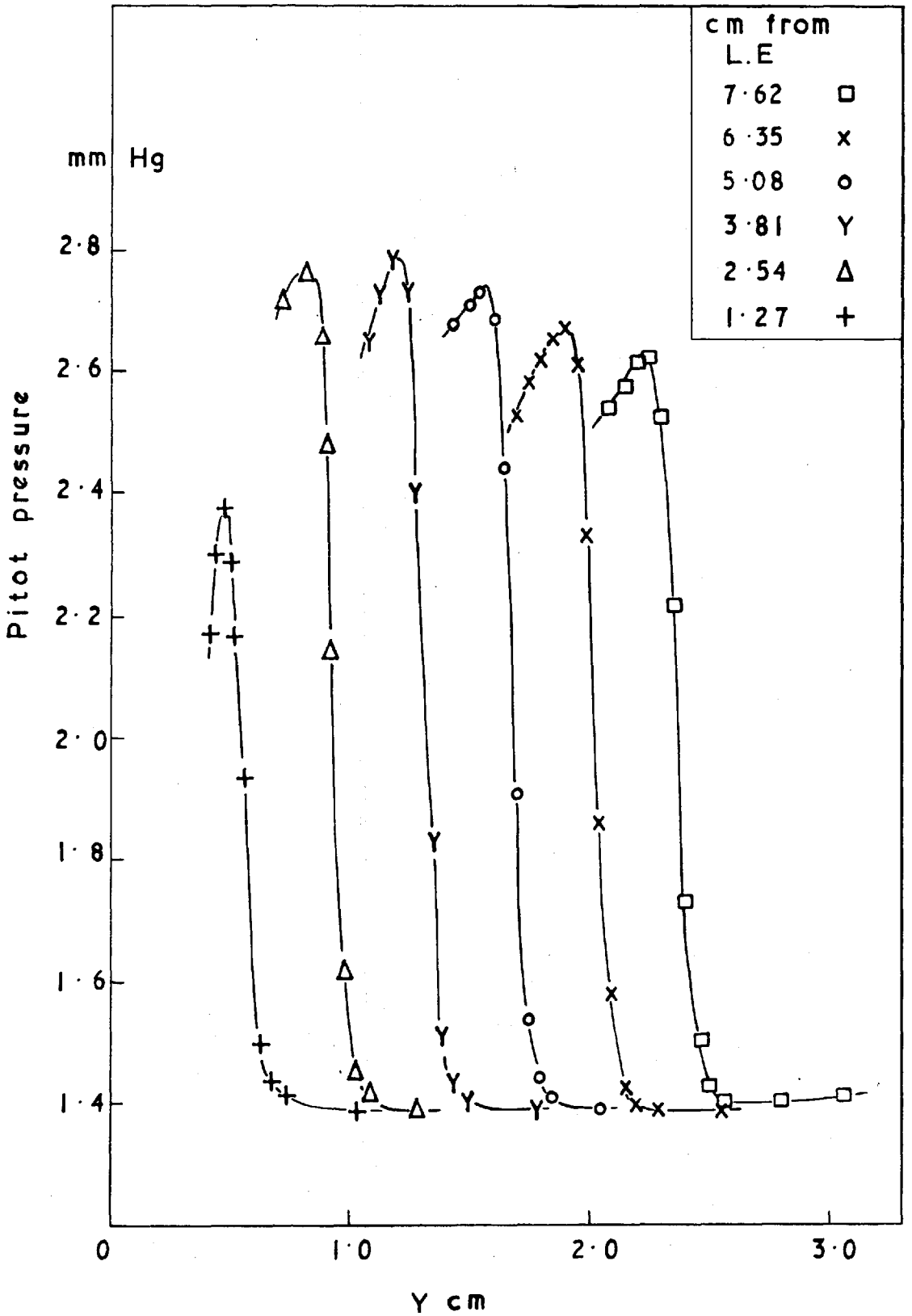

FIG. 21 Pitot traverses through the shock layer $M = 6{\cdot}3$ $Re_\infty/cm = 390$.

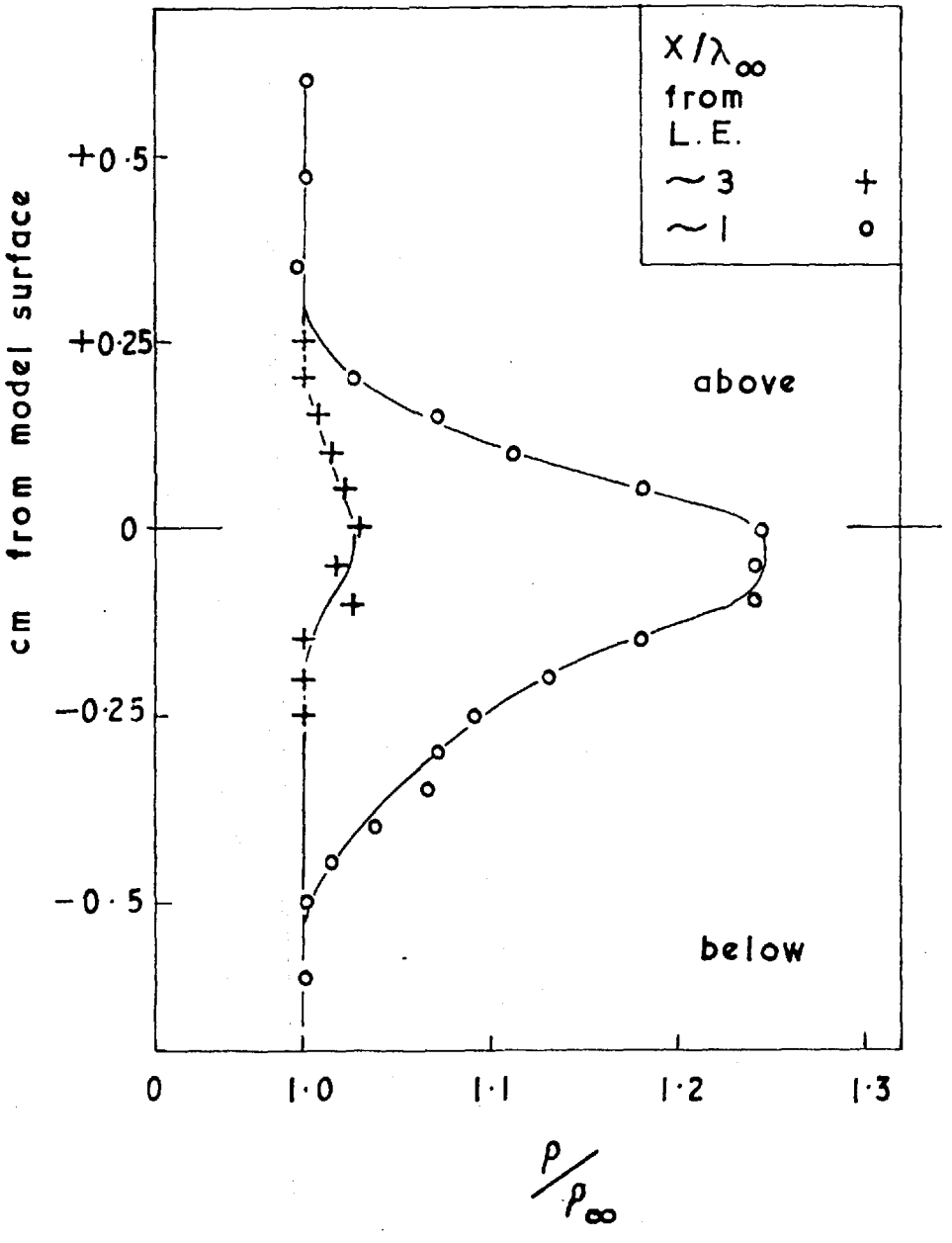

FIG.22. Density profiles ahead of leading edge M = 5·74 Re_∞/cm = 130.

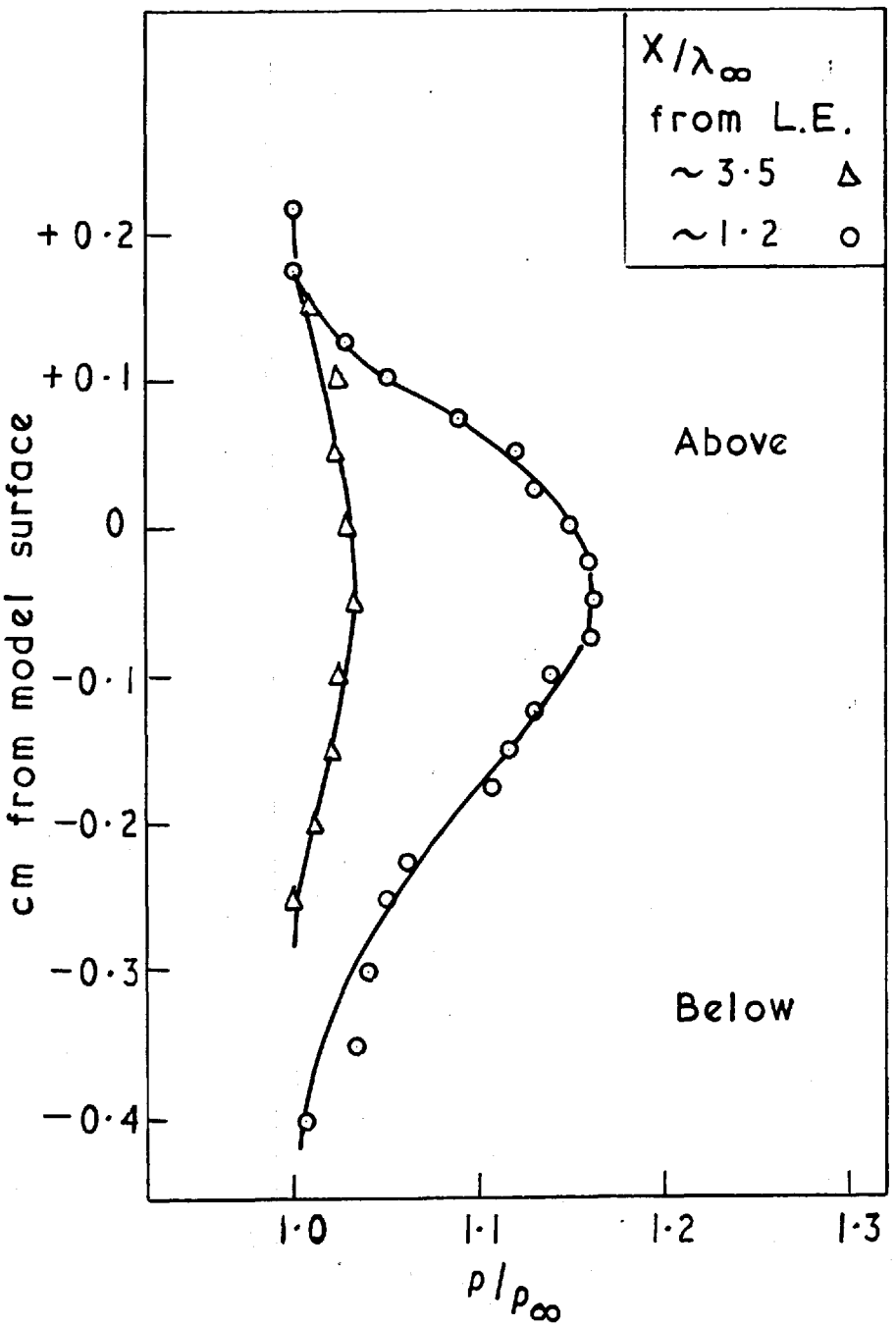

FIG.23 DENSITY PROFILES AHEAD OF LEADING EDGE: $M=5{\cdot}8$. $Re_\infty/cm=160$

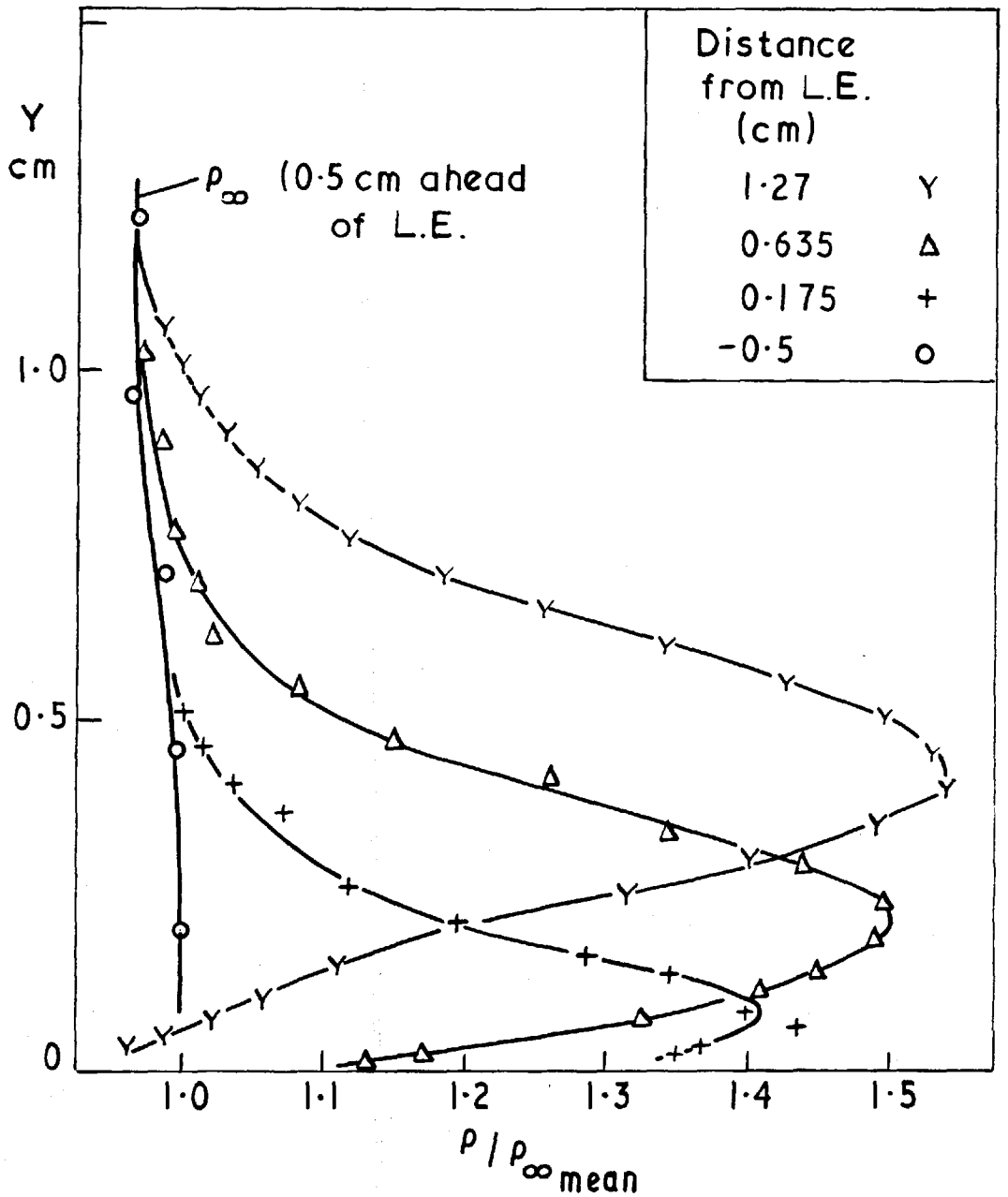

FIG. 24 TYPICAL DENSITY PROFILES THROUGH THE SHOCK LAYER: $M = 5{\cdot}8$. $Re_\infty / cm = 160$

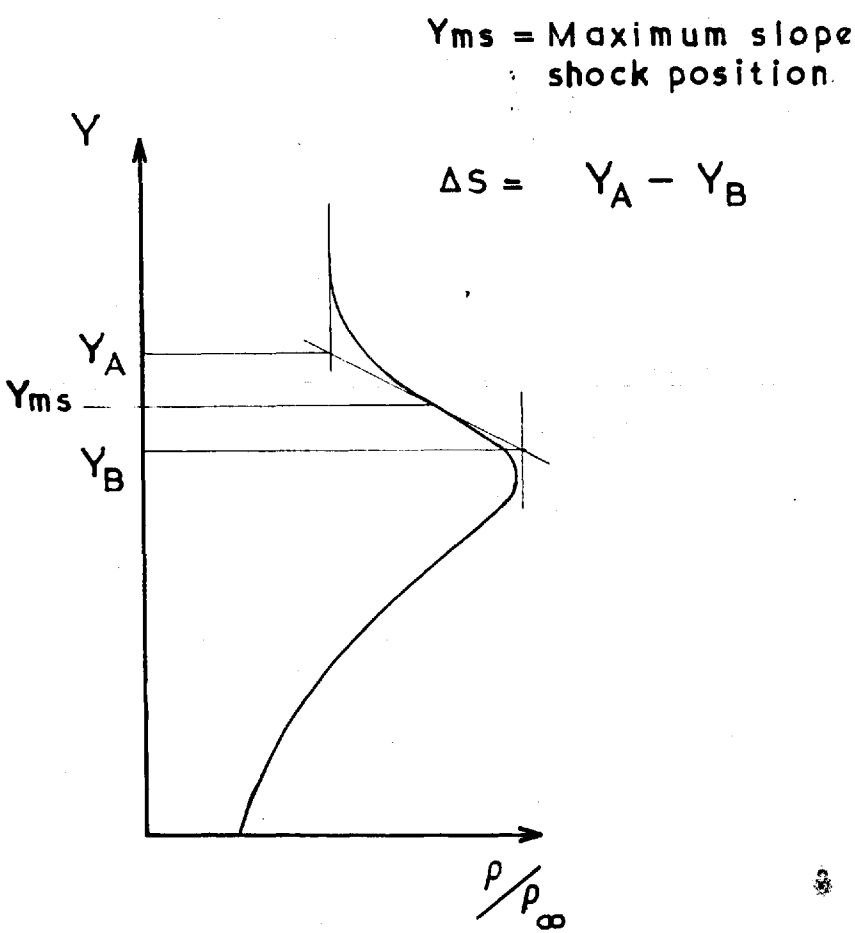

FIG. 25 (a) Maximum slope definition of shock wave.

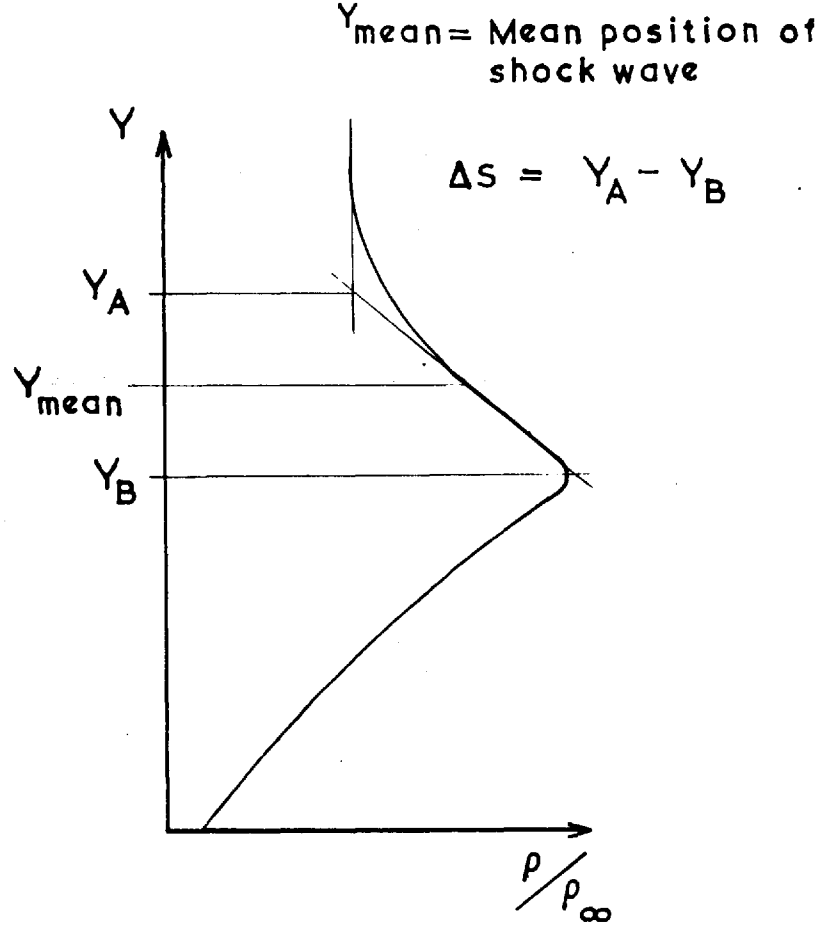

FIG. 25 (b) Definition of shock near leading edge.

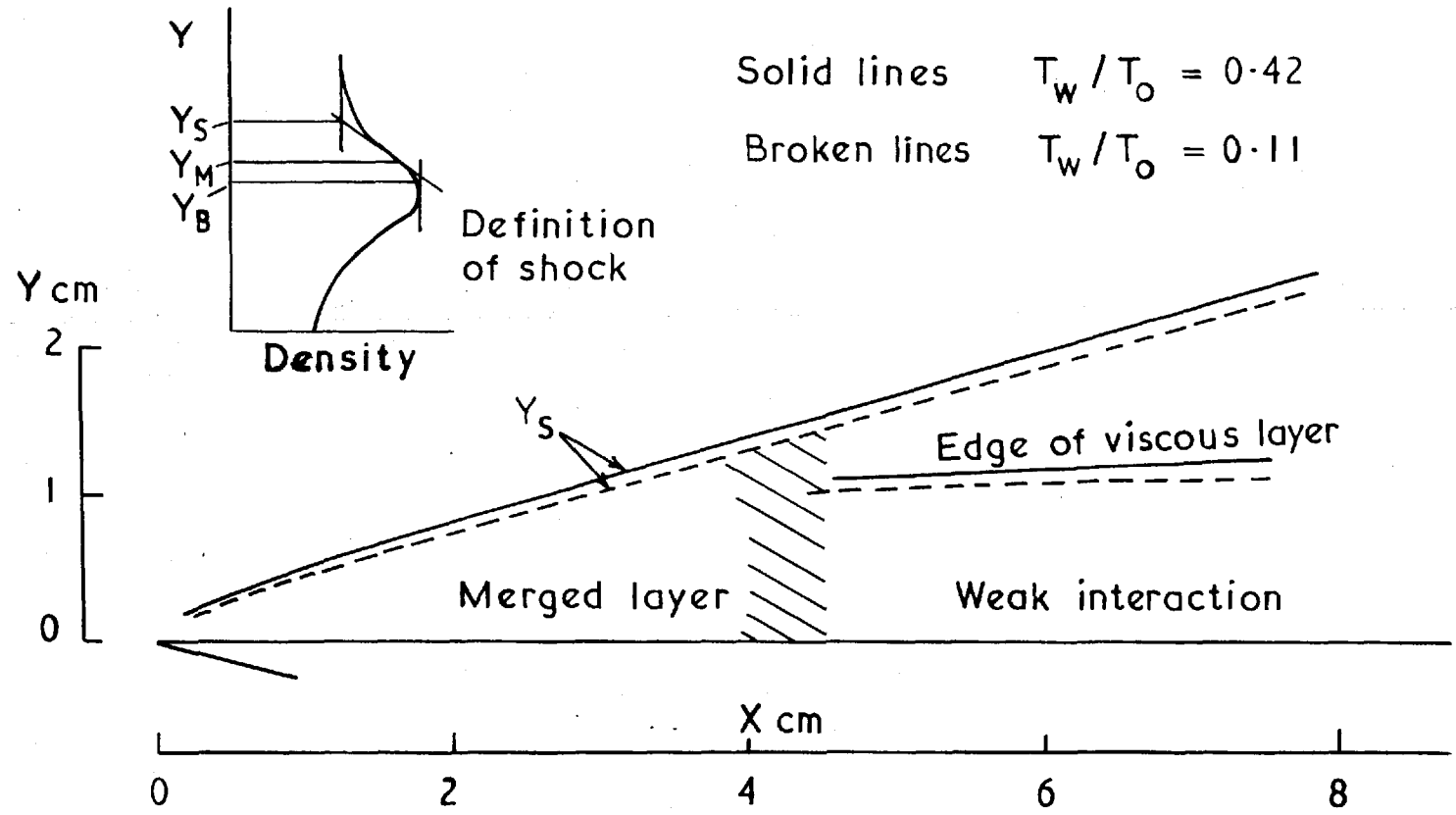

FIG.26 FLOW FIELD MODEL DETERMINED FROM ELECTRON BEAM DATA. M = 6·08 : Re/cm = 260

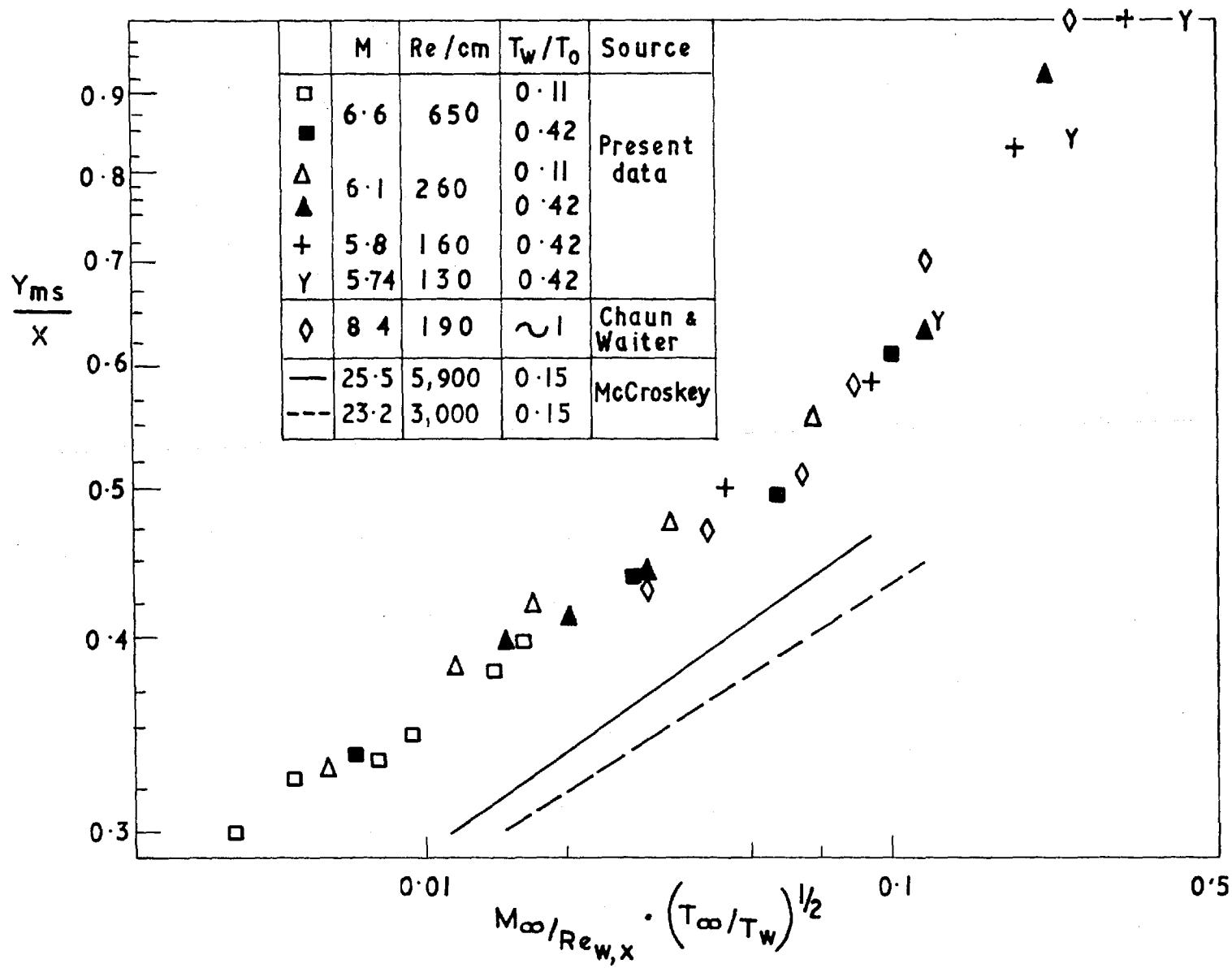

FIG. 27. Correlation of shock shape

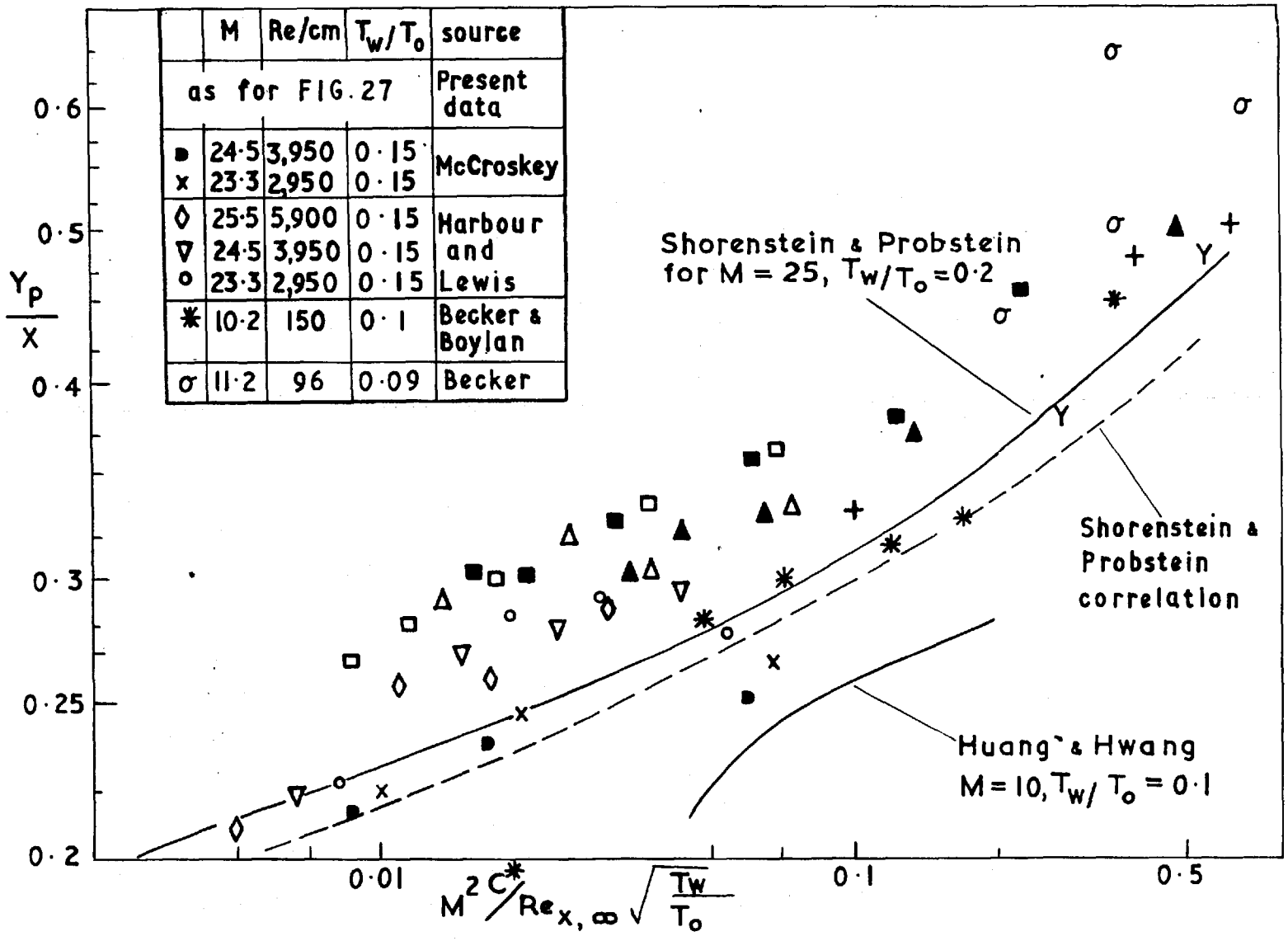

FIG. 28 Comparison of experimental and theoretical shock positions.

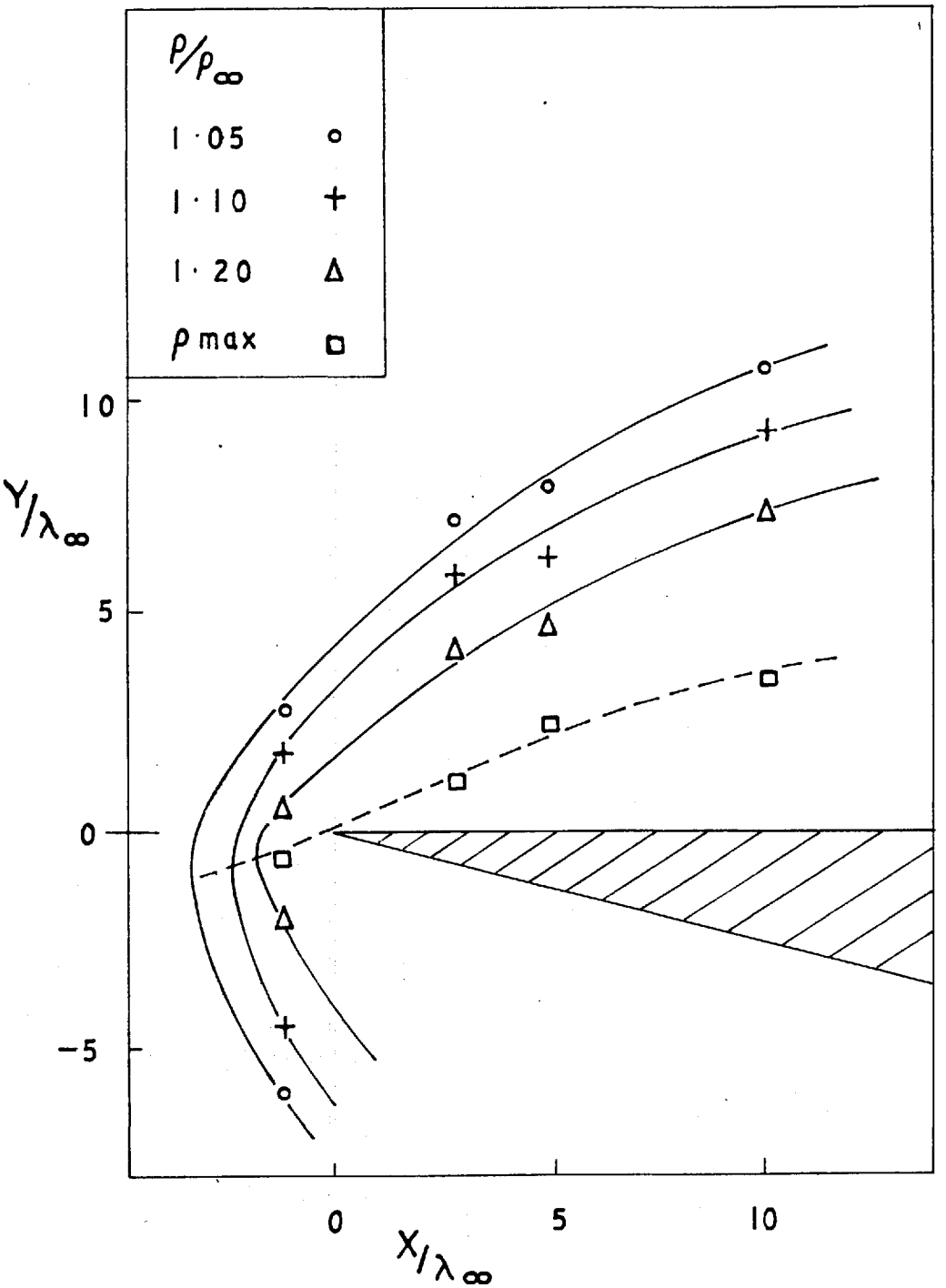

FIG. 29. Contours of constant density for M = 5·74 λ_∞ = 0·64 mm.

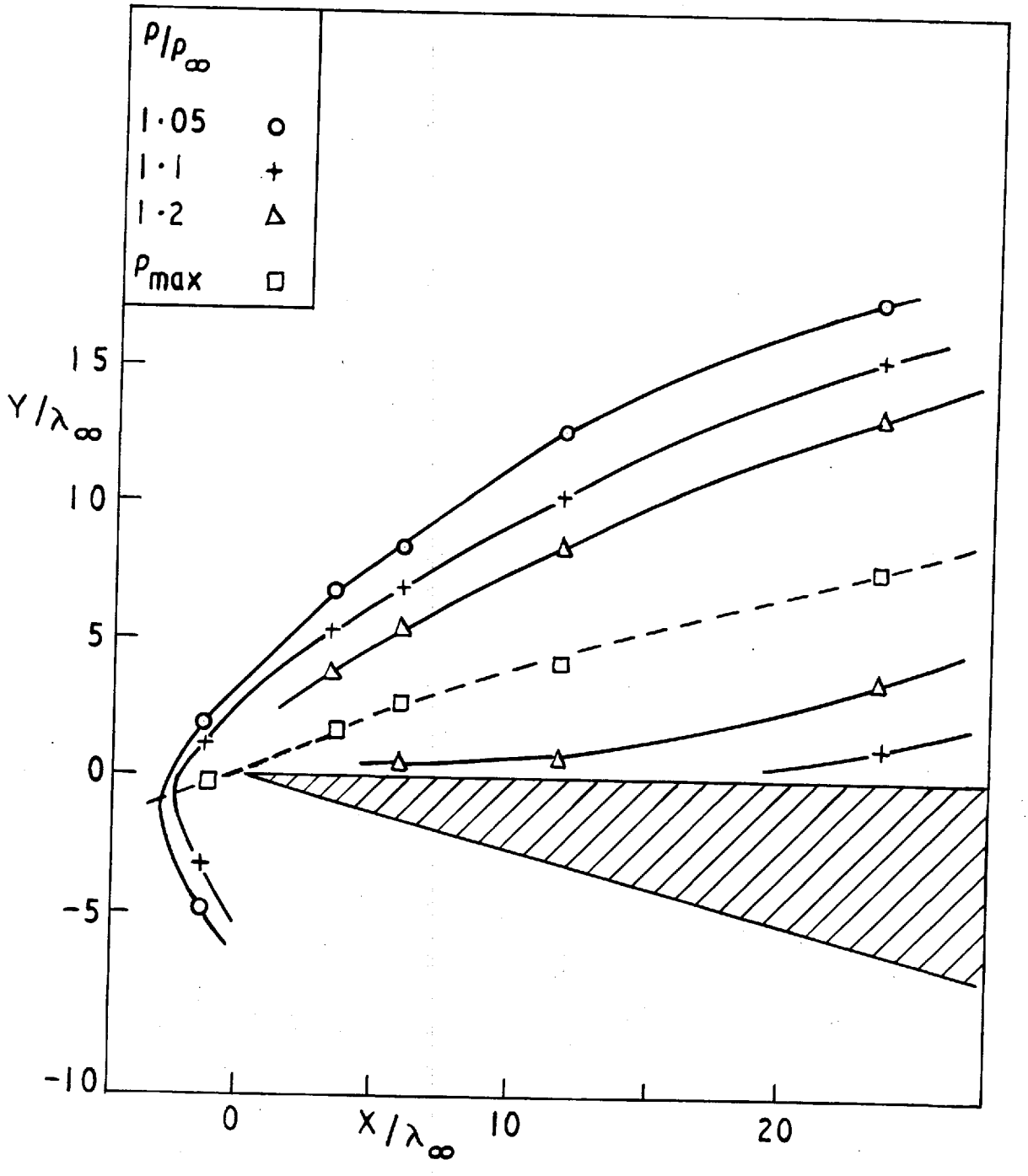

FIG. 30 CONTOURS OF CONSTANT DENSITY FOR $M = 5 \cdot 8$. $\lambda_\infty = 0 \cdot 54$ mm

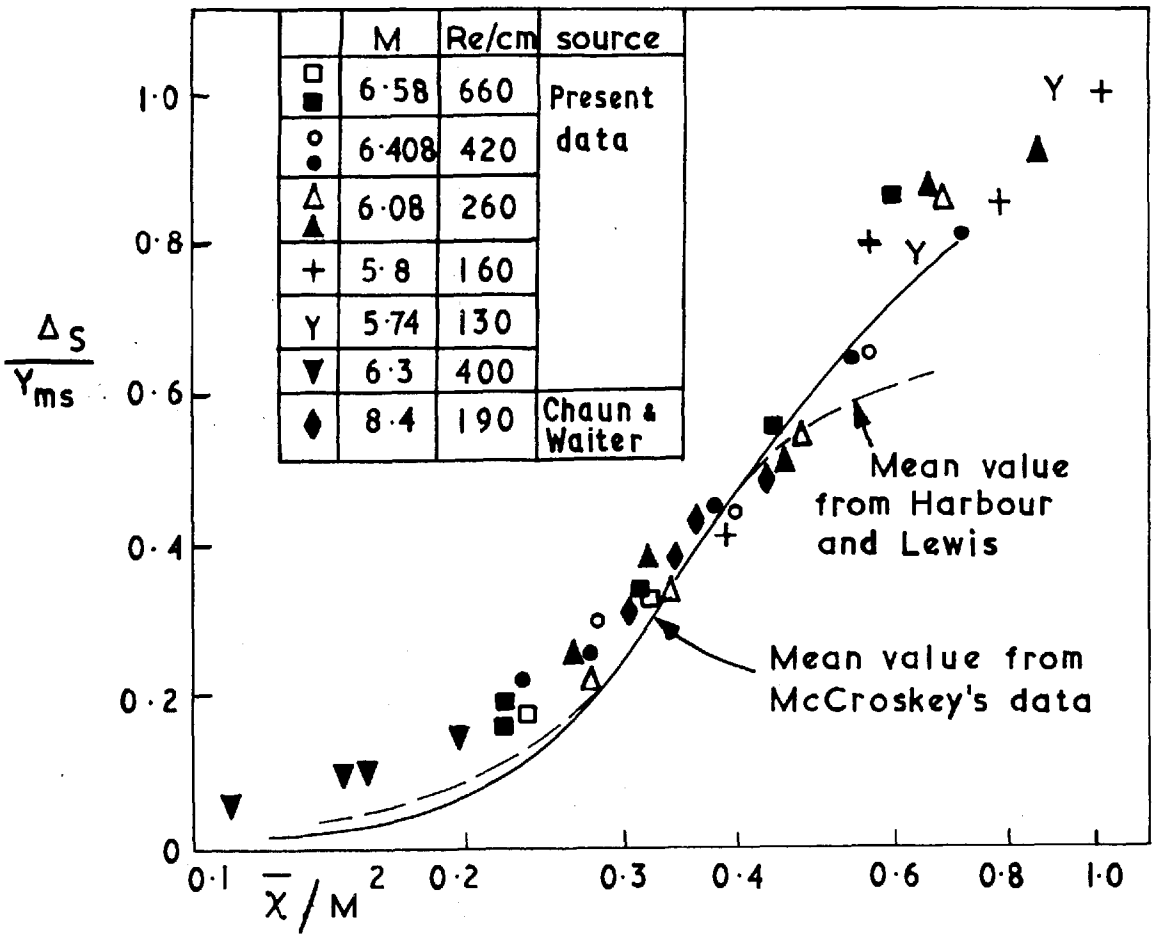

FIG.31. Correlation of shock thickness

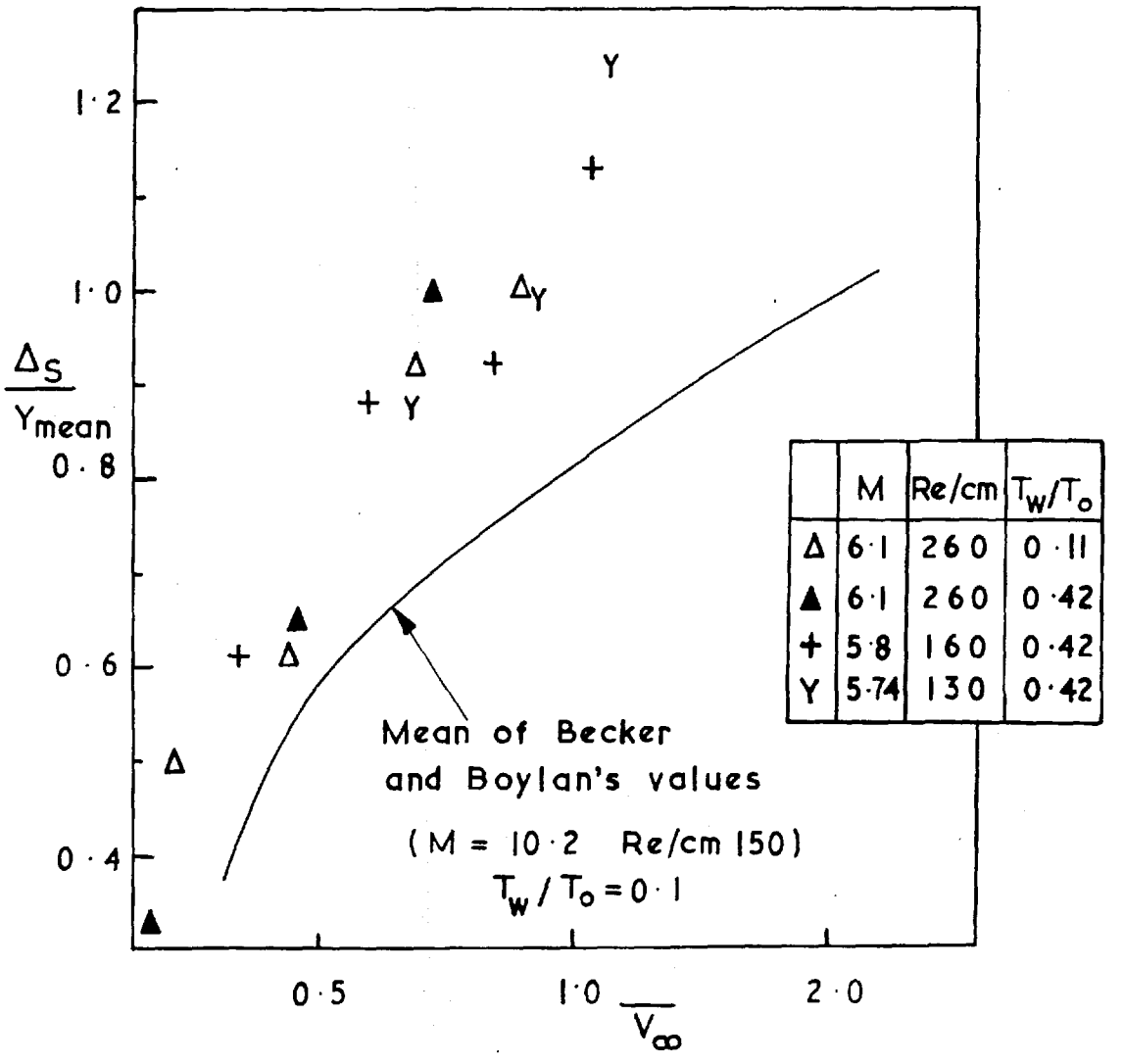

FIG. 32 Shock thickness defined in terms of Y_{mean}.

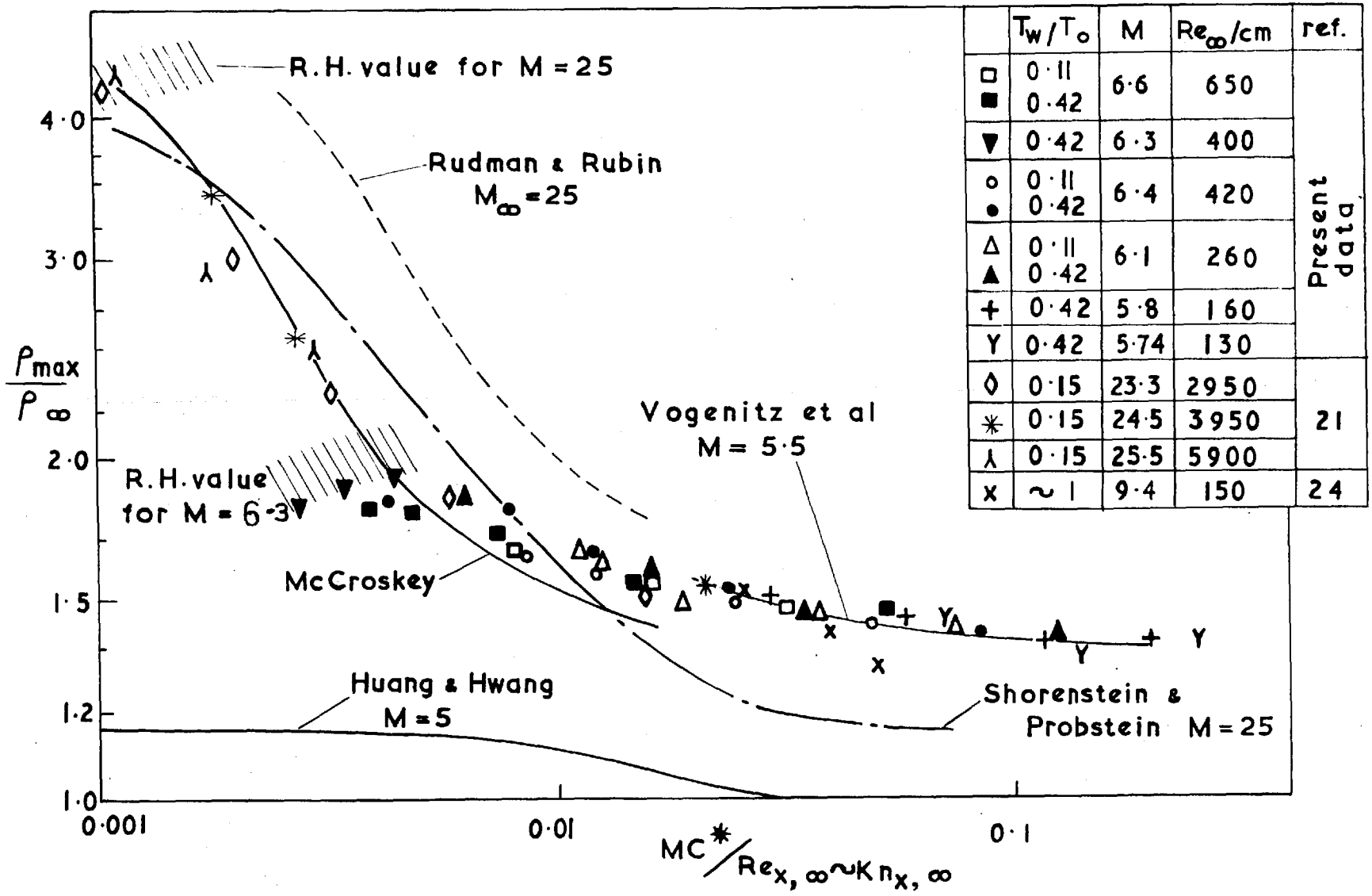

FIG. 33 Correlation of shock strength ρ_{max}/ρ_∞.

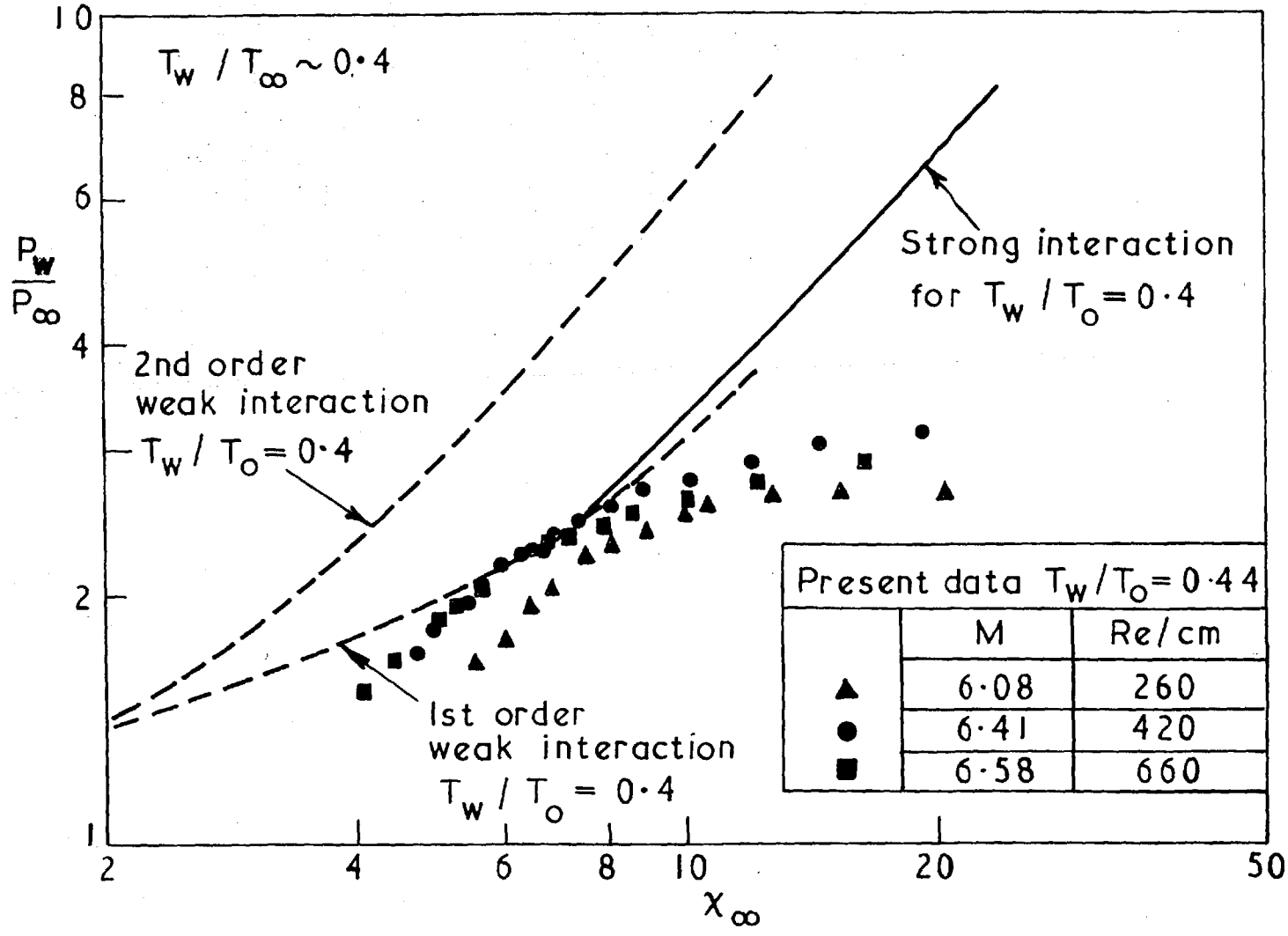

FIG 34. Surface Pressure

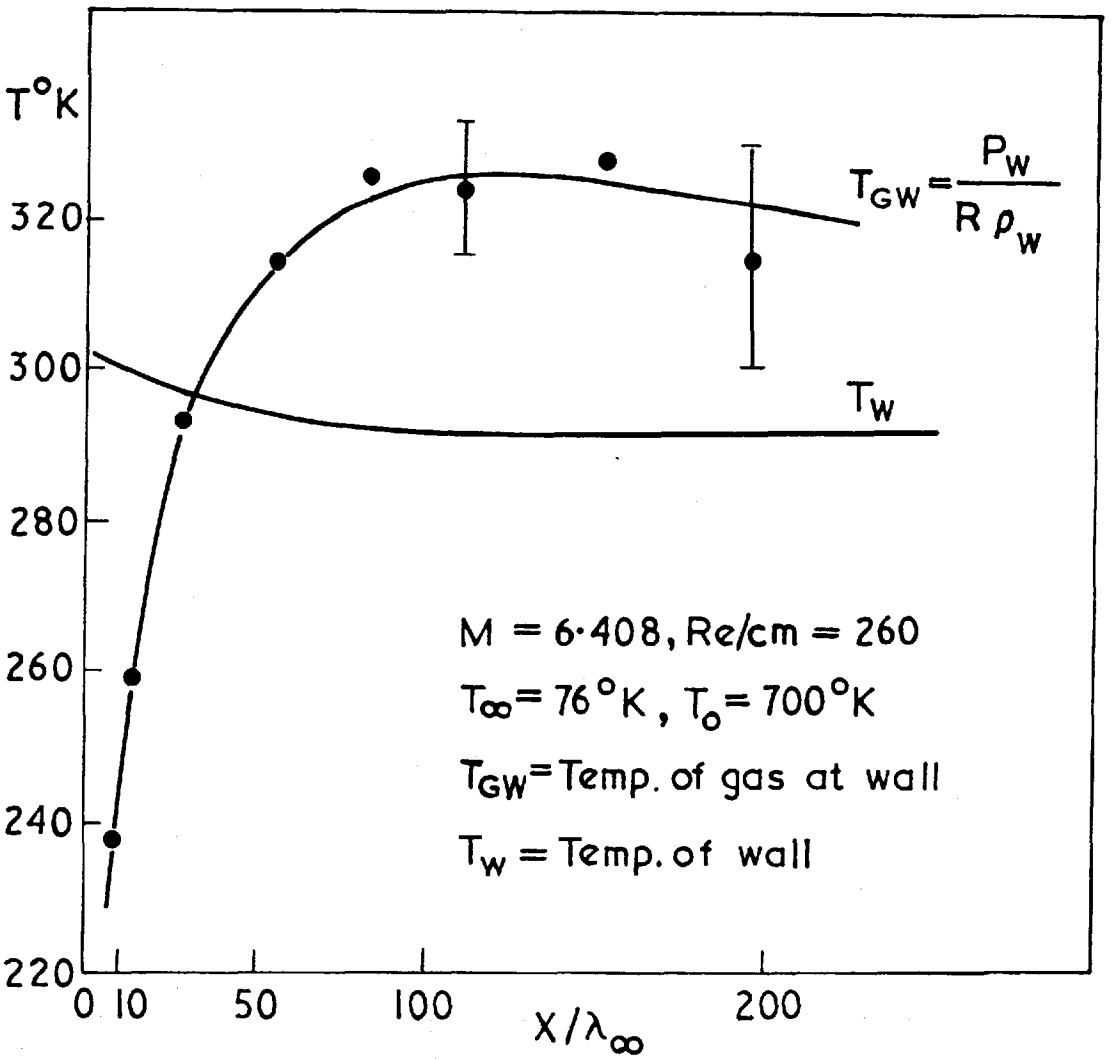

FIG.35 TEMPERATURE OF GAS AT THE SURFACE OF MODEL

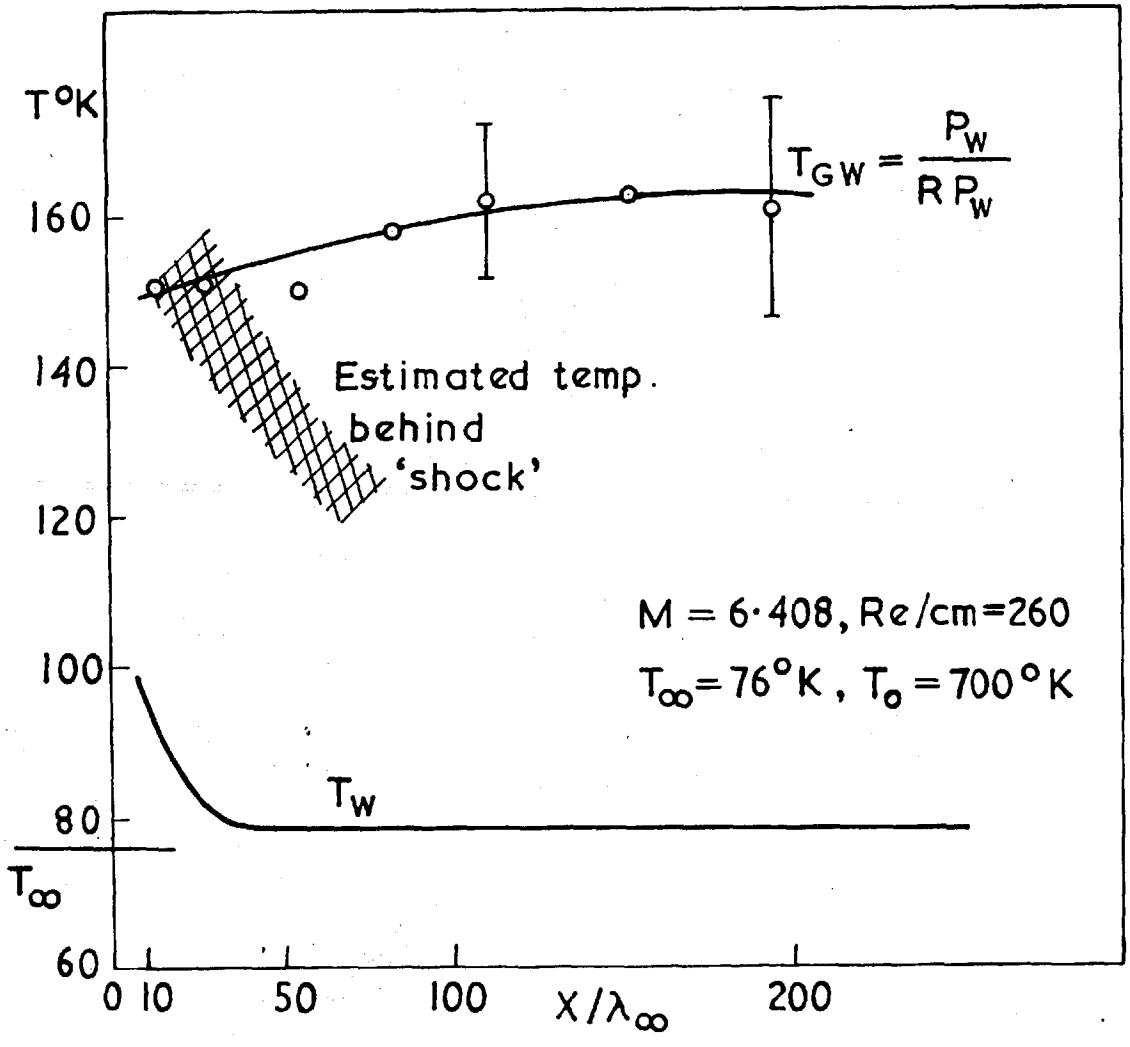

FIG.36 TEMPERATURE OF GAS AT SURFACE OF MODEL

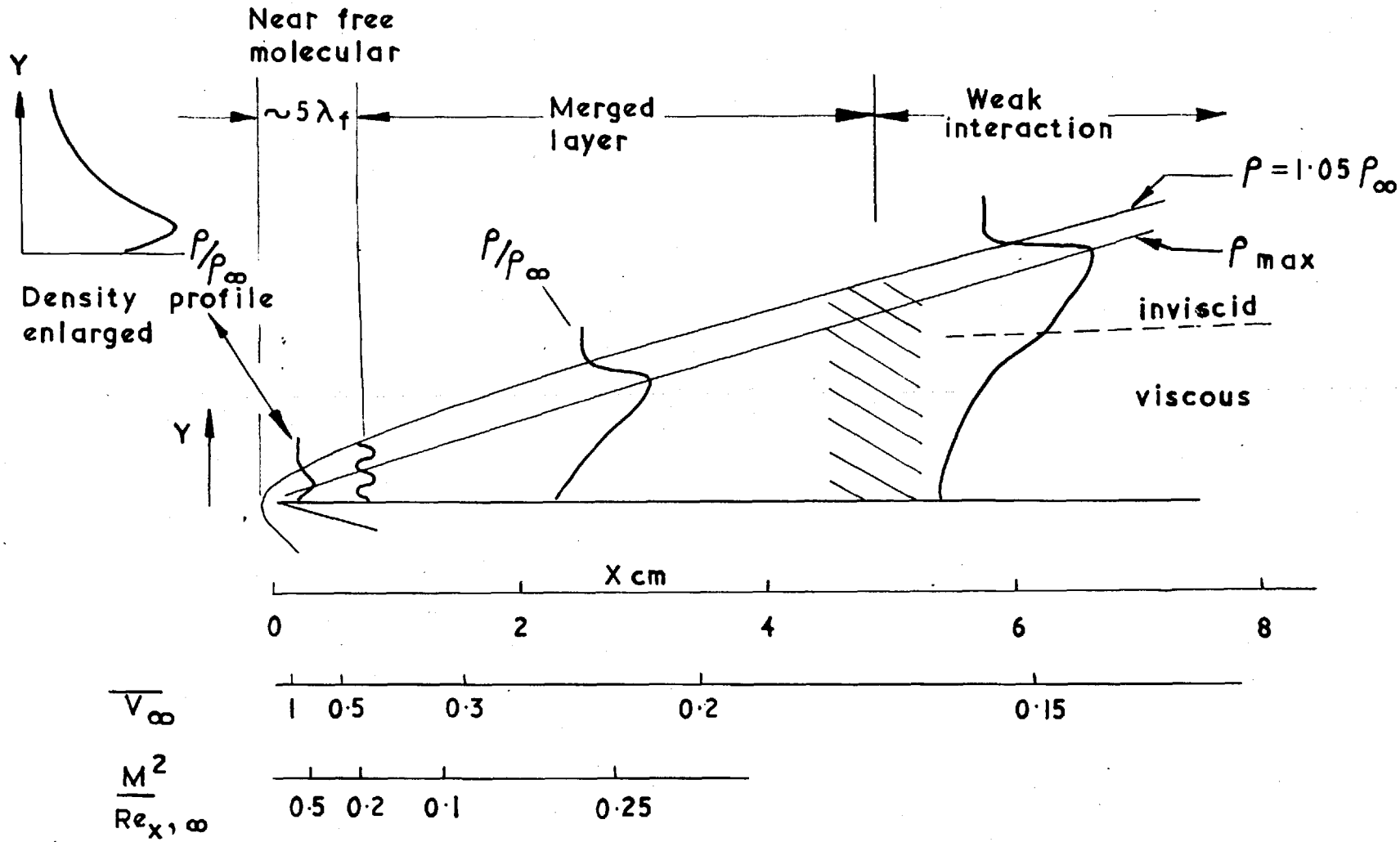

FIG. 37. Schematic representation of flow field. $M \triangleq 6$, $\lambda_\infty = 0.35$ mm, $T_w/T_o = 0.42$ and density profiles.

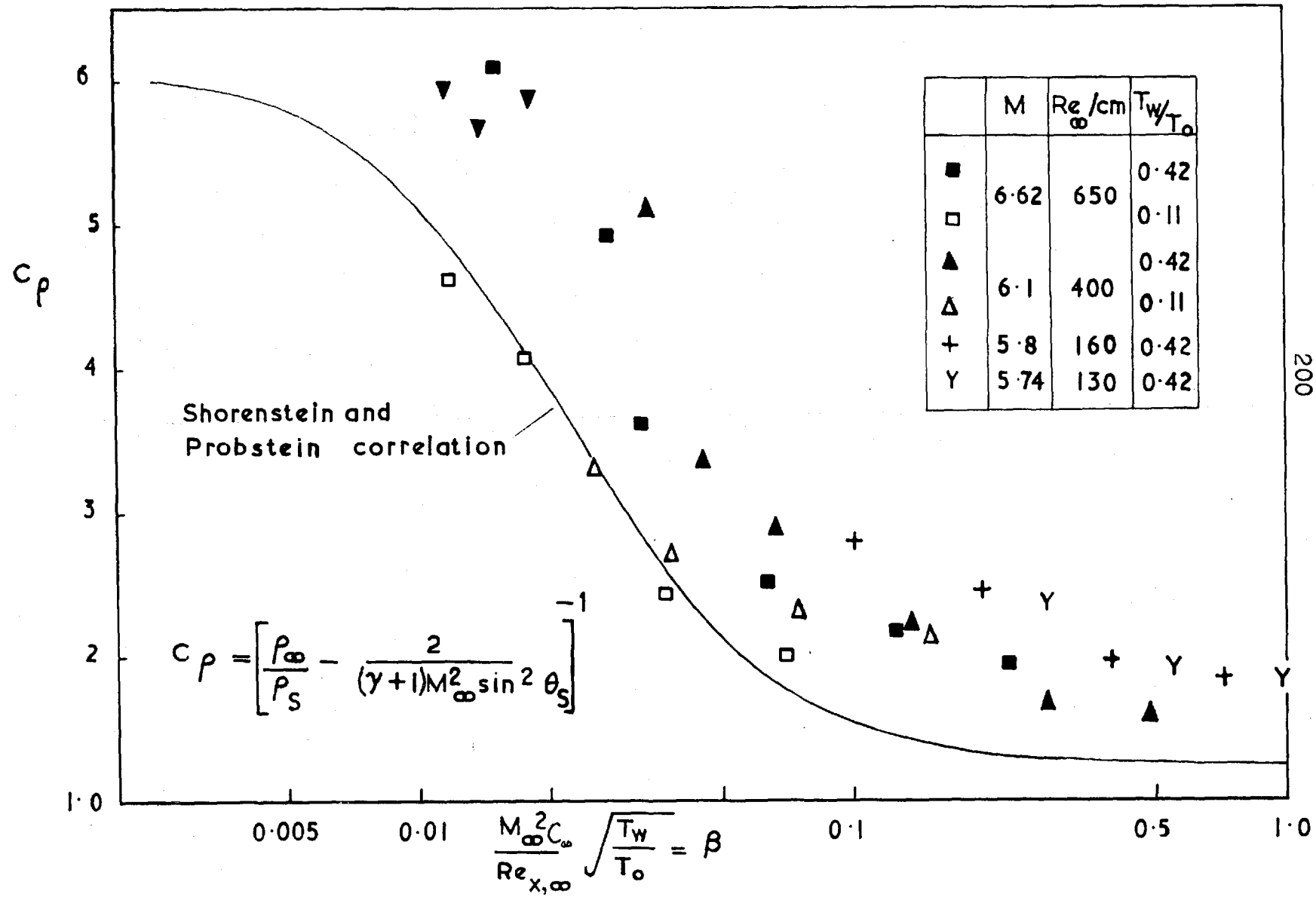

FIG. 38 Shock strength compared with correlation formula

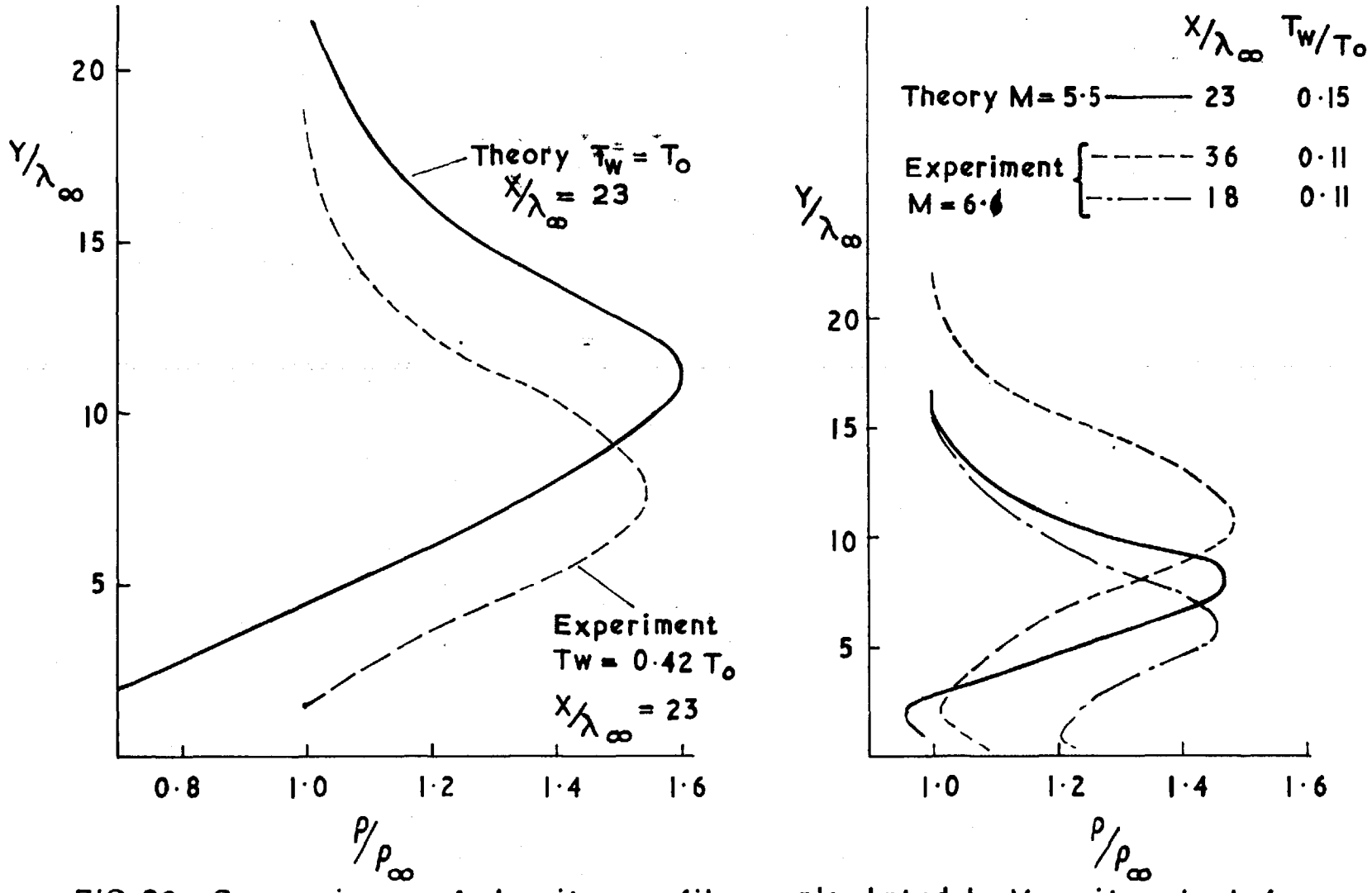

FIG. 39 Comparison of density profiles calculated by Vogenitz et al for M = 5·5, with present experiment for M = 5·8 To 6·1.

TABLE A1·1

Mean flow conditions used in the experiments

Small nozzle T_o 700 °K			
H_o mm Hg	M	Re_∞/cm	$\rho_\infty \frac{GRM}{cm^3} \times 10^7$
120	6·59	650	2·64
74·6	6·5	410	1·71
40	6·1	260	1·24
Large nozzle T_o = 632 °K			
60	6·3	390	1·78
20	5·8	160	·85
15	5·74	130	·67

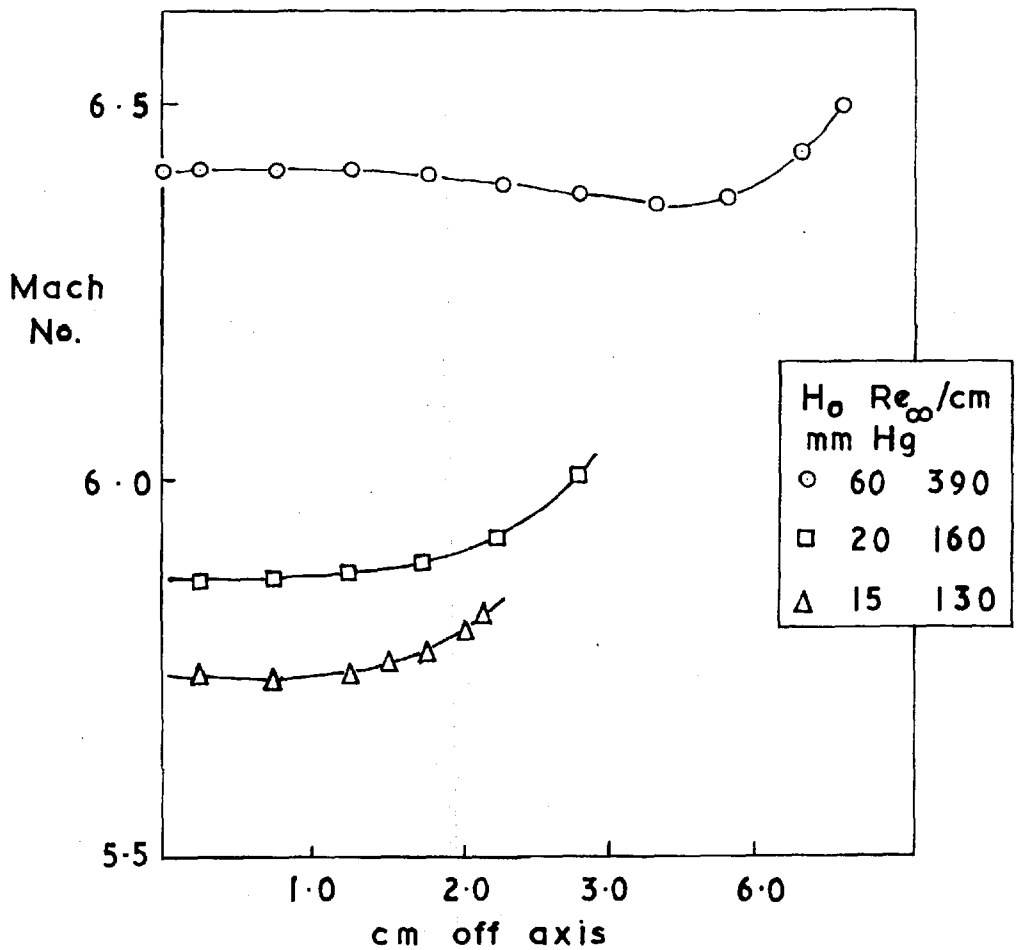

FIG. A1.1. Cross traverses at exit plane large nozzle – 14 cm exit diameter.

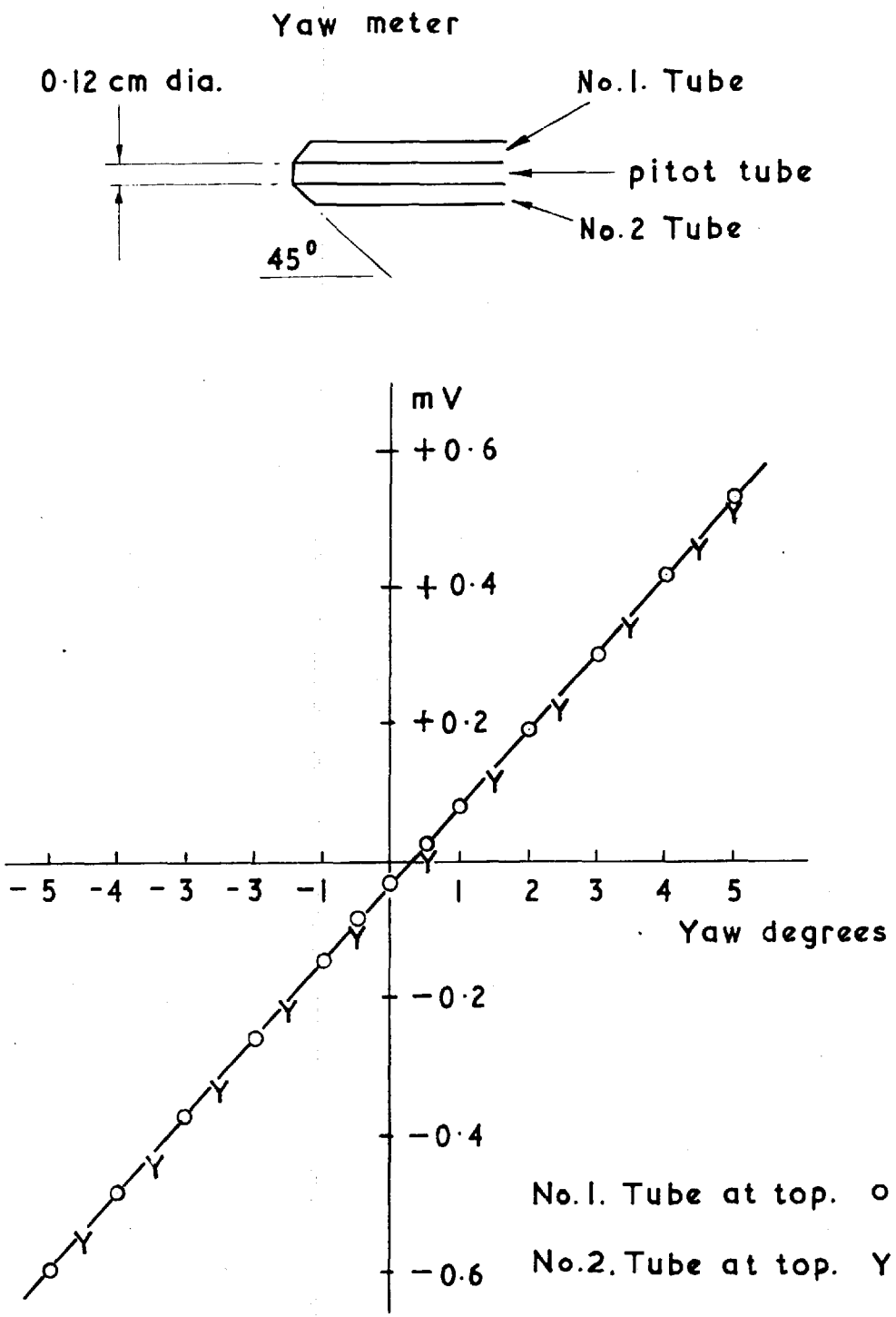

FIG. A1.2. Calibration of yaw meter.

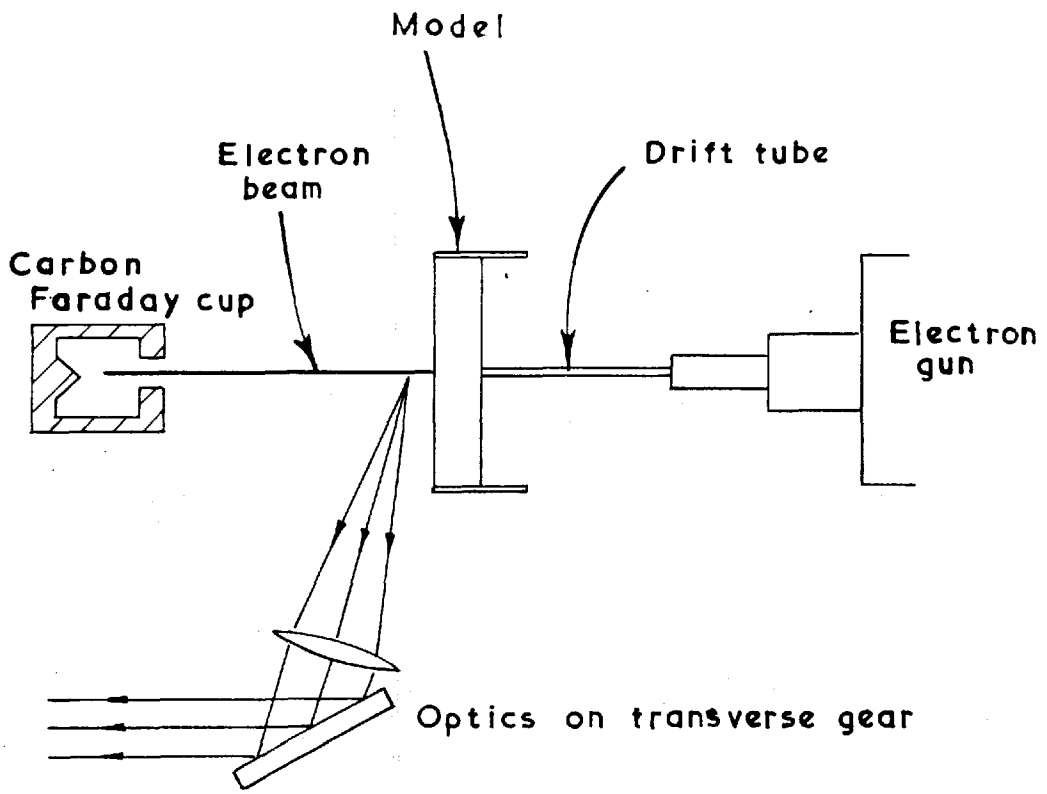

FIG. A2·1. Electron beam arrangement for density measurements.

(view from downstream of model).

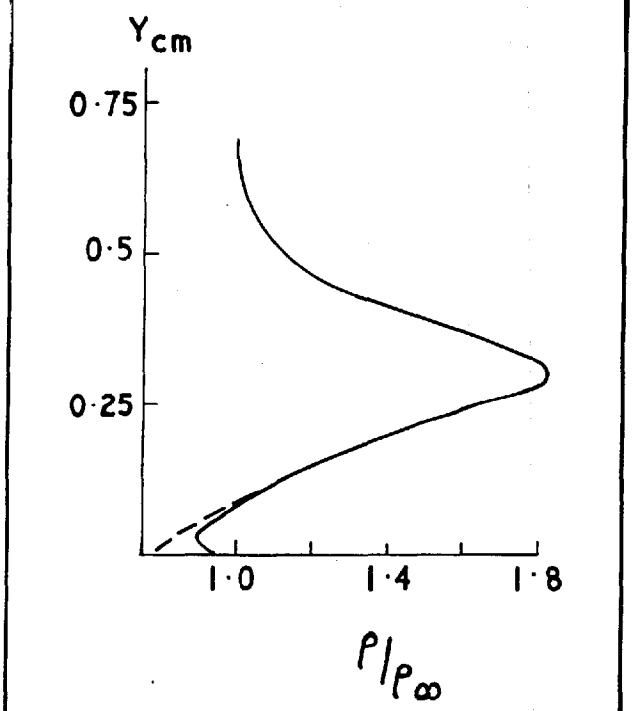

FIG. A2·2 Density profile: uncooled flat plate X=0·76 cm.

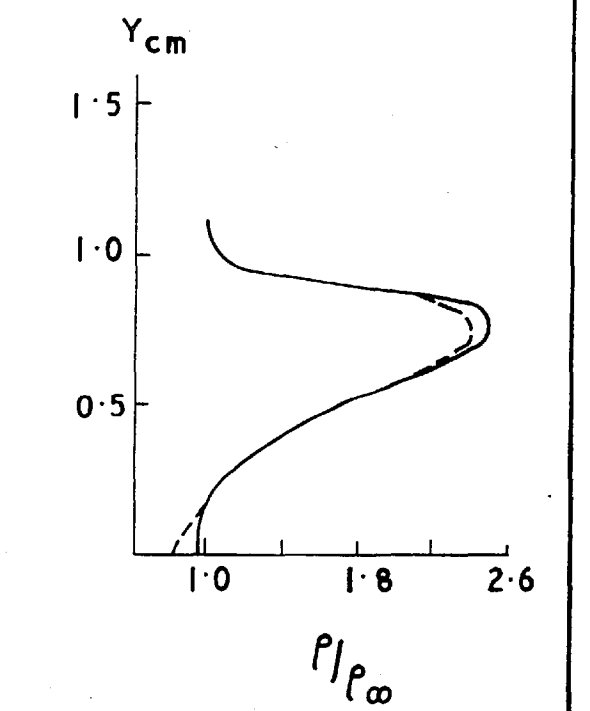

FIG. A2·3. Density profile: uncooled 15° wedge X= 2·54 cm.

M= 6·41 Re_∞ 410 cm^{-1}
No drift tube ——
Drift tube used----

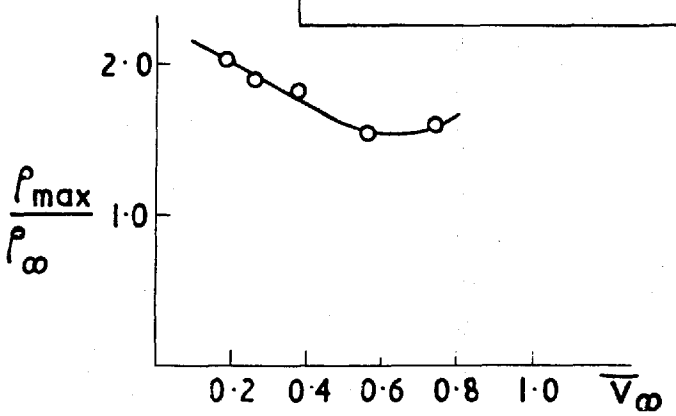

FIG. A 2·4 Density ratio across the shock for uncooled flat plate

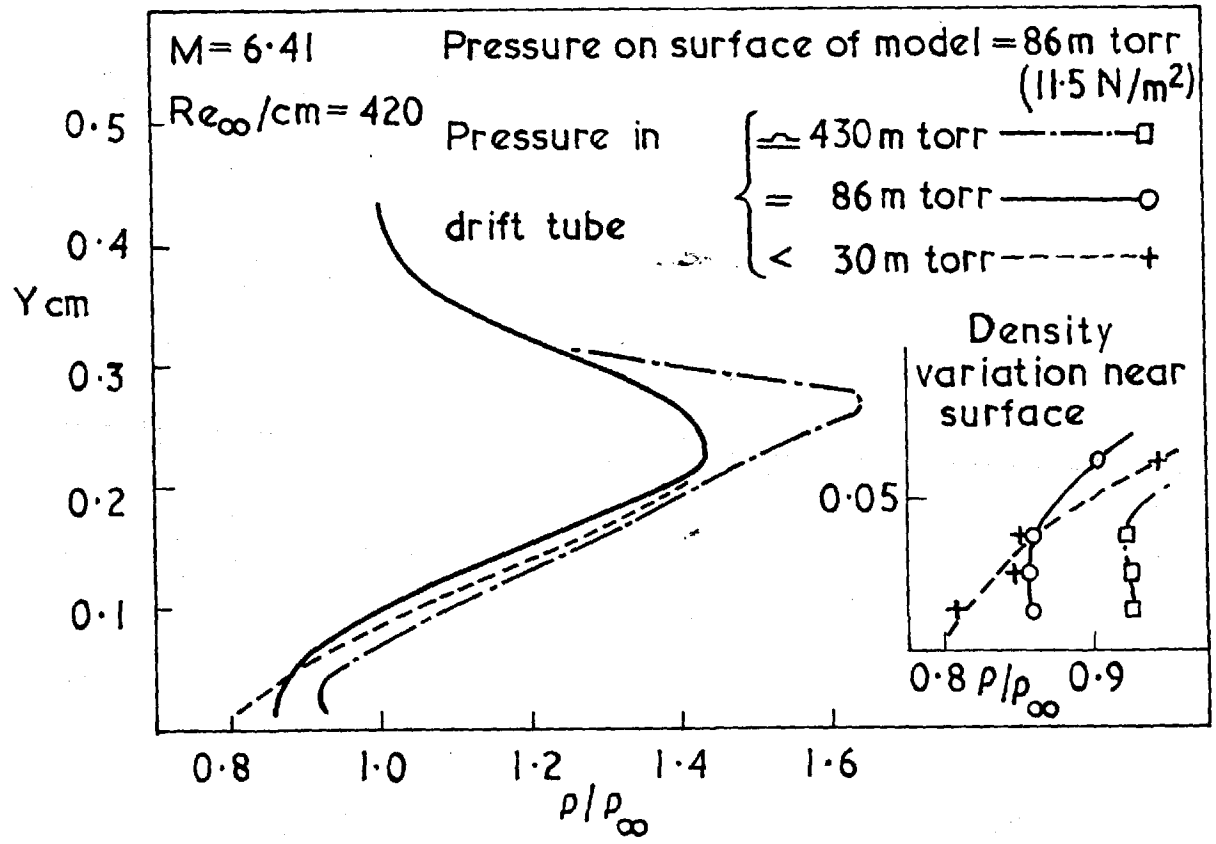

FIG A2·5 The effect of varying the pressure in the Drift Tube

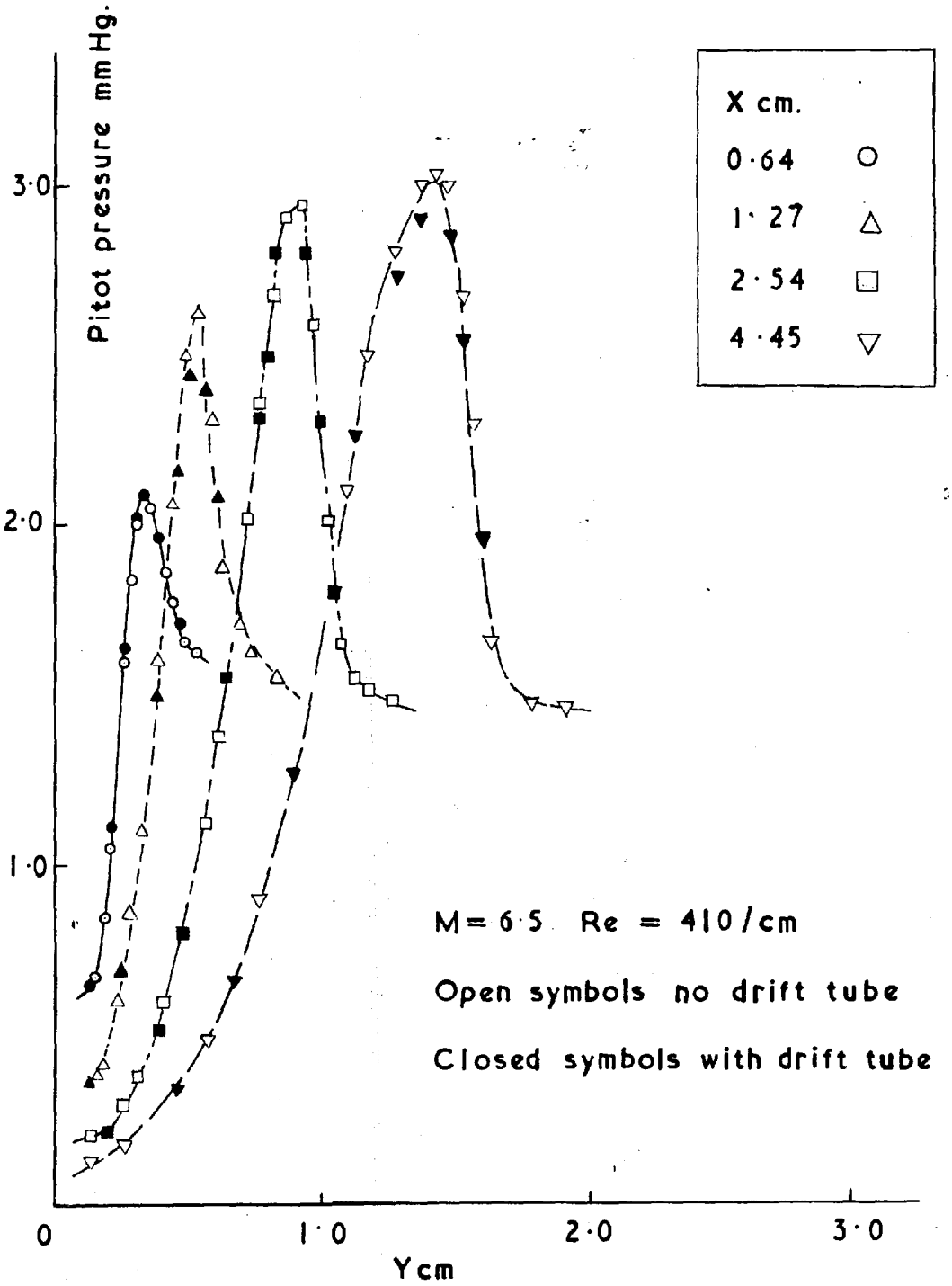

FIG. A 2·6 Pitot traverses through the shock layer with and without drift tube 0·175 cm from L.E.

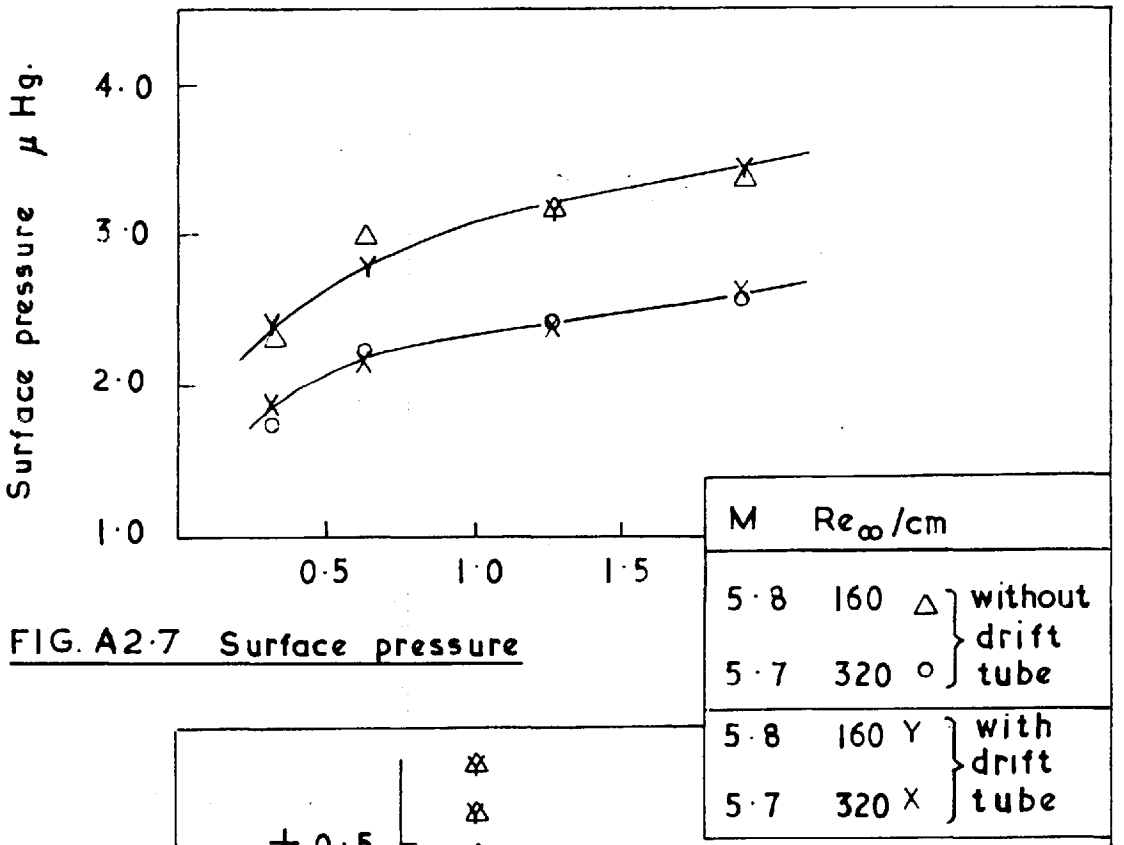

FIG. A2·7 Surface pressure

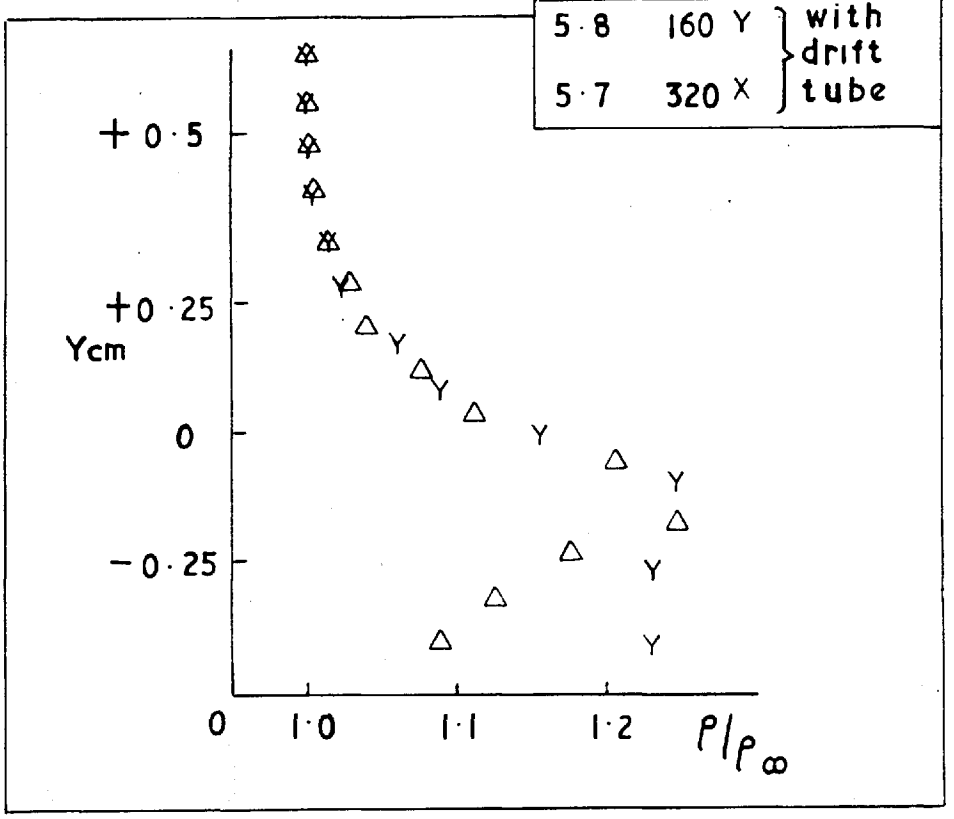

FIG. A2·8 Density profile 0·076 cm upstream of model leading edge.

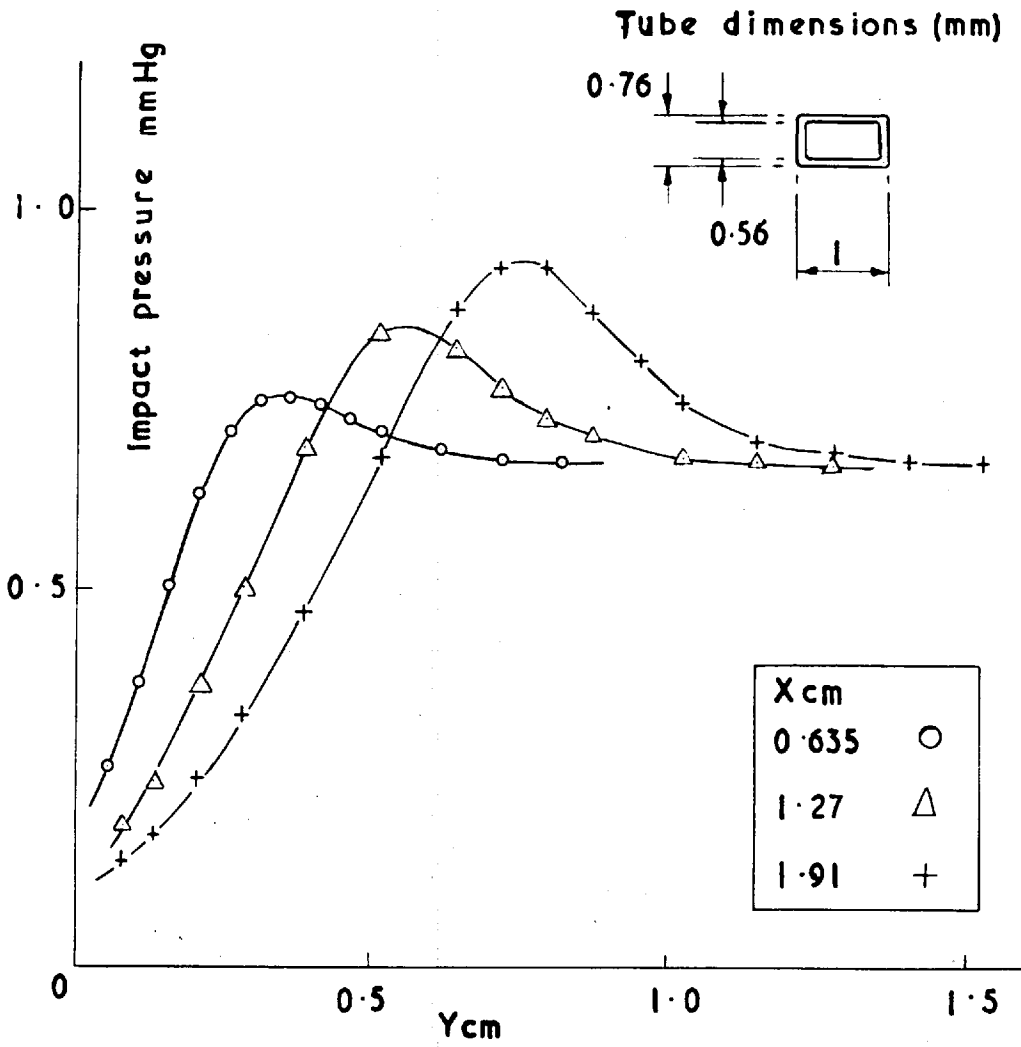

FIG. A2·9 Pitot traverses for $M = 5 \cdot 8$ and $Re_{\infty} = 160/cm.$

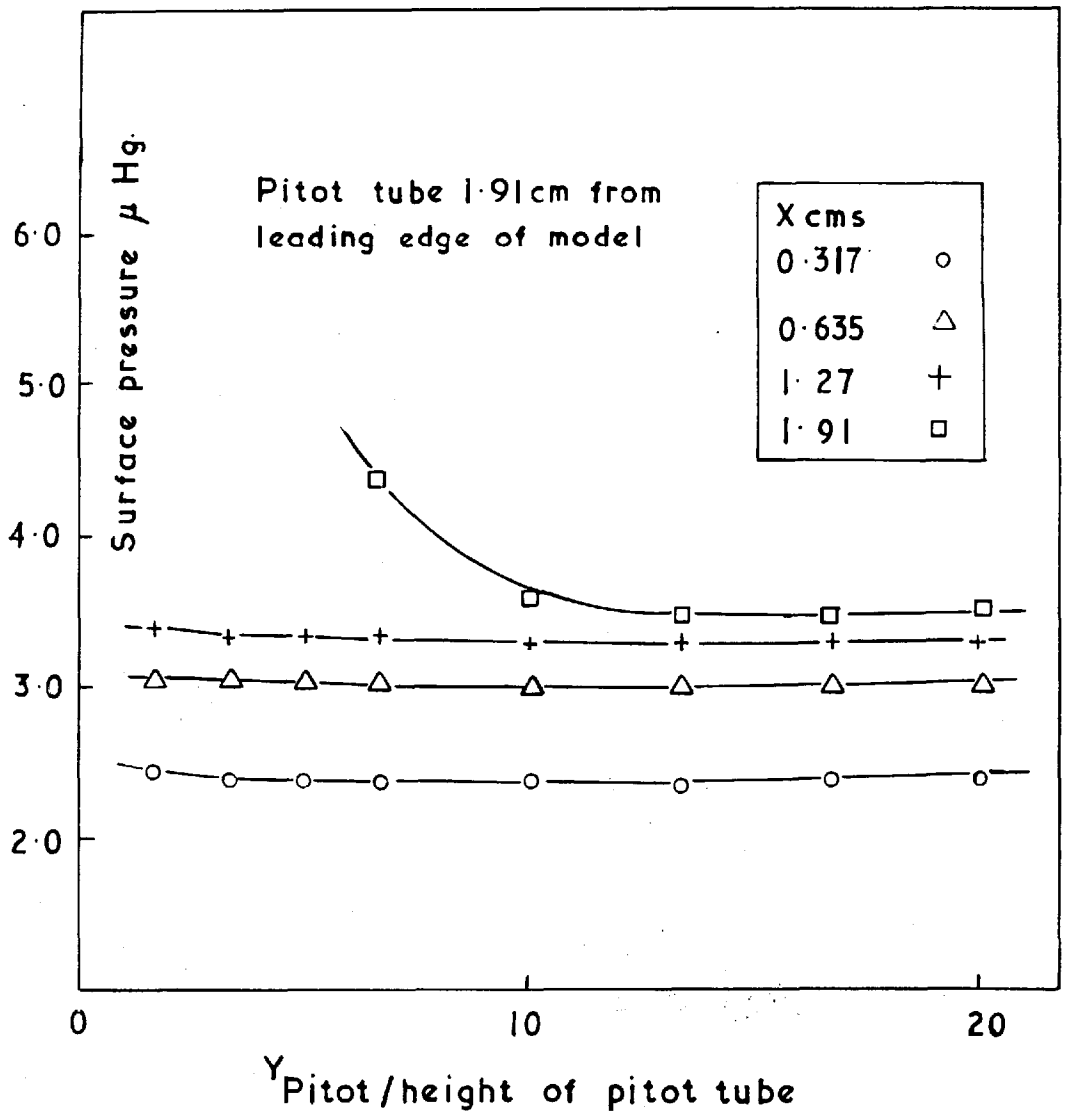

FIG. A2·10 Measured surface pressure as function of height of pitot tube above surface (Y_{pitot}).

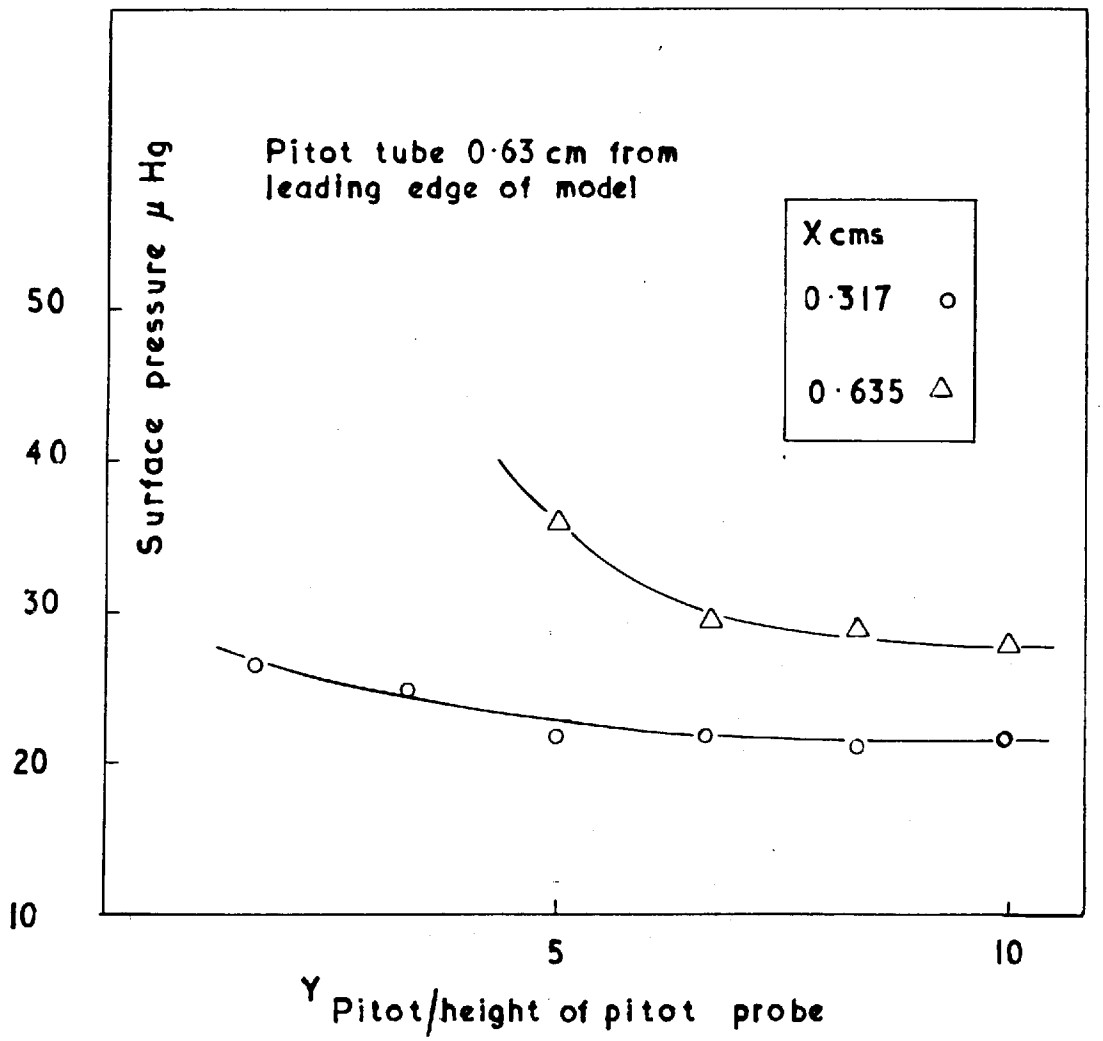

FIG.A2·11 Measured surface pressure as function of height of pitot tube above surface (Y_{pitot})

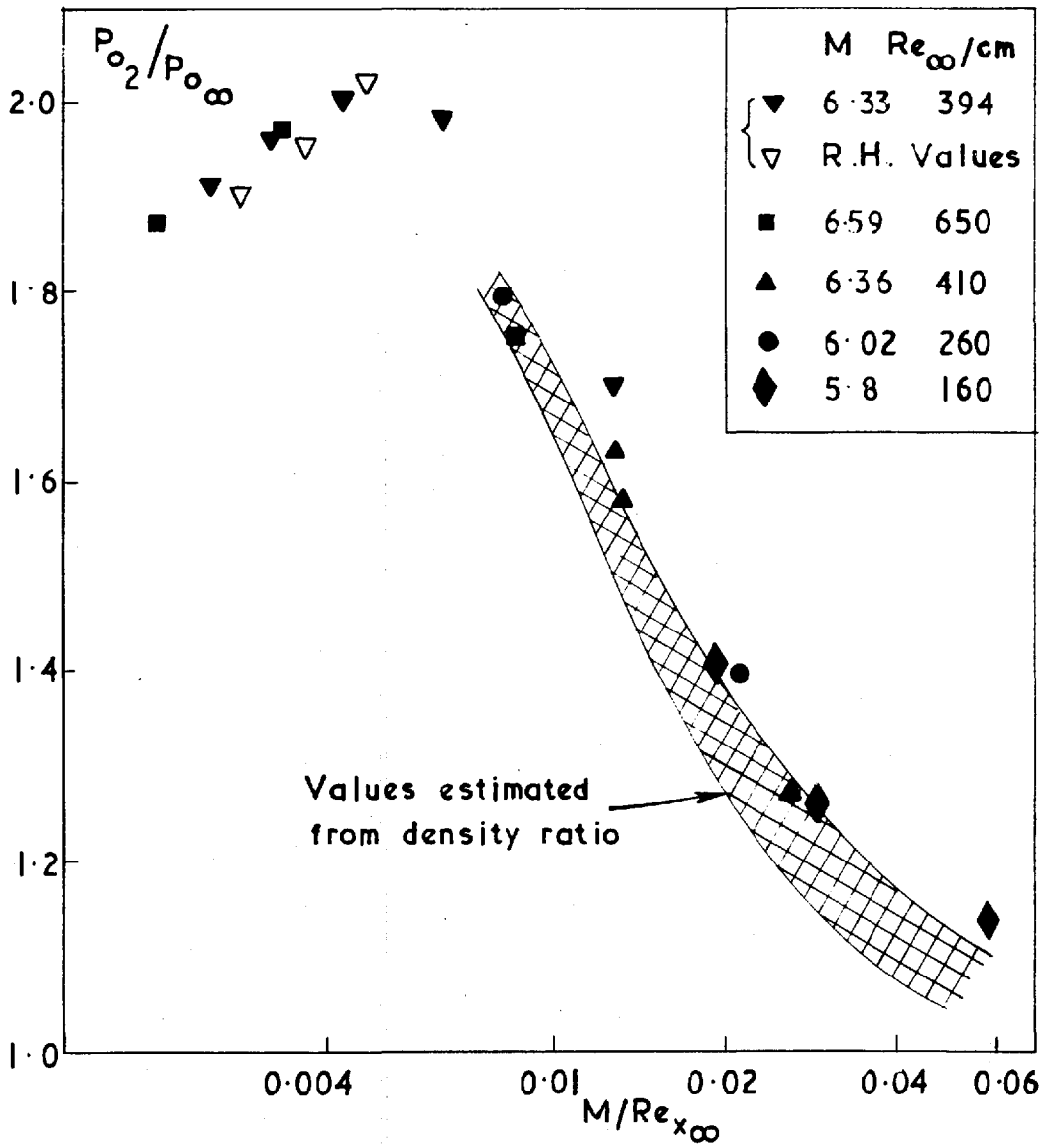

FIG.A2·12 Measured and calculated Pitot pressure ratio across the 'shock wave'.

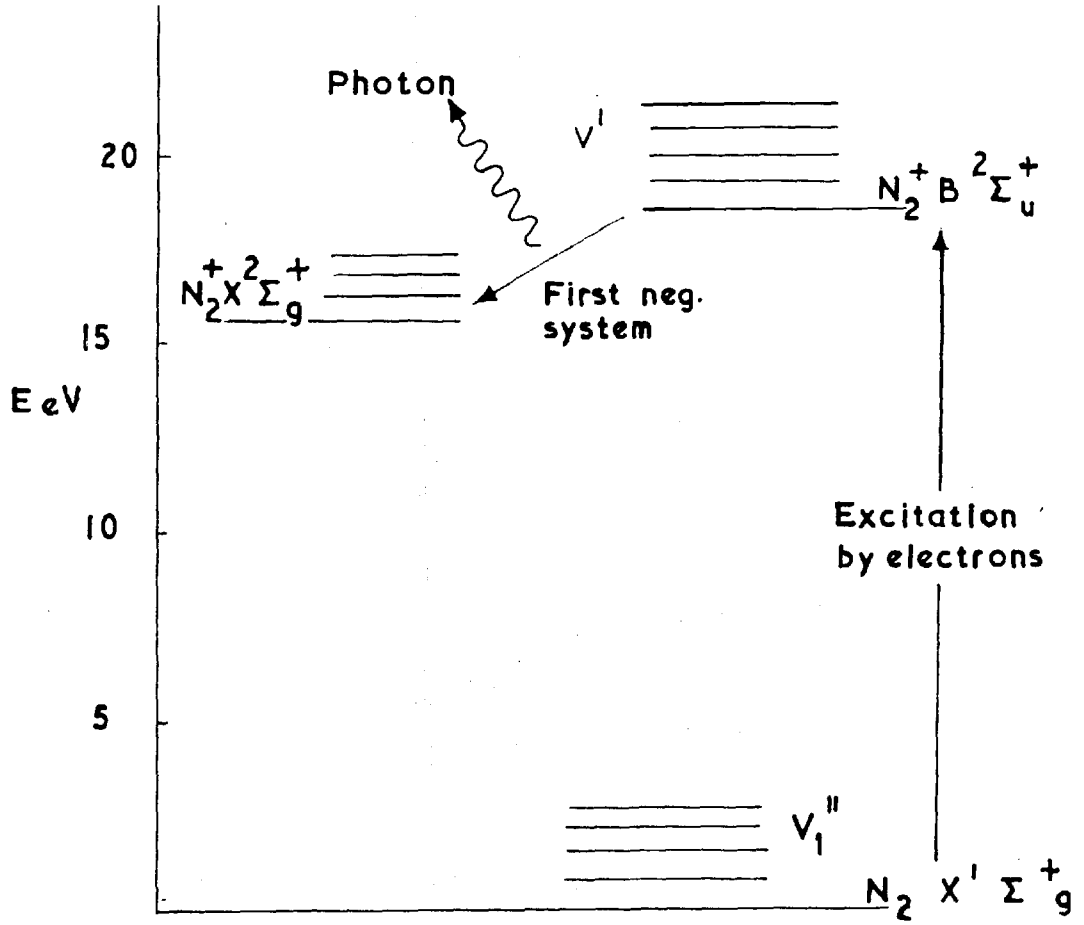

FIG. A 3·1 Excitation – emission path for first negative system

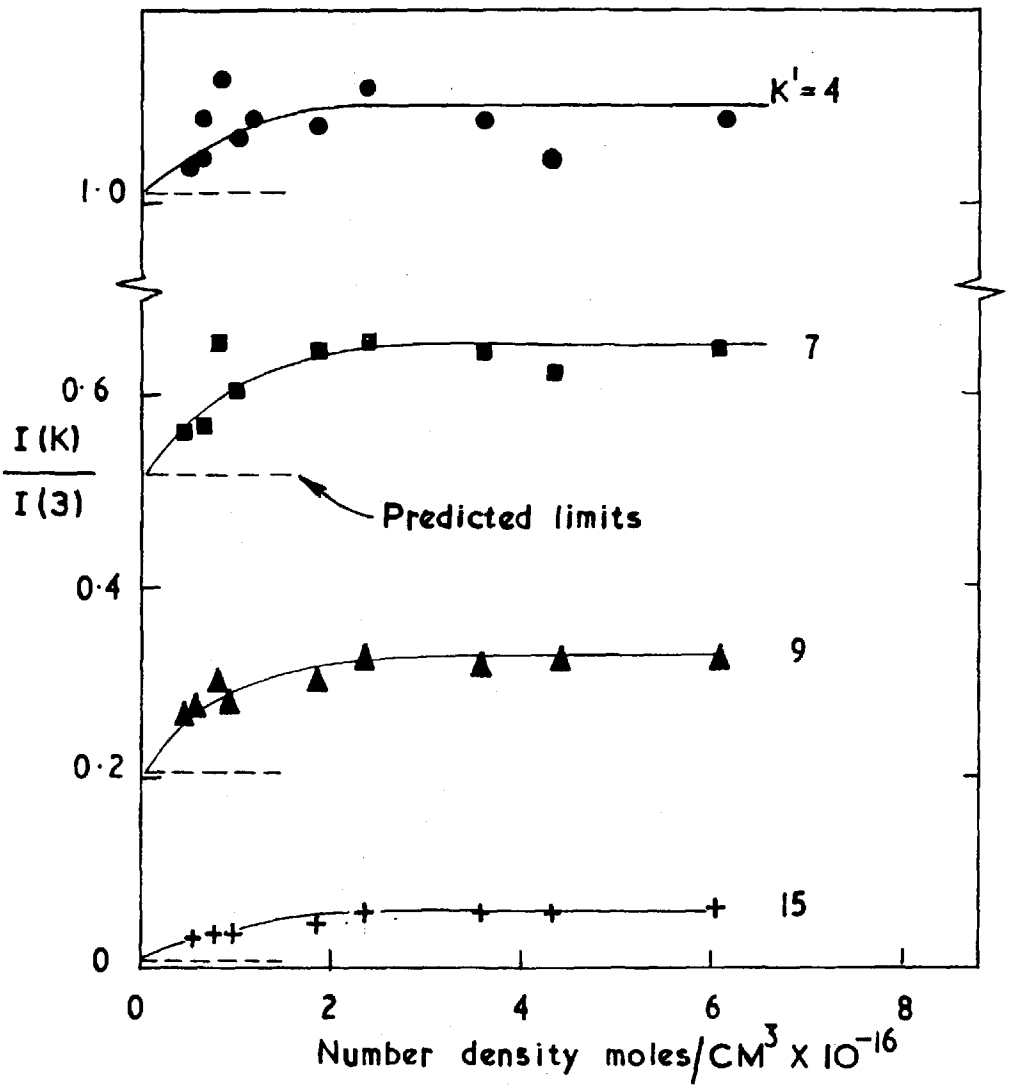

FIG.A 3·2 Normalised line intensities

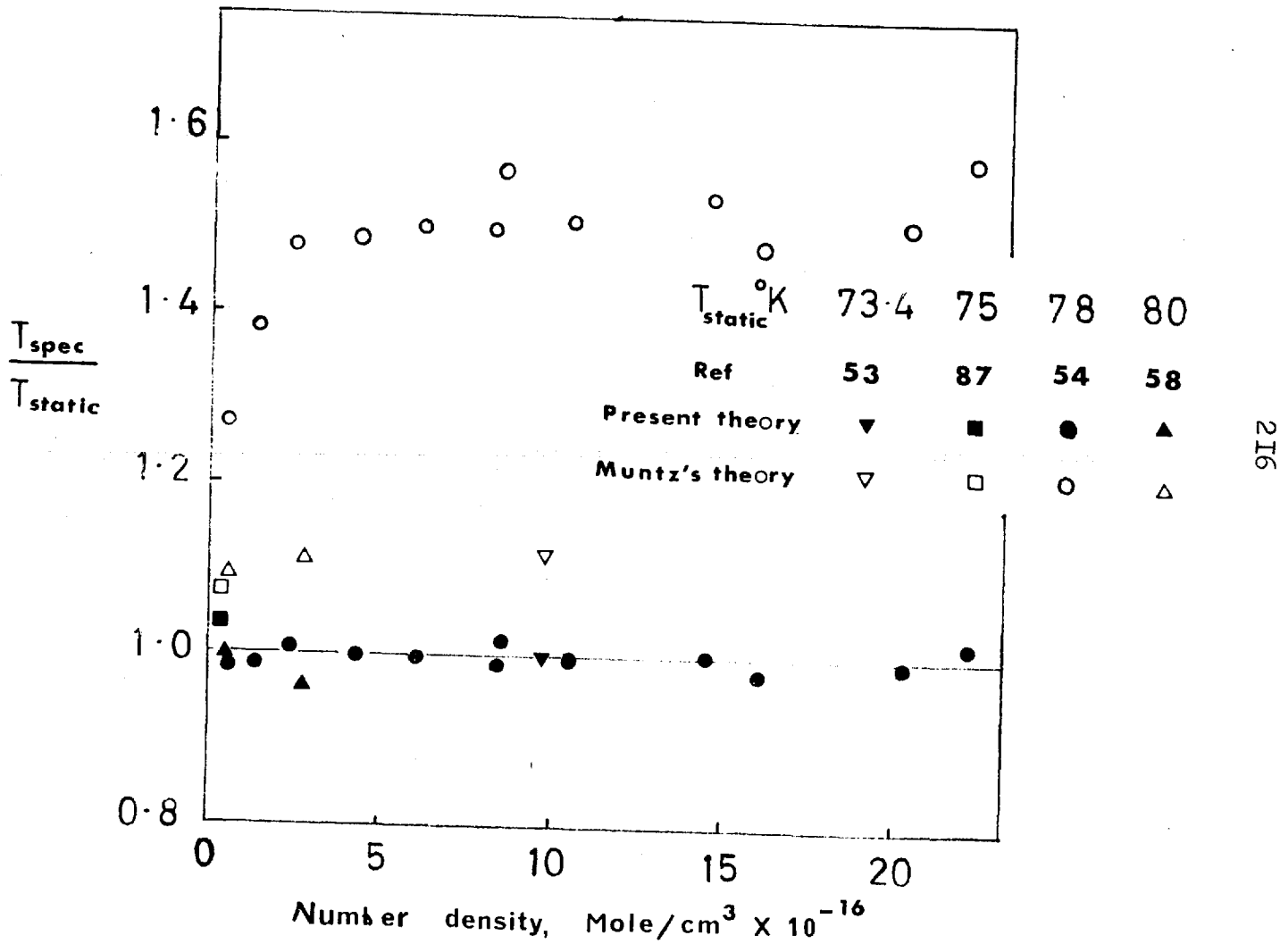

FIG A3·3 Comparison of theories

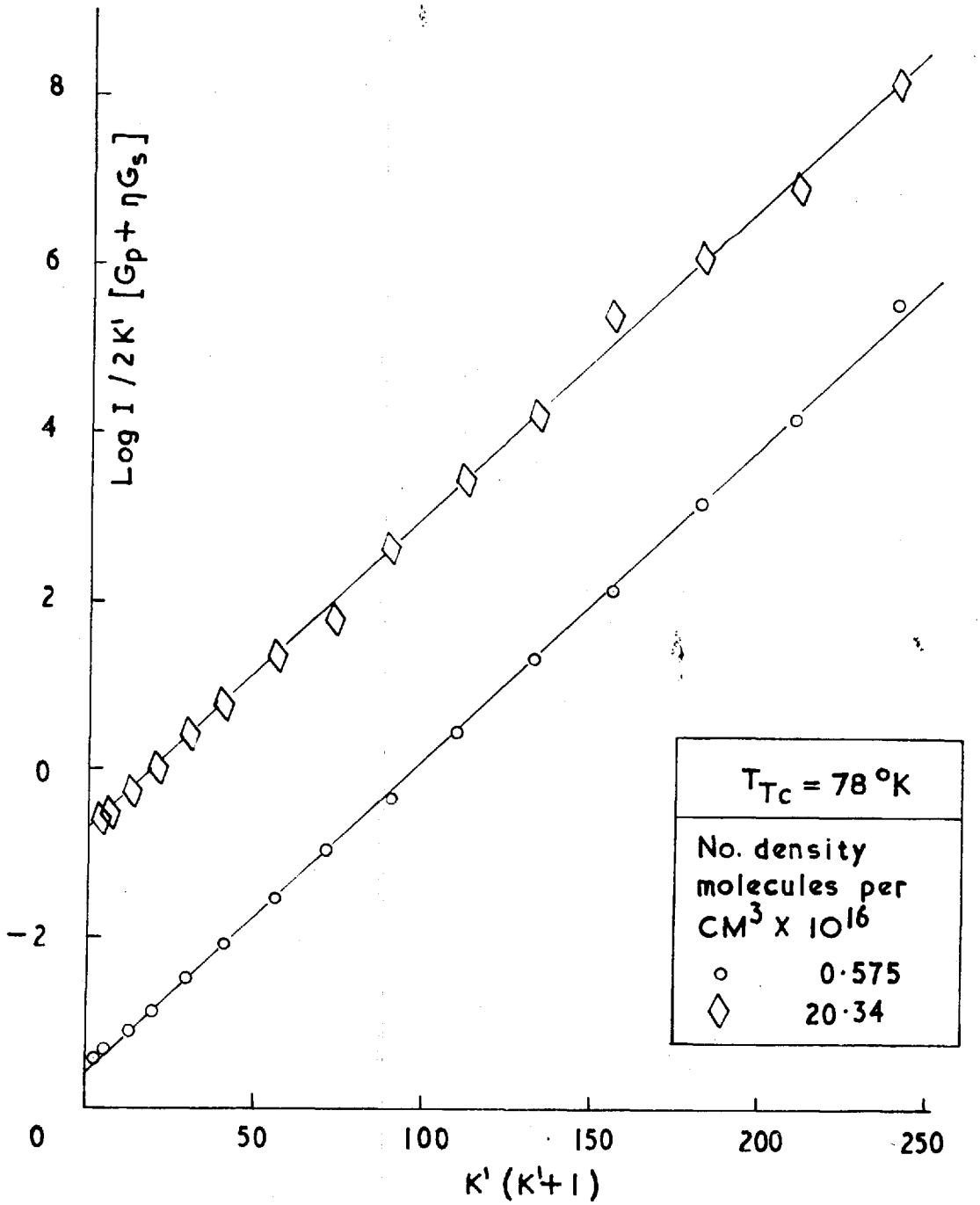

FIG. A 3·4. Typical plots of $\text{Log}_e I / 2K' [G_p + \eta G_s]$ against $K'(K'+1)$.

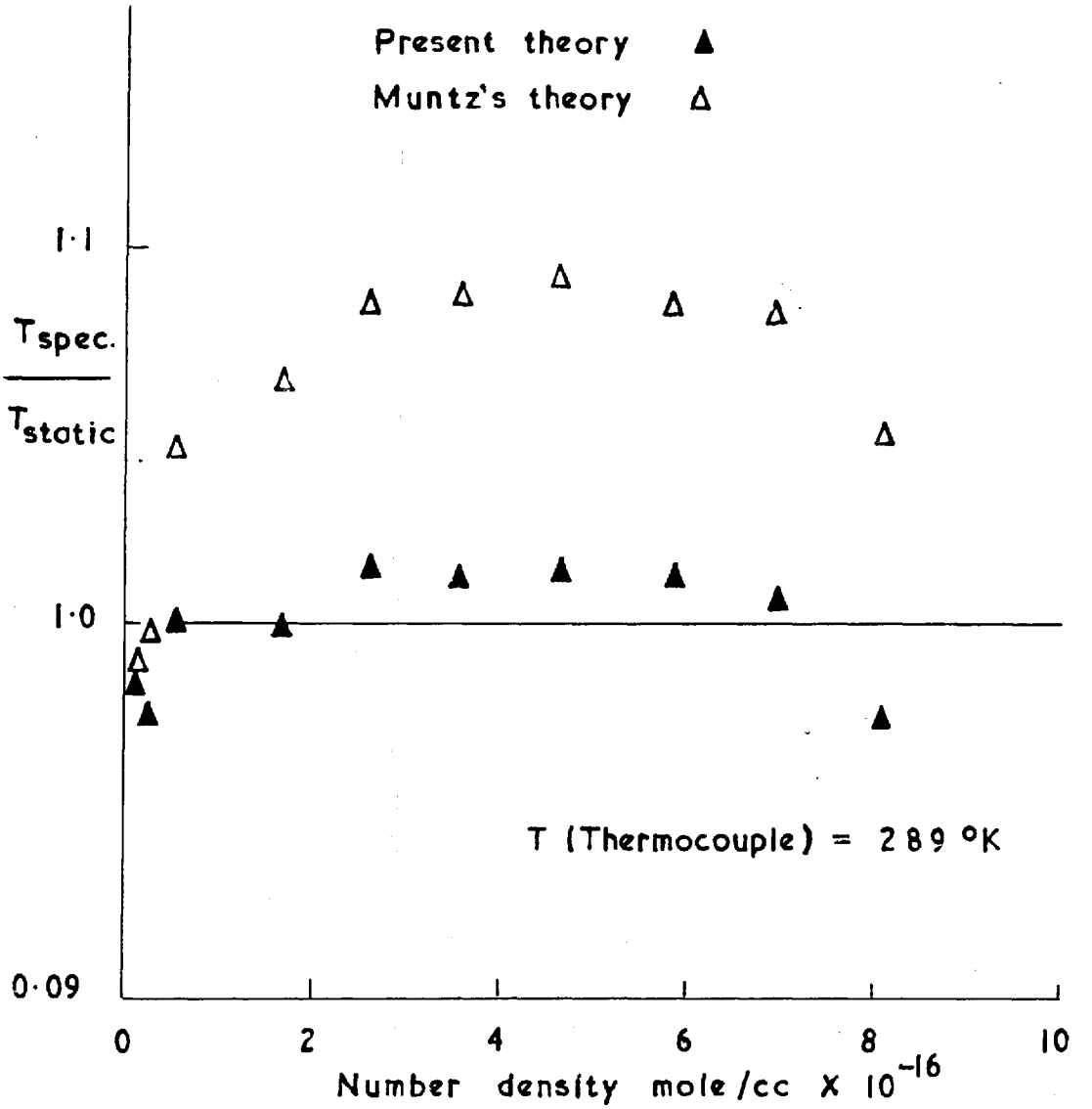

FIG. 3·5 Comparison of theories using 15 lines

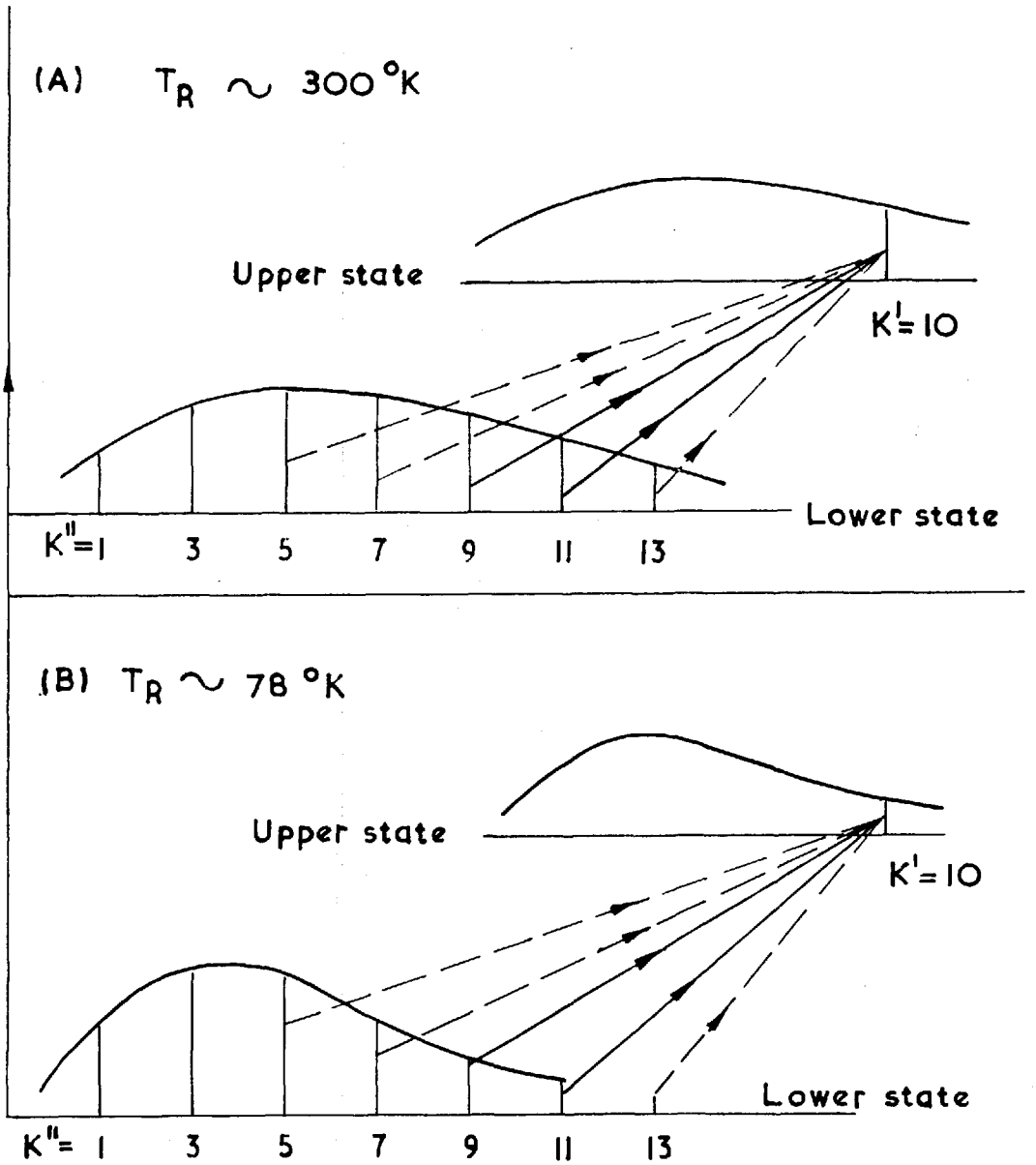

FIG. A 3·6 Schematic diagram of excitation to $K'=10$ Level by allowed. $\Delta K = \pm 1$, and forbidden, $\Delta K = \pm 3, \pm 5 \ldots$, transitions.

Table A 3 · 1 Values of $G(K^1 . T_R)$

K^1 =	1	2	3	4	5	6	7	8	9	10	11	12	13	14	15
T = 78 °K															
$G(K^1 T_R)$ =	1·08	1·09	1·05	1·13	1·15	1·26	1·27	1·40	1·68	2·04	2·92	3·38	6·30	11·5	23·2
T = 289°K															
$G(K^1 T_R)$ =	2·64	2·77	2·60	2·66	2·60	2·68	2·62	2·75	2·76	2·82	2·80	2·86	2·94	3·13	3·14